DETERMINATION OF THE TEMPERATURE DISTRIBUTION DUE TO NEUTRON AND GAMMA HEATING IN A SPACE-REACTOR SHIELD

A Thesis

Submitted to the Graduate Faculty of the
Louisiana State University and
Agricultural and Mechanical College
in partial fulfillment of the
requirements for the degree of
Master of Science in Nuclear Engineering

in

The Department of Nuclear Science

by
Satyajit Nadkarny
M.S., Louisiana State University, 1984
December 1988

ACKNOWLEDGEMENTS

This study was carried out as part of a project funded by a research grant from Oak Ridge National Laboratory, Oak Ridge, Tennessee. I would like to thank my major professor Dr. Mark L. Williams, associate professor of Nuclear Engineering at LSU, for procuring the grant, allowing me to utilize this project for thesis study, and for his invaluable guidance and support throughout the period of this study. I would like to thank Dr. Adnan Yucel, assistant professor of Nuclear Engineering at LSU, for his help and suggestions in matters related to "heat conduction" in this project.

I am grateful to D. T. Ingersoll, L. R. Williams, and W. W. Engle Jr., all three of the Engineering Physics and Mathematics Division at Oak Ridge National Laboratory, for providing all the calculational data needed in this study. I am also thankful to W. H. Harless Jr. of Advanced Nuclear Technology Operation Division, General Electric, Sunnyvale, California, for clarifying numerous doubts concerning the SP-100 space reactor model utilized in this study.

I am grateful to Dr. J. C. Courtney, professor of Nuclear Engineering at LSU, Dr. L. M. Scott , assistant professor of Nuclear Science at LSU, and Dr. V. A. Cundy, associate professor of Mechanical Engineering at LSU for kindly agreeing to serve on my thesis examining committee.

I am indebted to Richard Teague, Electronics Technician at the Nuclear Science Center, LSU, for his help in problems related to computer usage.

TABLE OF CONTENTS

LIST OF TABLES

LIST OF FIGURES

ABSTRACT

Nuclear heating due to radiation (neutrons and gammas) deposited in the shield materials of space power reactors becomes significant at high reactor power levels. The radiation shield is composed of lithium hydride (LiH) for neutron attenuation and tungsten for gamma attenuation. The physical properties of LiH require the temperatures in the LiH regions in the shield be maintained in the 600°K-680°K range for the shield to maintain its structural integrity.

In this thesis, the transport code DOT-IV, and DOS-HEATING6, a modified version of the heat conduction code HEATING6 developed at LSU in conjunction with this study to compute the nuclear heat source, have been used for two-dimensional (RZ) steady state and transient nuclear heating analysis of the radiation shield of a SP-100 space nuclear reactor design developed by General Electric in 1984.

Results of the steady state analysis indicate that the shield temperatures in the original design do not lie in the recommended 600°K-680°K range. Thereafter several modifications to the preliminary shield design are made in an attempt to obtain an acceptable temperature distribution, while meeting weight and radiation dose constraints. Among the shield designs examined, it is found that a design in which enriched LiH at the front of the shield is replaced by beryllium and the insulation around the tungsten is removed, appears to be closest to optimum. The resultant temperature distribution is close to the required 600°K-680°K range.

Transient heat conduction calculations using DOS-HEATING6 for the beryllium shield model indicate that the thermal time constant of the shield is extremely small. Therefore during 'pulsed mode' operation of the SP-100 reactor, shield temperatures will not be of much concern since they will remain well below the full power steady state temperature distribution during reactor operation. During power-up and shut-down operations the shield temperature will require several days to reach steady state conditions.

1. INTRODUCTION

1.1 The U.S. SP-100 Space Nuclear Reactor Program

1.1.1 Historical Background

Nuclear reactors are considered to be the main contenders as space power sources for high power level requirements (100 kWe to several MWe). They offer several advantages over other conventional power sources [1.1, 1.2] such as solar cells, chemical fuel cells, radioisotopic thermoelectric generators (RTG's) etc., among which are : (1) high specific power (40 - 50 W/kg); (2) long operational lifetimes (7 - 10 years); (3) high durability (e.g., better suited to operate in hostile environments) and (4) ability to deliver both steady state and pulsed power.

In the U.S., research work concerning space nuclear power began in the mid-1950s [1.3] with the NERVA (Nuclear Engine for Rocket Vehicle Application) program which was primarily intended for developing nuclear propulsion systems. The SNAP (Systems for Nuclear Auxiliary Power) project which commenced in 1961 focussed on developing nuclear electric power sources. However both the programs were phased out during the mid-1970s due inadequate funding and because of the emergence of the Space Shuttle program as a higher priority. Nevertheless, this developmental period of about fifteen to twenty years was quite fruitful in that much knowledge was gained and documented concerning the type of reactor, radiation shield, thermal to electric power conversion method etc. that would be most suitable.

The early 1980s saw a revival of interest in space nuclear reactors

when nuclear power became necessary to meet the future space objectives. The renewed interest was primarily due to the need for a high power source that could be placed in orbit as part of the Strategic Defense Initiative (SDI). However many of the goals of the civilian space program were also recognized as being dependent upon development of a simimlar type of power source. Three federal agencies viz. National Aeronautics and Space Administration (NASA), Department of Energy (DOE), and the Department of Defense (DOD) agreed to jointly fund a program called "SP-100" (Space Power Reactor - 100 kWe) for furthering research in space reactor technology. The program which commenced in 1983 is actively being pursued to date by various contractors including General Electric, Westinghouse, Los Alamos National Laboratory, Oak Ridge National Laboratory, Jet Propulsion Laboratory etc. The main objectives of the SP-100 project are to develop the best overall design for a 100 kWe space nuclear reactor (the design should be modular and scaleable to 1000 kWe) and compare its feasibility with that of other power sources.

RTG's have already been successfully put into orbit serving low power satellites. The highly successful Voyager-2 space craft which is currently approaching Neptune has its electronics systems powered by a RTG. However, to date, only one critical nuclear reactor has been launched by the United States (the 500 We SNAP-10A on April 3, 1965). The reactor operated successfully in its permitted orbit for forty three days before a series of false electronic signals caused it to shut down. The Soviet Union, on the other hand, has placed numerous critical reactors in earth orbit.

A number of civilian and defense applications in space requiring

high power levels have been identified. In the SDI program a nuclear reactor may be required to power advanced lasers and particle beam weapons. Plans are underway at NASA to construct a space station to be used as a science base and for space manufacturing. Although the initial station (expected to be operational by mid 1990s) will need only about 75 kWe of power, the final version complete with all facilities is expected to need about 2 MWe - 10 MWe [1.4]. Other applications include lunar bases, deep space missions to Mars, space based radars and laser communication satellites, hauling payloads fron LEO (low earth orbit) to GEO (geosynchronous earth orbit), satellite maintenance platforms in GEO etc [1.3].

The current phase of the SP-100 project is expected to be completed by mid 1990s [1.5]. The immediate future of space nuclear power depends on whether the space nuclear power applications identified are funded or not. However in the long run it appears that space-based nuclear power systems are an inevitable component in establishing extra-terrestrial bases.

1.1.2 General Features of the SP-100 Space Nuclear Reactor

A rough consensus has now evolved as to the general SP-100 design and subsystems. Fig. 1.1 shows a typical SP-100 type space nuclear reactor power system currently being considered. The space nuclear power system may be broadly subdivided into four subsystems, viz. the nuclear reactor, radiation shield, thermal to electrical power conversion subsystem, and the waste heat rejection subsystem.

The reactor itself is a fast reactor employing liquid metal (Na, Li, or NaK) as coolant [1.6]. The reasons for the choice of a fast reactor

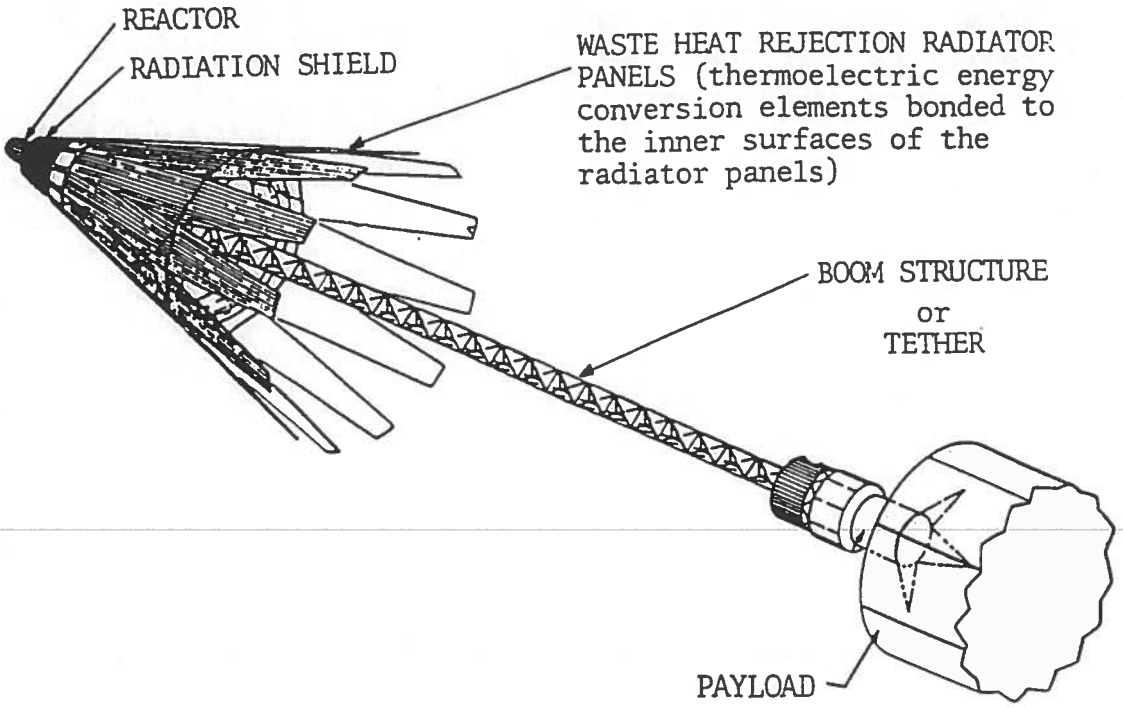

Fig. 1.1 A typical SP-100 space nuclear power system (Ref. [1.2])

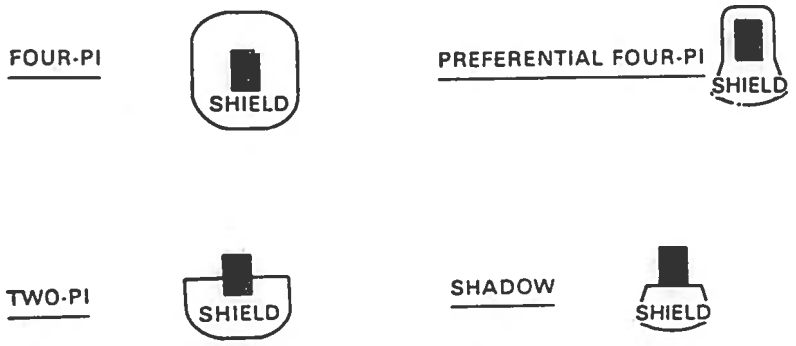

Fig. 1.2 Different types of radiation-shield geometries (Ref. [1.2])

are numerous, the main reason being the fact that a fast reactor core is smaller than for thermal or epithermal reactors. Liquid metal coolants are preferred for their excellent heat transfer properties and low vapour pressure at high temperatures.

The radiation shield is mounted directly behind the reactor core. Its purpose is to protect the payload (crew and sensitive electronic equipment) from reactor core radiation (neutrons and gammas). The SP-100 nominal seven year neutron fluence and gamma dose specifications at the 25 m doseplane (25 m behind the reactor midplane towards the payload end) are 1.0E13 neutrons/cm^2 and 0.5 Mrads respectively [1.7]. Fig. 1.2 shows four basic shield types that could be employed to reduce the radiation intensity. The choice of a particular shield type depends upon the mission shielding requirements. Fig. 1.3 shows a typical "shadow shield" configuration which is the type most often considered for the SP-100 due to the lower weight. The shield contains two component shielding materials, one for neutron attenuation and the other for gamma attenuation. Materials containing nuclides with low atomic weights (e.g. H, Be etc.) make good neutron attenuators due to the effective moderating capability, whereas materials containing nuclides with high atomic numbers and high mass densities make good gamma attenuators. Lithium hydride is preferred over other candidate materials for neutron shielding because of its high hydrogen content (5.9E22 hydrogen atoms/cc), low mass density (0.82 gm/cc), high melting point (960°K), and its ability to capture neutrons with very little secondary gamma production. The lithium hydride is cast into a stainless steel honeycomb matrix to give structural integrety to the shield. Tungsten is usually preferred over

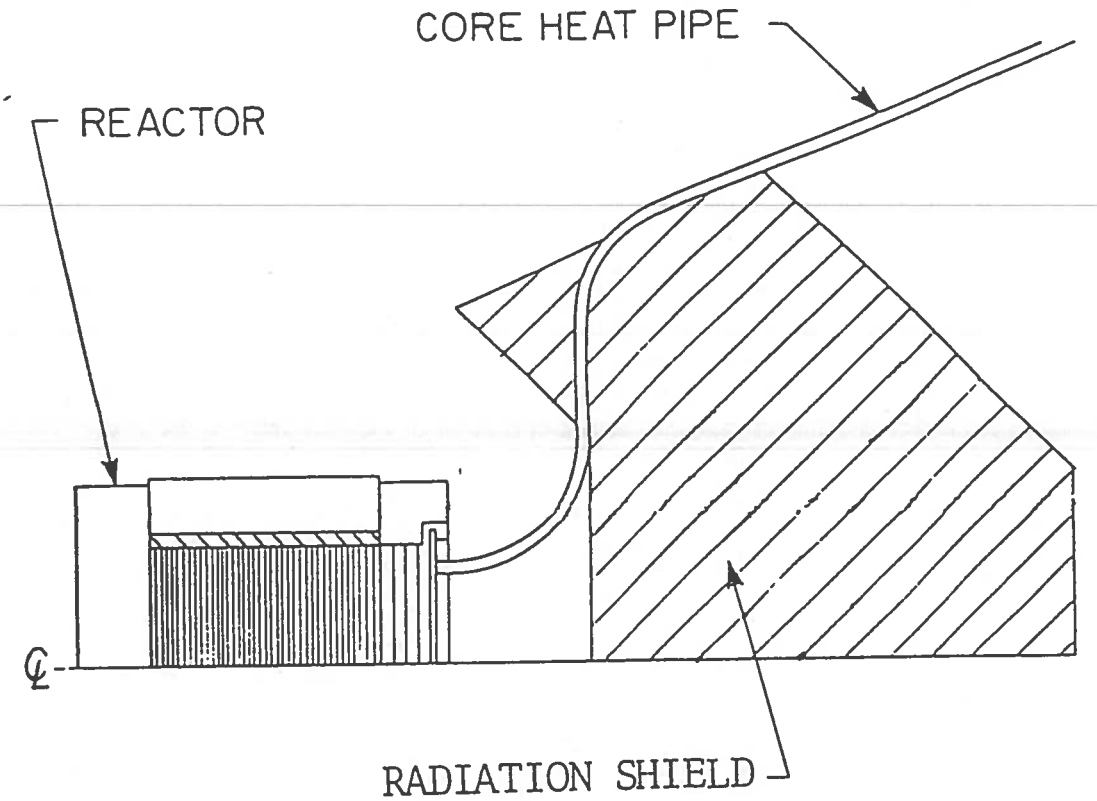

Fig. 1.3 A typical "shadow" shield configuration (only upper half shown) (Ref. [1.2]).

other candidate materials for gamma shielding especially from the minimum shield weight point of view. Tungsten also has a high melting point (3683°K). Design of the shield configuration and the relative placement of LiH and tungsten within the shield is driven by the need to minimize the shield mass (the shield mass could account for almost 20% - 30% of the total system mass [1.8]).

The thermal to electric power conversion subsystem converts the reactor thermal energy into electrical energy. The following three power conversion methods seem to be most promising : Thermoelectric, Thermionic, and the Sterling Engine. The first two are static conversion systems in that no mechanical moving parts are involved, and the latter is a dynamic system [1.3]. The Thermoelectric and Stirling Engine converters are placed outside the reactor, whereas the Thermionic converter forms a part of the reactor core. Thermoelectric and Thermionic converters have low conversion efficiencies (~ 7% - 9%), whereas the Stirling Engine converter has a higher efficiency (~25% - 35%).

Waste heat from the thermal conversion (usually more than 90% of the reactor thermal output) is rejected into space by thermal radiation from the outer surface of the radiator panels located behind the radiation shield. The radiator operating temperature is typically in the 800°K - 850°K range. Design of radiator panels is driven by the need to minimize their surface area (the entire nuclear space power system must fit into the space shuttle's 60 ft long and 15 ft wide payload bay). This means that the reactor must operate at a high temperature to maintain thermodynamic efficiency. Reactor operating temperatures are typically

in the 1350°K - 1400°K range.

The payload section is located behind the radiator panels at a sufficient distance (~25 m from the reactor midplane) to meet dose constraints, and is connected to the radiator panel end by a tether or a boom structure. The reactor is launched "cold"; i.e. it is started only after it has reached its stable orbit. The SP-100 reactor is designed to have a 10 year life with a 7 year full power operation capability.

1.2 Thermal Analysis of the Radiation Shield

Thermal analysis of the radiation shield of an operating space nuclear reactor is an important consideration in validating the shield design. The shield is exposed to intense radiation (neutrons and gammas) and consequently it heats up due to the energy deposited by the incoming particles. Although the nuclear heating rate in a shield is usually less than 0.5% of the reactor thermal power, at high reactor power levels (100 kWe to several MWe), it becomes significant and can result in excessive shield temperatures and temperature gradients leading to high thermal stresses that could crack the shield. Moreover the only mechanism by which the shield loses heat is by radiating the thermal energy from its outer surface into space. In fact "thermal analysis" of the shield is typically followed by "stress-strain analysis" in order to establish the thermally induced shield stresses. Major concerns in using LiH as the neutron shield material are as follows :

(1) LiH has a very low thermal conductivity (0.063 W/cm/°K at 800°K). The shield design should be such that temperatures remain well below the melting point of LiH (960°K).

(2) Shield temperatures are required to be maintained in the 600°K - 680

°K range. A minimum temperature of 600°K is recommended to minimize swelling of the shield due to hydrogen production resulting from radiation induced dissociation of LiH. A maximum temperature of 680°K is recommended (especially for the outer portions of the shield) to avoid loss of dissociated hydrogen if the shield were punctured by meteorite impact (loss of hydrogen from the shield decreases the moderating capability of the shield).

(3) LiH is very brittle at high temperatures. Large temperature gradients are bound to induce excessive thermal stresses which could crack the shield and lead to undesirable neutron streaming and loss of dissociated hydrogen through the cracks.

It can be seen that in addition to determining the radiation attenuation properties of the shield, it is also necessary to obtain the spatial temperature distribution.

1.2.1 Previous Work Done in Radiation Shield Thermal Analysis

Much of the work concerning radiation shield design e.g. selection of shielding materials, radiation transport analysis of shields to ensure acceptable radiation doses at the dose plane, etc. was done during the SNAP program [1.9]. However, very little attention was given to thermal analysis of radiation shields during that time. Reference [1.9] mentions some thermal analysis work done by Beiriger [1.10], Thompson and Schwab [1.11], and Keshishian [1.12] during the SNAP program time period.

Since the inception of the SP-100 program in 1983, particularly with emphasis on designing space reactors involving high power levels wherein

nuclear heating in the shield becomes extremely significant, thermal analysis of shields has begun to recieve considerable attention. Since the early eighties, the University of New Mexico at Albuquerque has been actively involved in space reactor shield analysis. The most comprehensive work that is readily available is by Barattino et. al. [1.13, 1.14, 1.15] done during 1984 - 1985. Their work involved coupled radiation transport-steady state nuclear heating calculations for a hypothetical SP-100 space reactor shield, including development of in-house computer codes for the analysis. On the other hand, in this thesis, coupled radiation transport-steady state nuclear heating calculations have been carried out for the shield of a realistic SP-100 space reactor (designed by General Electric in 1984). This design has more complex features than assumed in the earlier works, and it was to assess the benifit of some of the unique design components proposed by G.E. Additionally, in this thesis, transient nuclear heating calculations have been conducted for the shield. Apparently, this topic has not been addressed in the work by Barattino et. al. or any of the previous works.

FEMP2D, the computer code developed and used for radiation transport calculations by Barattino et. al. in their studies, is a finite element code that solves the steady state multigroup Boltzmann transport equation for 2-D geometries, using the "spherical harmonics method" (P_1 approximation). In many shielding calculations it is necessary to employ higher order transport theory approximations to obtain accurate results. Therefore, in this thesis, radiation transport calculations have been performed using the DOT-IV computer code. DOT-IV solves the steady state

multigroup Boltzmann transport equation for 2-D geometries, using the "discrete ordinates" method (also called "S_N" method), which is more accurate than the low order spherical harmonics method used by FEMP2D, especially for deep penetration transport of neutrons and gammas such as encountered in this study. DOT-IV has very general capabilities (e.g., arbitrary scattering anisotropy,quadrature order, group structure, etc.) and is well established as an accurate code for performing complex shielding analysis.

SHLDTEMP, the computer code developed and used for shield temperature calculations by Barattino et. al. in their studies, is a finite element code (using simplex elements) that solves the steady state heat conduction equation using the Newton-Raphson iterative technique. This code is limited to XY and RZ geometries and has other limitations as well (e.g., simulating surface-to-surface radiative heat transfer across internal gaps such as encountered in the shield analyzed in the present study). Therefore, in this thesis, shield temperature calculations have been done using the HEATING6 computer code. HEATING6 is a finite difference code that has the capability to solve the steady state as well as transient heat conduction equation for 2-D as well as 3-D geometries, using a variety of numerical techniques.

Both DOT-IV and HEATING6 are thoroughly tested production oriented codes developed at Oak Ridge National Laboratory and are more generic in their application than FEMP2D and SHLDTEMP, the in-house codes developed and used in the calculations by Barattino et. al in their studies.

One thing that has been considered in the coupled radiation transport-nuclear heating calculations by Barattino et. al. in their

studies, but has not been accounted for in the coupled calculations performed in this thesis is the effect of temperature feedback on the nuclear properties (nuclear cross sections, atom densities) of the shield materials and consequently on the energy deposition in the shield. However, Barattino et. al. have shown that the effect of temperature feedback on energy deposition in the shield is significant only for reactors operating in the multi-MWe range). In this thesis, since the reactor considered is a 100 KWe reactor, neglecting temperature feedback effects should not introduce serious errors in the shield temperature calculations.

1.3 Thesis Objectives

The main objectives of this thesis are as follows :

(1) to make program modifications to HEATING6 in order to provide capability for performing nuclear heating calculations.

(2) to test the modified version of the code (called DOS-HEATING6) on sample cases so as to validate its accuracy.

(3) to perform coupled radiation transport-heat conduction calculations using DOT-IV and DOS-HEATING6 for the radiation shield of an actual SP-100 reactor design, in order to determine the steady state temperature distribution in the shield, as well as the neutron and gamma radiation dose and flux throughout the system.

(4) if the temperatures are not in the desired 600°K -°680 K band, then make design modifications to the basic shield configuration so as to obtain shield temperatures in that range.

(5) to perform transient heat conduction calculations using DOS-HEATING6 in order to estimate the thermal response time of the shield.

Chapter 2 describes neutron and gamma interactions that lead to shield nuclear heating. Chapter 3 gives an overview of the calculational procedure involved in shield "thermal analysis". Chapter 4 and Chapter 5 describe in brief the theory and numerical techniques underlying DOT-IV and HEATING6, respectively. Chapter 6 describes the main features of DOS-HEATING6. Chapter 7 describes in detail, all nuclear heating calculations performed. Lastly, Chapter 8 briefly summarizes the main results of the nuclear heating calculations performed in this study.

2. EVENTS CAUSING NUCLEAR HEATING IN THE RADIATION SHIELD

Nuclear heating in the radiation shield of the space reactor is mainly due to fast neutrons leaking from the reactor core, primary gammas coming from the reactor core, and secondary gammas produced as a result of inelastic scatter of fast neutrons, and radiative capture of thermal neutrons in the radiation shield [2.1].

Neutron Heating

Fast neutrons (average energy ~ 2 MeV) originate in the reactor core as a result of fission reactions :

$$_{92}U^{235} + {}_{0}n^{1} \longrightarrow \text{Fission products} + 2.47\ {}_{0}n^{1} + \gamma\text{'s} + 200\ \text{MeV energy} \qquad (2.1)$$

These neutrons deposit their kinetic energy as heat through succesive scattering collisions with the shield nuclei. Elastic scattering is dominant in light elements (low atomic number) whereas inelastic scattering is dominant in heavy elements. After suffering collisions with the shield nuclei, the fast neutrons may slow down and become low energy thermal neutrons.

Some light elements such as B^{10}, Li^{6} etc. capture thermal neutrons and emit charged particles which cause highly localized heating as they plough their way through the medium causing ionization. Of particular importance in LiH is the following [n,α] reaction that Li^{6} undergoes:

$$_{3}Li^{6} + {}_{0}n^{1} \longrightarrow {}_{1}H^{3} + {}^{++}_{2}He^{4} \qquad (2.2)$$

Natural lithium contains 7.56 at% Li^{6} and 92.44 at% Li^{7}. To reduce charged particle heating and build up of helium in the shield (build up of helium in the shield might result in high pressures in the shield

casing (stainless steel containers)) due to the $Li^6[n,\alpha]$ reaction, a portion of the LiH used in the radiation shield is sometimes composed of enriched LiH (almost 100% Li^7 enrichment).

Gamma Heating

The source of gammas may be traced to three main events :

(1) Primary gammas from the reactor core due to fission and decay of fission products. The average energy of these gammas is about 1 MeV.

(2) Secondary gammas due to inelastic scatter of neutrons in the reactor core, reflector, and the shield ([n,n'] reaction which occurs mostly in heavy elements, and for high neutron energies) :

$$ {}_Z X^A + {}_0 n^1 \longrightarrow \left[{}_Z X^{A+1}\right]^* \longrightarrow \left[{}_Z X^A\right]^* + {}_0 n^1 \; ; \; \left[{}_Z X^A\right]^* \longrightarrow {}_Z X^A + \gamma \qquad (2.3) $$

(3) Secondary gammas due to radiative capture ([n,γ] reaction) of thermal neutrons in the reactor core, reflector, and especially in the radiation shield :

$$ {}_Z X^A + {}_0 n^1 \longrightarrow \left[{}_Z X^{A+1}\right]^* \longrightarrow {}_Z X^{A+1} + \gamma \qquad (2.4) $$

These gammas mostly have energies in the 10 KeV - 10 MeV range which they deposit in the radiation shield by undergoing one of the following three types of interactions :

(1) Photoelectric absorption (E < 0.1 MeV)

(2) Compton scatter (0.1 MeV < E < 5 MeV)

(3) Pair Production (E > 5 MeV)

In fact, secondary gammas account for most of the nuclear heat generated in the radiation shield. Heating due to energy degradation of fast

neutrons is significant only in the front portion of the radiation shield close to the reactor core.

3. OVERVIEW OF CALCULATIONAL METHODOLOGY

Determination of the steady state temperature distribution in the shield involves the following three steps :

(1) The first step is to carry out radiation transport analysis of the entire reactor-shield system. This involves solving the coupled neutron/gamma steady state multigroup Boltzmann transport equation with the entire reactor-shield system as the solution domain. This step yields the spatial distribution of the multigroup scalar flux of particles (neutrons and gammas) in the reactor-shield region, i.e., $\Phi_g(\hat{r})$ where $\hat{r} \in$ reactor-shield region. It is necessary to know $\Phi_g(\hat{r})$ in order to determine neutron and gamma radiation dosage as well as determine the nuclear heating rates in the shield.

(2) The second step is to determine the spatial distribution of the nuclear heating rates throughout the shield by folding the multigroup scalar flux of particles obtained from step (1) with certain energy deposition data called "kerma factors", i.e.

$$q_N(\hat{r}) = \sum_{g=1}^{g=IGM} \Phi_g(\hat{r})\, \Sigma_g^k(\hat{r}) \qquad (3.1)$$

where $q_N(\hat{r})$ ≡ nuclear volumetric heat generation rate [W/cm^3] at spatial point $\hat{r}$.

$\Phi_g(\hat{r})$ ≡ group 'g' scalar flux [particles/cm^2/sec] at spatial point $\hat{r}$.

$\Sigma_g^k(\hat{r})$ ≡ group 'g' macroscopic kerma factor [J/cm] for the material at spatial point $\hat{r}$.

IGM ≡ total number of energy groups employed in transport calculations.

(3) The last step is to carry out heat conduction analysis of the shield

region. This involves solving the steady state heat conduction equation with only the shield region as the solution domain, using the nuclear heating source determined in step (2) [Note : thermal analysis of the core is another important topic, but it is not germane to this work]. The steady state heat conduction equation in the shield region may be written as :

$$\hat{\nabla} \cdot (k \hat{\nabla} T(\hat{r})) = - q_N(\hat{r}), \quad \hat{r} \in \text{shield region} \qquad (3.2)$$

where $T(r) \equiv$ temperature [$^\circ$K] at the spatial point $\hat{r}$.

$k = k(T(\hat{r})) \equiv$ thermal conductivity [W/cm/$^\circ$K] of the material at spatial point $\hat{r}$.

$q_N(\hat{r}) \equiv$ volumetric nuclear heating rate at spatial point $\hat{r}$ [W/cm^3].

Solving Eqn. (3.2) yields $T(\hat{r})$, the steady state temperature distribution in the shield. Fig. 3.1 illustrates the steps outlined above in the form of a flowchart. It is evident that any computer code capable of solving the steady state heat conduction equation (step 3) may be used for nuclear heating analysis of the shield, if it is adapted to (a) read the multigroup neutron and gamma scalar fluxes from step (1), (b) read multigroup kerma factors for all materials involved, and (c) calculate the nuclear heating rates in the shield by folding the fluxes with the kerma factors according to step (2). In the present study, the computer code DOT-IV has been used to carry out step (1). Subsequent steps (2) and (3) have been carried out using the computer code DOS-HEATING6, which is a modified version of the HEATING6 code, adapted to calculate the nuclear heating rates from the DOT-IV fluxes and input kerma factors. The major problem with coupling DOT-IV and HEATING6 is the incompatibility between spatial meshes in the two codes. It becomes

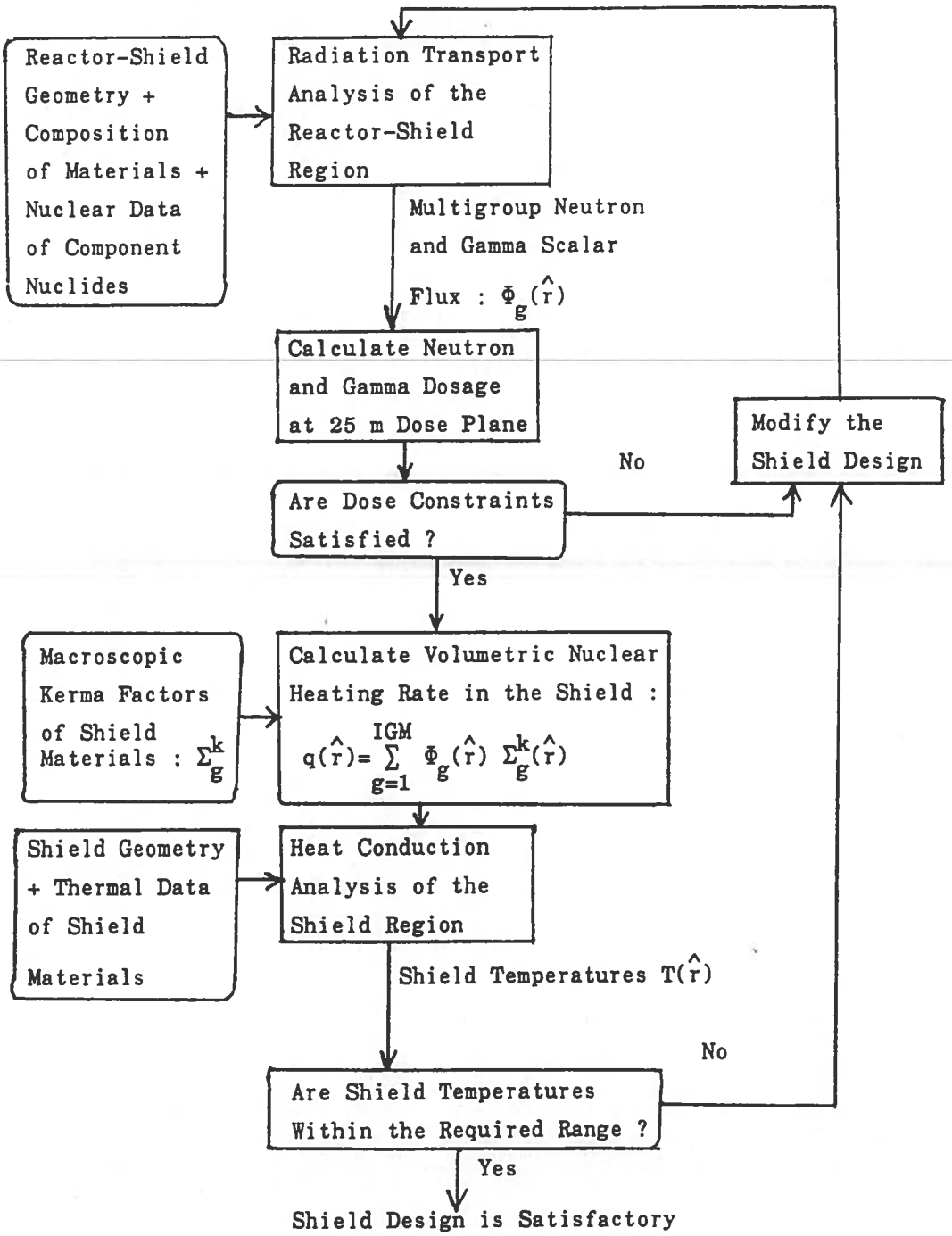

Fig. 3.1 Flowchart indicating the basic procedure involved in coupled radiation transport-steady state nuclear heating analysis of a shield

necessary to interpolate the DOT-IV scalar fluxes to the HEATING6 mesh before calculating the nuclear heat source according to step (2). This feature of DOS-HEATING6 is discussed in detail in Chapter 6.

4. REVIEW OF PARTICLE TRANSPORT CODE "DOT-IV"

The DOT-IV computer program [4.1] solves the steady-state Boltzmann Transport Equation numerically using the method of "Discrete Ordinates". In doing so it determines the space and energy-dependent angular flux of particles in 2-D cartesian/cylindrical geometric systems resulting from sources of particles that are either externally incident (surface source) or generated internally in the geometric system (volume source). Although it exists as a functional module in the "DOS" (Discrete Ordinates Systems) family of inter-related radiation transport codes [4.2], it may also be run as a stand-alone program. DOT-IV has evolved from earlier versions of DOT and is the latest version distributed by the Radiation Shielding Information Center. It is mostly used in deep penetration calculations for the transport of neutrons and gammas such as encountered in shield analysis, although it also has the capability of performing criticality (k-type and search) calculations. In the present study it has been used to compute the neutron and gamma particle flux, which is then used in calculating the nuclear heat source for the heat conduction analysis.

4.1 The Steady State Boltzmann Transport Equation

The Boltzmann equation expresses particle conservation (losses = productions) within a six dimensional differential phase space control volume '$dVdEd\hat{\Omega}$'. It may be written as follows:

$$[\hat{\Omega}.\hat{\nabla}+\Sigma_t(\hat{r},E)]\Psi(\hat{r},E,\hat{\Omega})=\int_{\hat{\Omega}'}d\Omega'\int_{E'}\Sigma_s(\hat{r},E'\rightarrow E,\hat{\Omega}'\rightarrow\hat{\Omega})\Psi(\hat{r},E',\hat{\Omega}')dE' + S(\hat{r},E,\hat{\Omega}) \qquad (4.1)$$

where $\hat{r}$,E,and $\hat{\Omega}$ are the six independent variables required to describe particle transport : i.e.,

$\hat{r}$ is the spatial position with respect to an arbitrary reference spatial coordinate system. In general $\hat{r}$ is a three dimensional vector, but DOT-IV is limited to two dimensional geometries;

E is the energy of the particle;

$\hat{\Omega}$ is a unit vector in the direction of particle travel specified with respect to a local directional coordinate system with its origin at $\hat{r}$;

The direction vector $\hat{\Omega}$ is completely specified by giving the values of two of its direction cosines μ and η. The third direction cosine ξ is related to μ and η by $\xi^2 = 1 - (\mu^2+\eta^2)$. Fig. 4.1 shows the spatial and directional coordinate systems for cartesian and cylindrical geometries. The macroscopic cross sections (units of cm^{-1}) in Eqn. (4.1) are $\Sigma_t(\hat{r},E)$, the total cross-section at $\hat{r}$ for a particle with energy E; and $\Sigma_s(\hat{r},E'\rightarrow E,\hat{\Omega}'\rightarrow\hat{\Omega})$, the double differential scatter cross section at $\hat{r}$ for a particle with energy E′ and direction Ω' to emerge from a scattering reaction with energy E and direction $\hat{\Omega}$. The variable $S(\hat{r},E,\hat{\Omega})$ is the source emission density for sources other than scatter (i.e. fission or external sources). The dependent variable in Eqn. (4.1) is $\Psi(\hat{r},E,\hat{\Omega})$, the particle angular flux which has units of particles/cm^2/sec/eV/steradian. The angular flux is used in DOT to calculate the scalar flux $\Phi(\hat{r},E)$ (units of particles/cm^2/sec/eV), defined as :

$$\Phi(\hat{r},E) \equiv \int_{\hat{\Omega}} \Psi(\hat{r},E,\hat{\Omega})d\Omega \qquad (4.2)$$

The "Discrete Ordinates Method" (also called "S_N Method") essentially involves discretizing each of the independent variables viz.

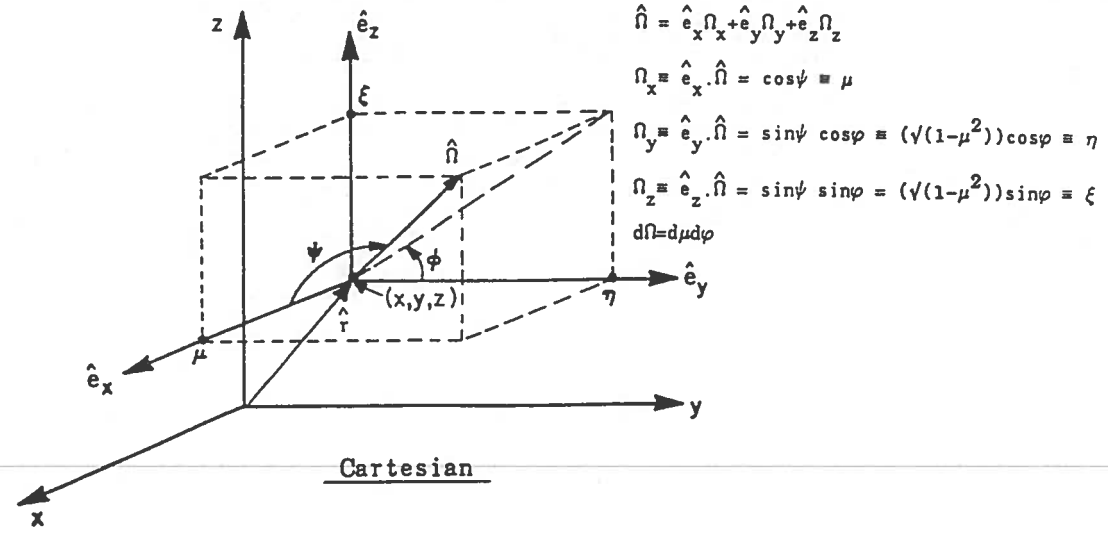

Cartesian

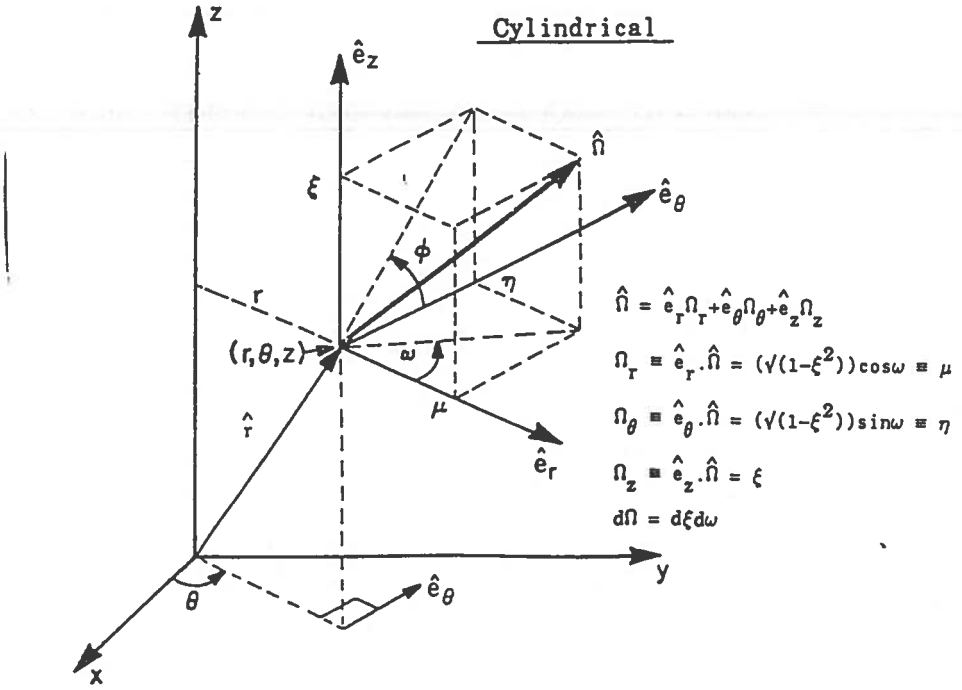

Cylindrical

Fig. 4.1 Spatial and directional coordinate systems used to describe particle transport (Ref. [4.3])

$\hat{r}$,E,and $\hat{\Omega}$ [4.3, 4.4]. Since the discretization of the flux must be understood in order to numerically compute the nuclear heat source, a brief description of the discrete ordinates approach is given in the next five sections.

4.2 Spatial Discretization

The 2-D spatial domain is represented by finite mesh intervals. There are two options in DOT-IV for specifying the mesh. These are (a) Fixed Mesh, in which the mesh intervals corresponding to the 'i' index (X/R axis) are the same for all 'j' (Y/θ/Z) levels; (b) Variable Mesh, in which the mesh intervals corresponding to the 'i' index are allowed to vary with each 'j' level. A distinct 'i' mesh structure is called an 'ISET'. A fixed mesh will have only one ISET whereas a variable mesh will have more than one ISET.

Fig. 4.2 illustrates examples of the variable mesh feature in DOT-IV for XY/RZ and Rθ geometric systems. Variable meshes are employed to represent irregular geometric features, with a minimum of mesh intervals. Fig. 4.3 shows the DOT-IV 2-D mesh elements (spatial control volumes) and their associated volumes.

4.3 Directional Discretization

The infinite number of directions in which the particle can travel through space is represented by a set of discrete directions or rays $\hat{\Omega}_n$, n=1..MM where MM is the total number of directions in the set. The locus of the tip of the unit vector $\hat{\Omega}$, as $\hat{\Omega}$ takes on all possible directions, is a sphere of unit radius with its center located at the origin of the directional coordinate system. The surface of this unit sphere can be

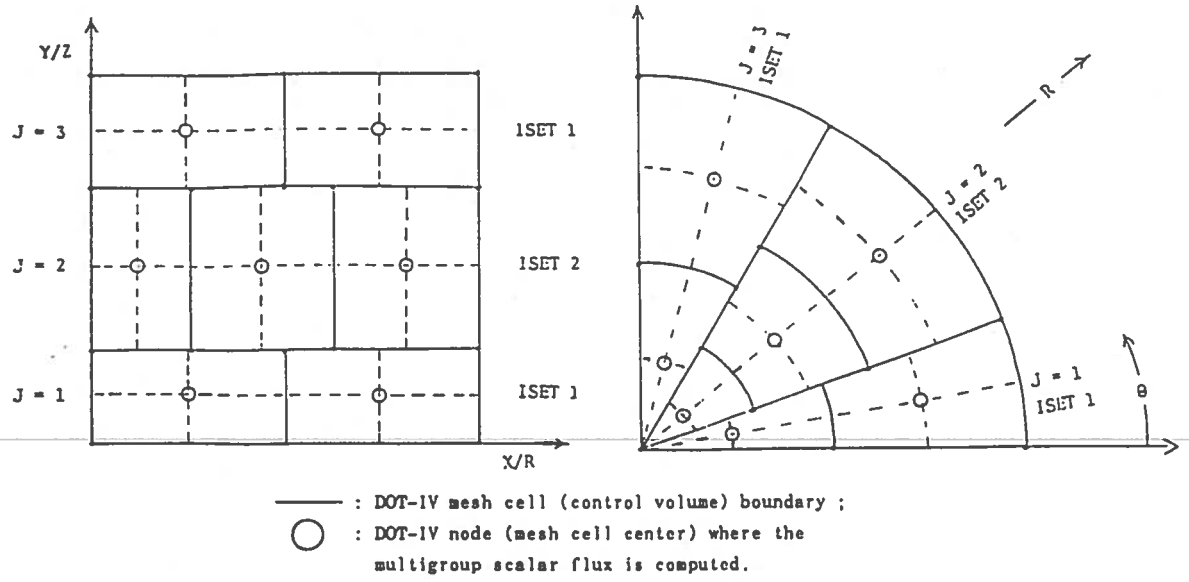

Fig. 4.2 Examples of DOT-IV "variable mesh" in XY/RZ and RΘ geometries

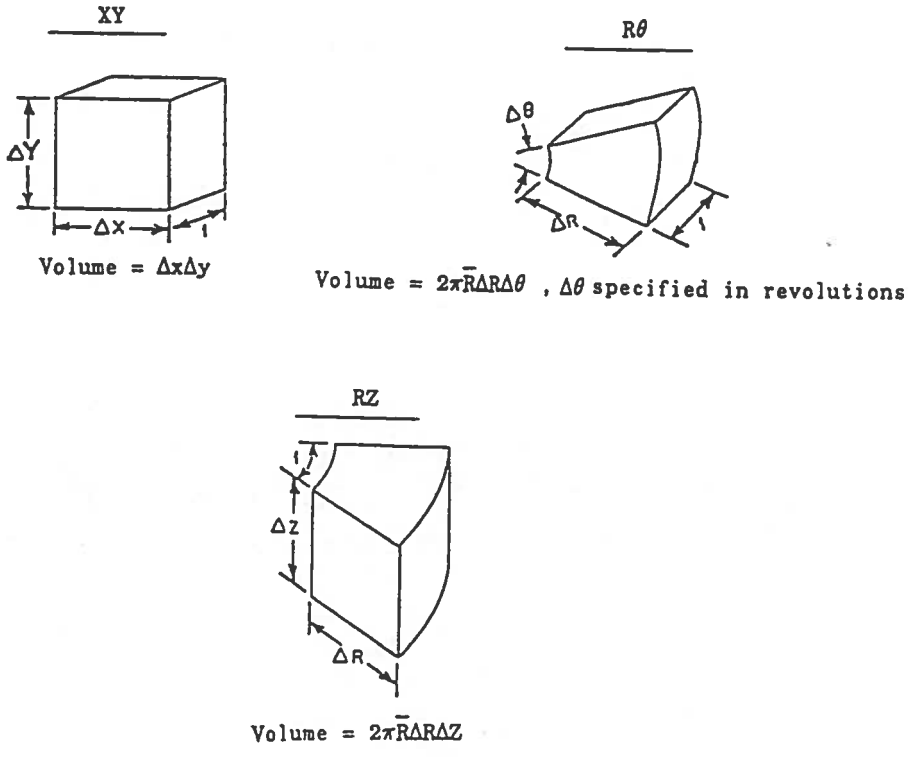

Fig. 4.3 DOT-IV elemental 2-D mesh cells

divided into a series of MM area elements such that the MM discrete directions intersect the unit sphere at the centers of these area elements. A typical such division is shown in Fig. 4.4 (only an upper octant shown). Each direction vector $\hat{\Omega}_n$ points to the center of an area element with area ΔA_n on the unit sphere which subtends a solid angle $\Delta\Omega_n$. The magnitude of $\Delta\Omega_n$ in steradian units will be equal to ΔA_n because of the fact that the radius of the sphere is unity. To each direction vector $\hat{\Omega}_n$, a directional weight W_n, may be assigned where W_n is equal to the fraction of the surface area of the unit sphere i.e.

$$W_n \equiv \frac{\Delta A_n}{4\pi} = \frac{\Delta\Omega_n}{4\pi} \qquad (4.3)$$

The entire unit sphere is covered by all directions so that $\sum_{n=1}^{MM} W_n = 1$.

The set of discrete directions $\hat{\Omega}_n$ and their associated weights is called a discrete ordinates "Quadrature Set". The quadrature directions are defined in a systematic manner on the surface of the unit sphere. The η values determine latitude levels on the sphere. The total number of latitude lines is called "S_N Order" of the quadrature. In 2-D geometries, the angular flux is symmetric in the right and left hemispheres of the unit sphere so that only the directions in a single hemisphere need to be specified. A symmetrical (i.e., non-biased) S_N quadrature set will have N latitude levels on the unit sphere : N/2 levels above and below the equator, respectively. Each η level is subdivided into discrete μ values. For symmetric quadratures the same (η,μ) values exist above and below the equator. Fig. 4.5 shows the arrangement of the directions in an S_4 quadrature set (only the upper quadrant shown; the same pattern is repeated in the lower quadrant). The

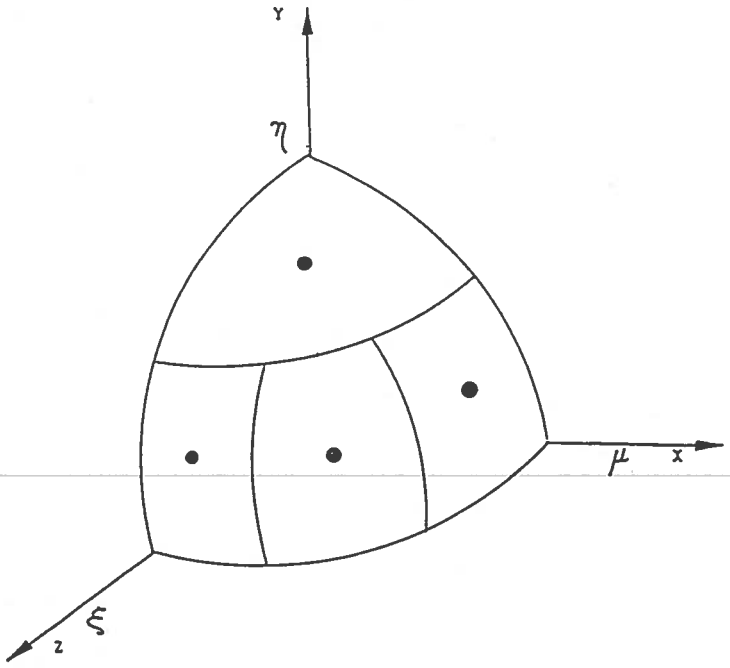

Fig. 4.4 Discretization of the direction variable '$\hat{\Omega}$' (only an upper octant shown)

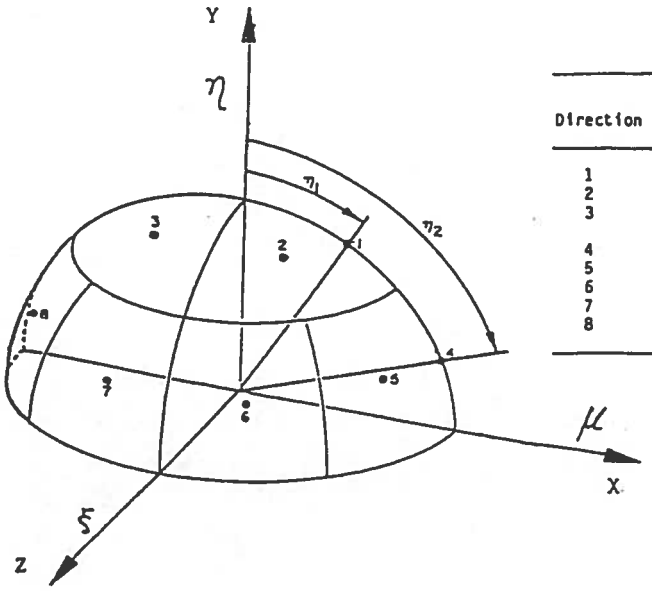

Direction	Weight, W	Ω_y, η	Ω_x, μ
1	0.0	.88192	.4714
2	.08333	.88192	.33333
3	.08333	.88192	-.33333
4	0.0	.33333	.94281
5	.08333	.33333	.88192
6	.08333	.33333	.33333
7	.08333	.33333	-.33333
8	.08333	.33333	-.88192

Fig. 4.5 Arrangement of directions in an S_4 quadrature set (only an upper quadrant shown)

total number of directions in a quadrature set of order N is given by MM = N(N+4)/2 .

4.4 Energy Discretization

The range of particle energies is divided into IGM intervals called "energy groups" (see Fig. 4.6 shown below).

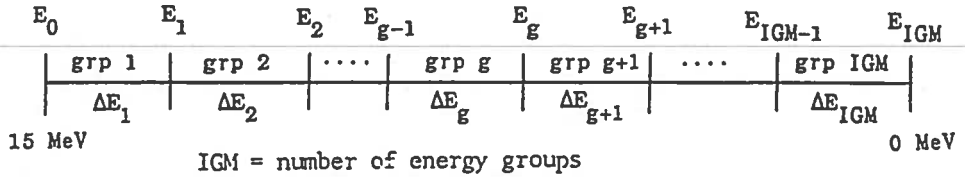

Fig. 4.6 Discretization of the energy variable 'E'

The partitioning of energy into energy groups leads to the definition and use of "group-wise" or "multigroup" dependent variables and cross sections :

$$\text{e.g. } \Psi_g(\hat{r},\hat{\Omega}) \equiv \int_{E_g}^{E_{g-1}} \Psi(\hat{r},E,\hat{\Omega})dE \quad ...(4.4) \quad ; \quad \Phi_g(\hat{r}) \equiv \int_{E_g}^{E_{g-1}} \Phi(\hat{r},E)dE \qquad (4.5)$$

$$\sigma_g(\hat{r}) \equiv \frac{\int_{E_g}^{E_{g-1}} \sigma(\hat{r},E)w(E)dE}{\int_{E_g}^{E_{g-1}} w(E)dE} \qquad (4.6)$$

where w(E) is a weighting function representing the approximate energy variation of the particle flux within the group. Multigroup microscopic

cross sections (units of "barns") are generated for various energy group structures from basic nuclear data using an appropriate weighting function for the generic problem of interest and stored on tape in the form of data libraries which can be accessed by multigroup codes like DOT. The energy group structure used in DOT-IV is essentially determined by the multigroup cross section library that is input.

4.5 Discretized Boltzmann Transport Equation

Eqn. (4.1) can be integrated over each energy group ΔE_g, each mesh cell (i,j), and each direction interval $\hat{\Omega}_n$ to obtain the discretized multigroup version of Eqn. (4.1), in terms of the group angular fluxes. This set of equations expresses conservation of particles in each direction interval $\Delta\Omega_n$ about $\hat{\Omega}_n$, in each spatial mesh cell (i,j) about $\hat{r}$, and in each energy group ΔE_g, and the discrete flux can be viewed as the average flux density in the discrete phase space control volume $\Delta V_{ij}\Delta E_g\Delta\Omega_n$. Thus Eqn.(4.1) becomes

$$[\hat{\Omega}_n.\hat{\nabla}+\Sigma_{tg}(i,j)]\Psi_g(i,j,\hat{\Omega}_n)=\sum_{n=1}^{MM}\Delta\Omega_{n'}\sum_{g'=1}^{IGM}\Sigma_{s,g'\to g}(i,j,\hat{\Omega}_{n'}\to\hat{\Omega}_n)\Psi_{g'}(i,j,\Omega_{n'}) + S_g(i,j,\hat{\Omega}_n) \qquad (4.7)$$

In DOT-IV, the angular fluxes are normalized by a factor of 4π larger than the familiar angular flux per steradian, due to the units of the angular weights in the quadrature :

$$\Psi_g(i,j,\hat{\Omega}_n) \text{ in DOT-IV} = 4\pi(\ \Psi_g(i,j,\hat{\Omega}_n) \text{ in steradians }\ )$$

In the above equation (4.7) the limits of the indices are g=1..IGM; n=1..MM; i=1..maximum 'i' index; and j=1.. maximum 'j' index. Eqn. (4.7) is not the final discretized form since the gradient on the left

hand side of Eqn. (4.7), i.e. $\hat{\Omega}_n.\hat{\nabla}\,\Psi_g(i,j,\hat{\Omega}_n)$ is replaced by its finite difference form which is equivalent to integrating Eqn. (4.7) over mesh cell (i,j). It is also customary to express the scatter source as a spherical harmonic expansion (see section 4.6) The resulting set of coupled algebraic equations is solved by DOT-IV iteratively for the multigroup angular flux $\Psi_g(i,j)$. The multigroup scalar flux $\Phi_g(i,j)$, which has units of particles/cm^2/sec, is calculated as

$$\Phi_g(i,j) = \sum_{n=1}^{MM} W_n\,\Psi_g(i,j,\hat{\Omega}_n) \qquad (4.8)$$

The value of $\Phi_g(i,j)$ corresponds to an average value over the volume of the cell (i,j) and may be thought of as the value at the center of the mesh cell (i,j).

4.6 Treatment of Scatter

Scattering is generally independent of the initial direction $\hat{\Omega}'$, and the scatter cross section can be expressed as a function of the scatter cosine $\mu_0 \equiv \hat{\Omega}'.\hat{\Omega}$ rather than as a function of the individual initial and final directions $\hat{\Omega}'$ and $\hat{\Omega}$ respectively. Scatter is said to be isotropic if the incoming particles are scattered uniformly in all outgoing directions. In reality however, most scattering events tend to be anisotropic in the laboratory system. Anisotropic scattering is treated in DOT-IV by expanding the scatter cross section in terms of Legendre Polynomials of the scatter cosine (μ_0). An 'N'th order expansion may be written as

$$\Sigma_{s,g'\to g}(\mu_0)=\Sigma_{0,g'\to g}P_0(\mu_0)+\Sigma_{1,g'\to g}P_1(\mu_0)+\ldots+\Sigma_{N,g'\to g}P_N(\mu_0) \qquad (4.9)$$

where $P_N(\mu_0)$ represents the Nth order Legendre Polynomial. The order of the cross section expansion is given by the parameter ISCT in the DOT input.

For many neutron and photon transport calculations, a 3rd order (1st 4 terms in the expansion) representation suffices. The coefficients of the Legendre Polynomials in Eqn. (4.9) are called "Cross Section Moments". The first coefficient, $\Sigma_{0,g'\rightarrow g}$, is equal to the familiar group to group scatter cross section matrix. The matrix $\Sigma_{1,g'\rightarrow g}$ is equal to three times the average cosine of scatter for a particle going from group g' to group g, multiplied by the P_0 cross section. The sum of all the cross section moments multiplied by the corresponding Legendre Polynomials will be positive for all values of μ_0 only if an infinite number of terms is taken in the cross section expansion. Since the expansion is carried out only upto a finite number of terms, it is possible that negative scalar fluxes can result in some extreme problems. However DOT-IV has an option available that will approximately correct this behaviour.

Finally, to conclude this chapter Fig. 4.7 shows a block diagram of the DOT-IV input and output. The primary quantity of interest for coupled radiation transport-thermal analysis of the space reactor shield is the multigroup scalar flux $\Phi_g(i,j)$ which is saved in an output dataset called a VARFLM file (written on logical unit number specified by the parameter NTFOG : the second entry of the 61$$ array in DOT-IV input). The scalar flux is needed to compute the nuclear heat source.

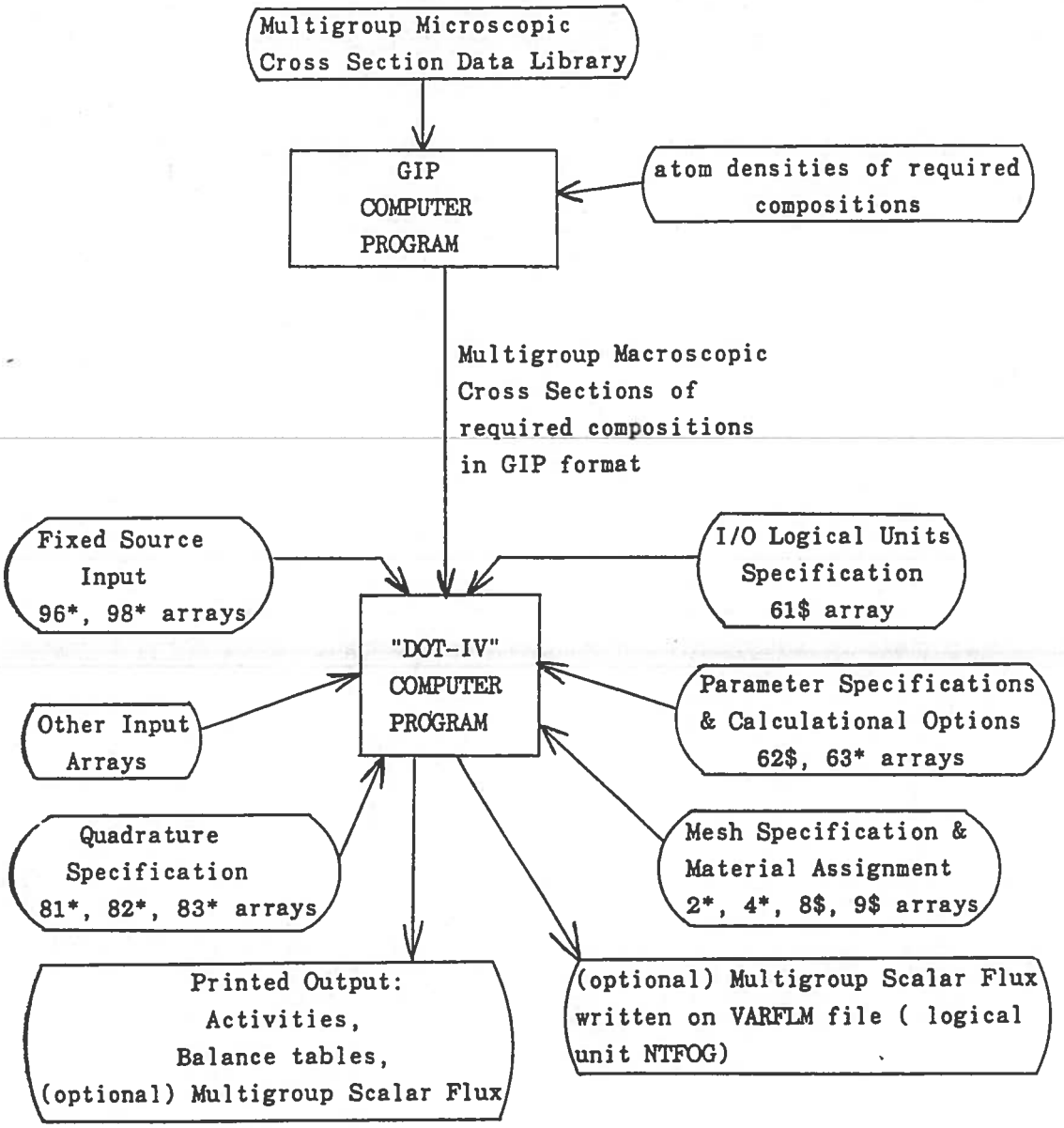

Fig. 4.7 Block diagram of DOT-IV input and output

5. REVIEW OF HEAT CONDUCTION CODE "HEATING6"

The HEATING6 computer program [5.1] solves the steady state or transient heat conduction equation numerically (by the "finite difference" method) for 1-D/2-D/3-D Cartesian/Cylindrical geometries or for 1-D spherical geometries. HEATING6 is the latest version of the "HEATING" (Heat Engineering and Transfer in Nine geometries) series of codes. It was developed at Oak Ridge National Laboratory. HEATING6 exists as a functional module in the "SCALE" system [5.2] (a family of codes for licencing evaluation of nuclear systems); however it can also be run as a stand-alone program.

The code utilizes thermal properties (e.g. conductivity, density, specific heat) which may vary with spatial position, and temperature. Heat generation rates may vary with spatial position, temperature, and time. Boundary conditions which may be applied along the surfaces of the configuration of the problem may be of different types; e.g. specified temperatures or any combination of prescribed heat flux, forced convection, natural convection, and radiation. Convective and radiative heat transfer coefficients may be specified as functions of spatial position, temperature, and time. Boundary temperatures may be specified as functions of spatial position, and time. The code can simulate radiative heat transfer across internal air gaps, and can even simulate the thermal efficiency of certain finned surfaces. Selected materials may undergo phase change during transient calculations involving one of the explicit methods. The code also comes with an extensive "Materials Properties Library" containing temperature-dependent conductivities, heat

capacities, etc., which it can optionally access.

The code is very generic, allowing a wide variety of problems to be solved. It is coded in standard FORTRAN-IV, with several of the original subroutines having been modified and new routines added for this study. The theory discussed in this chapter is confined to 2-D geometric systems because the modified code "DOS-HEATING6" is limited to 2-D analysis. However the original HEATING6 code can treat 3-D geometries.

5.1 The Heat Conduction Equation

The general form of the heat conduction equation is obtained by applying heat balance (heat buildup = heat generation - heat losses) for an elemental control volume 'dV' surrounding a spatial point $\hat{r}$, and may be written as

$$C \frac{\partial T}{\partial t} = q + \hat{\nabla}.(k \hat{\nabla} T) \qquad (5.1)$$

where "t" is the time ; $T=T(\hat{r},t)$ is the temperature ; $k=k(\hat{r},T(\hat{r}))$ is the thermal conductivity ; $q=q(\hat{r},t)$ is the volumetric heat generation rate ; $C(\hat{r},T(\hat{r}))$ is the heat capacitance which is equal to the product of density $\rho(\hat{r},T(\hat{r}))$ and specific heat $c(\hat{r},T(\hat{r}))$. For steady state conditions to exist, the quantities in Eqn. (5.1) should be independent of time i.e.

$$\hat{\nabla}.(k \hat{\nabla} T) = - q \qquad (5.2)$$

where $T=T(\hat{r})$ and $q=q(\hat{r})$.

HEATING6 uses finite differences to numerically solve Eqn. (5.1) (transient analysis) or Eqn. (5.2) (steady state analysis). The spatial variable $\hat{r}$ is discretized by representing the spatial domain by a spatial mesh. For transient analysis, the time variable 't' is broken up

into a series of time steps.

5.2 Spatial Discretization

The entire spatial domain of the problem is divided into regions. A region cannot contain more than one material. The lines bounding a region must be parallel to the coordinate axes. For example in XY geometry, a region cannot be bounded by more than four lines (two lines parallel to the X axis and two lines parallel to the Y axis). A region boundary cannot be subjected to more than one type of boundary condition. Grid lines are of two types : (a) Gross grid lines : these are used for specifying unequally spaced intervals within a region. They must appear along all region boundaries ; (b) Fine grid lines : these are used for specifying equally spaced intervals between any two adjacent gross grid lines. The point where any two grid lines meet is called a "node". If the point where two grid lines meet happens to lie in a gap region (a region which does not contain any material i.e. a void) then HEATING6 does not consider that point to be a node. Also no nodes are placed at the r=0 grid line in the case of cylindrical geometries.

Temperatures are calculated at the nodes by applying heat balance to the "control volume" surrounding each node. Fig. 5.1 illustrates spatial meshes in XY, Rθ, and RZ geometric systems. In these figures, solid lines represent grid lines (gross/fine grid lines), and the broken lines which lie midway between grid lines represent control volume boundaries. Notice that the region in the control volume of a node is made up of component "subregions". The number of subregions associated with a node varies from one to four depending upon the location of the node. A subregion can contain only one material, however, two different

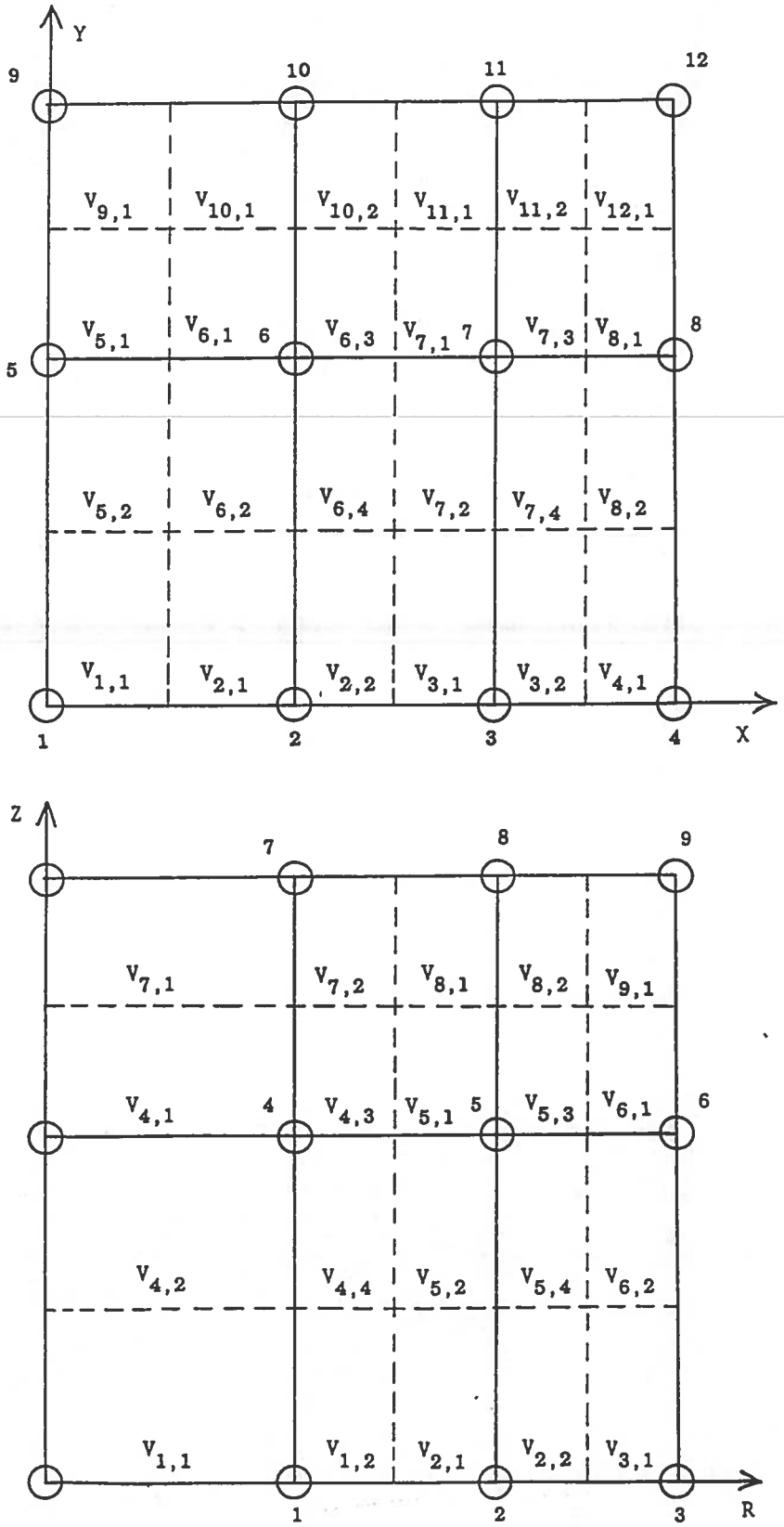

Fig. 5.1 Examples of HEATING6 spatial meshes

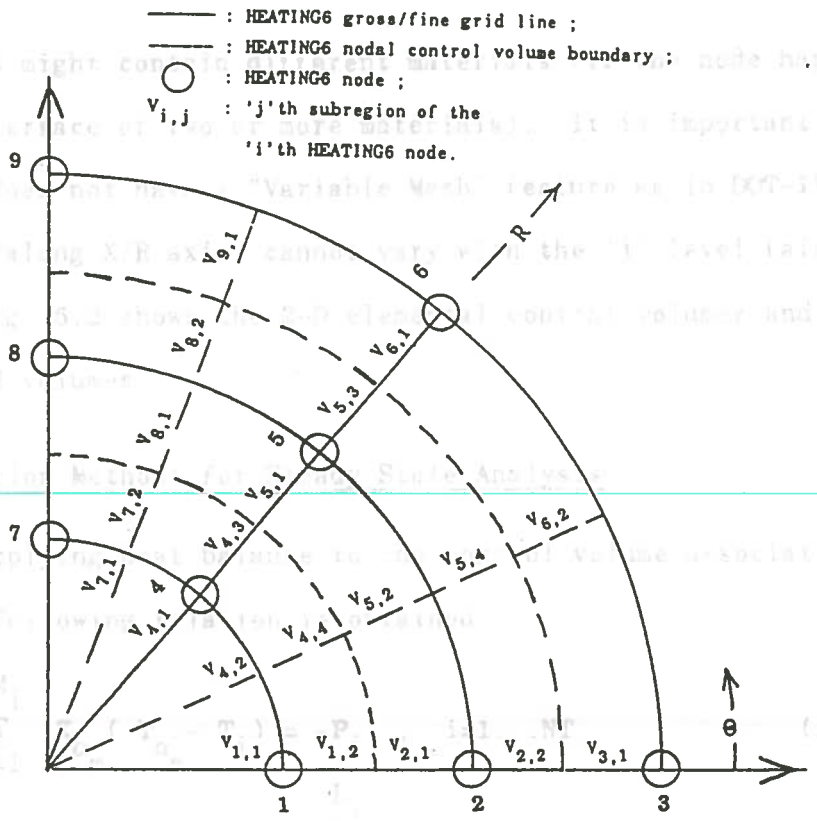

Fig. 5.1 (continued) : Examples of HEATING6 spatial meshes

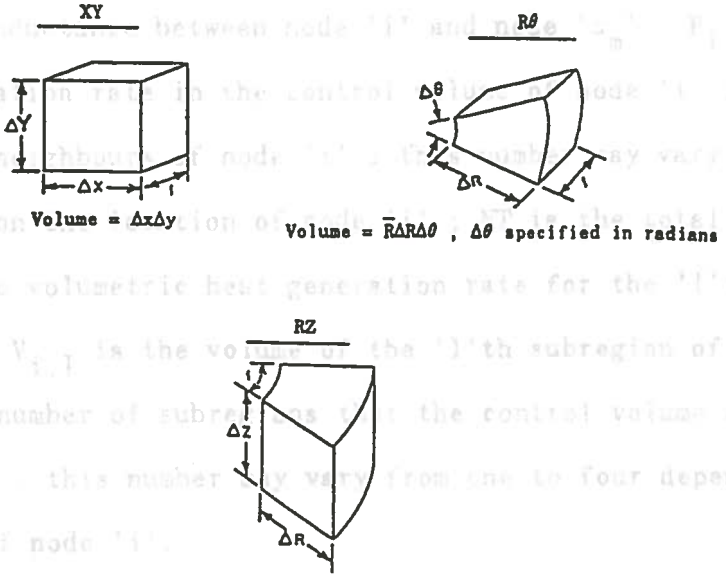

Fig. 5.2 HEATING6 2-D elemental control volumes

involving the NT unknown nodal temperatures. HEATING6 solves this set of equations by any one of the following two techniques :

SOR Method

The set of equations (5.3) is solved using the point succesive over-relaxation (SOR) iterative scheme. Briefly described, the method is as follows : from Eqn. (5.3), an estimate for T_i may be written as

$$\hat{T}_i^{n+1} = \frac{P_i + \sum_{m=1}^{M_i} {}_iK_{\alpha_m} T_{\alpha_m}^n}{\sum_{m=1}^{M_i} {}_iK_{\alpha_m}} \qquad (5.5)$$

where the superscript indicates the iteration number. To accelerate convergence by using the most recent values of T_{α_m} in Eqn. (5.5), the nodes are numbered in such a way that the 'i' index (along X/R axis) varies faster than the 'j' index (along Y/Θ/Z axis). If thermal conductivities are temperature dependent, then thermal conductances in Eqn. (5.5) must be evaluated at the latest available temperatures. The 'n+1'st iterate is then calculated as

$$T_i^{n+1} = T_i^n + \beta(\hat{T}_i^{n+1} - T_i^n) = (1-\beta)T_i^n + \beta\hat{T}_i^{n+1} \qquad (5.6)$$

with β ($0<\beta<2$) being the steady state relaxation factor. The procedure outlined so far is only a "bare bones" description. Actually, in order to increase the rate of convergence, HEATING6 uses a modified "Aitken δ^2 Extrapolation Procedure" to calculate T_i^{n+1}. Iterations are carried out

until $$\left| \frac{T_i^n - T_i^{n+1}}{T_i^{n+1}} \right|_{\text{max over all nodes}} < \epsilon$$

where 'ϵ' is the steady state convergence criterion.

Direct Method

The set of equations (5.3) may be rewritten in matrix form as

$$[A][T]=[B] \qquad (5.7)$$

where [A] is the coefficient matrix (banded), [T] is the vector of unknown nodal temperatures, and [B] is the vector of forcing functions consisting of terms related to heat generation rates and boundary conditions. HEATING6 solves the set of simultaneous linear equations (5.7) by calling appropriate subroutines from the LINPACK library (a library of linear algebra routines). For temperature-dependent properties [A] and [B] will be temperature dependent. In that case Eqn. set (5.7) may be reduced to a system of linear equations by evaluating [A] and [B] at currently available estimates of the nodal temperatures. This leads to an iterative process which is briefly described as follows : the system of equations $[A^n][T^{n+1}]=[B^n]$ is solved to determine $[T^{n+1}]$, where the superscript indicates the iteration number. Then the heat residual vector is determined as $[e^{n+1}]=[A^{n+1}][T^{n+1}]-[B^{n+1}]$. The 'i'th component of [e] gives the heat residual at the 'i'th node. The relative heat residual at each node is then determined by dividing the heat residual at the node by the average heat flow at that node (the average heat flow is the average of the absolute values of all the heat flows in and out of the node including the heat generation). The error at a node is taken to be the lesser of the two residuals viz. absolute residual and relative residual. For convergence, the maximum error determined over all the nodes must be less than ϵ.

For "small" and "moderate" sized problems, the Direct method is more accurate and efficient than the SOR method but it has the disadvantage of requiring significant core memory. For problems involving a large number of nodes, it is better to use the SOR method.

In order to gain confidence in the solution to a problem, one must experiment with the mesh spacing, and convergence criterion, ϵ. The HEATING6 default value of ϵ is 1.0D-5. However in the case of highly nonlinear problems such as encountered in the present study it was necessary to go as far as ϵ = 1.0D-12 (this is the minimum value of ϵ for an IBM 370 computer) in order to obtain a very accurate solution.

5.4 Solution Methods for Transient Analysis

On applying heat balance to the control volume associated with node 'i' the following equation is obtained :

$$C_i \frac{dT_i}{dt} = P_i + \sum_{m=1}^{M_i} K_{\alpha_m} (T_{\alpha_m} - T_i) \quad , \; i=1..NT \qquad (5.8)$$

where C_i is the heat capacitance associated with node 'i' and the rest of the symbols are the same as in Eqn. (5.3). On integrating Eqn. (5.8) with respect to time from $t=t_n$ to $t=t_{n+1}$ and approximating the integrands inside the definite integrals as weighted averages of their values at t_n and t_{n+1} (this concept is called "Theta Differencing" by some numerical analysts), the following relation is obtained:

$$C_i^{n+\theta} \frac{(T_i^{n+1}-T_i^n)}{\Delta t} = P_i^{n+\theta} + \theta\left[\sum_{m=1}^{M_i} {}_iK_{\alpha_m}^{n+\theta}(T_{\alpha_m}^{n+1}-T_i^{n+1})\right] + (1-\theta)\left[\sum_{m=1}^{M_i} {}_iK_{\alpha_m}^{n+\theta}(T_{\alpha_m}^{n}-T_i^{n})\right]$$

$$\text{for } i=1..NT \qquad (5.9)$$

where θ is the weighting parameter and the superscript $n+\theta$ implies that

the parameter is evaluated at time $t_{n+\theta}$. Solution methods for transient problems fall into two categories viz. explicit methods and implicit methods.

Explicit Methods

The Classical Explicit Procedure (CEP) corresponds to setting $\theta=0$ in Eqn. (5.9). On doing so, an explicit expression is obtained for T_i^{n+1} in terms of temperatures at time t_n.

$$T_i^{n+1}=T_i^n+\frac{\Delta t}{C_i}\left(P_i^n+\sum_{m=1}^{M_i} {}_iK_{\alpha_m}\left(T_{\alpha_m}^n - T_i^n\right)\right) \quad ,i=1..NT \qquad (5.10)$$

However, for the method to be stable, the following criterion should be satisfied:

$$\Delta t \leq \left[\frac{C_i}{\sum_{m=1}^{M_i} {}_iK_{\alpha_m}}\right]_{\text{minimum over all nodes}} \qquad (5.11)$$

Levy's Explicit Procedure (LEP) is a modification to the CEP and is similar to the Du Fort-Frankel Scheme. The expression for T_i^{n+1} is similar to Eqn. (5.10) except that the right hand side additionally involves T_i^{n-1}. The method is stable for any Δt.

Implicit Methods

These methods correspond to $0.5\leq\theta\leq1.0$. in Eqn. (5.9). The Classical Implicit Procedure (CIP) and the Crank-Nicolson Procedure (CNP) correspond to setting $\theta=1.0$ and $\theta=0.5$ in Eqn. (5.9) respectively. These methods are stable for any Δt. For these methods it is not possible to obtain an explicit expression for T_i^{n+1} in terms of temperatures at time t_n or previous times. Instead a set of NT linear equations in the NT

unknown nodal temperatures T_i^{n+1}, i=1..NT is obtained. Thus at each time step it is necessary to solve a system of equations. HEATING6 does this using the point successive over-relaxation method (SOR). Iterations are carried out until max{normalized heat residual at node 'i', i=1..NT} is less than the convergence criterion ϵ_1 (default value=1.0D-5). For problems involving temperature dependent properties, two iterative loops are involved. To begin with, thermal parameters are evaluated at the initial temperatures. Then the system of equations (5.10) is solved using SOR to obtain the temperature distribution at the new time level. Thermal parameters are then reevaluated and the entire procedure is repeated. The temperature disribution at time t_n is considered to have converged when

$$\frac{1}{NT}\sum_{i=1}^{NT}\left|\frac{T_i^{n,m} - T_i^{n,m-1}}{T_i^{n,m}}\right| \leq \epsilon_2$$

where 'm' is the outer loop iteration index and ϵ_2 is the convergence criterion for the outer loop (default value=1.0D-5).

The time step size for implicit schemes may be varied in a variety of ways. It may be specified to be constant for the entire calculation or during prescribed time intervals. It may also be varied by scaling it by a prescribed value every time step or it may be varied implicitly by specifying the maximum temperature change or the maximum % of relative temperature change allowed at a node over a time step.

The CNP method is the recommended procedure for solving transient problems. In order to gain confiμaxce in the solution to a problem it is advisable to experiment with the mesh spacing, time step, and convergence criteria.

Finally to conclude this chapter, Fig. 5.3 shows the input and output to HEATING6 in the form of a block diagram.

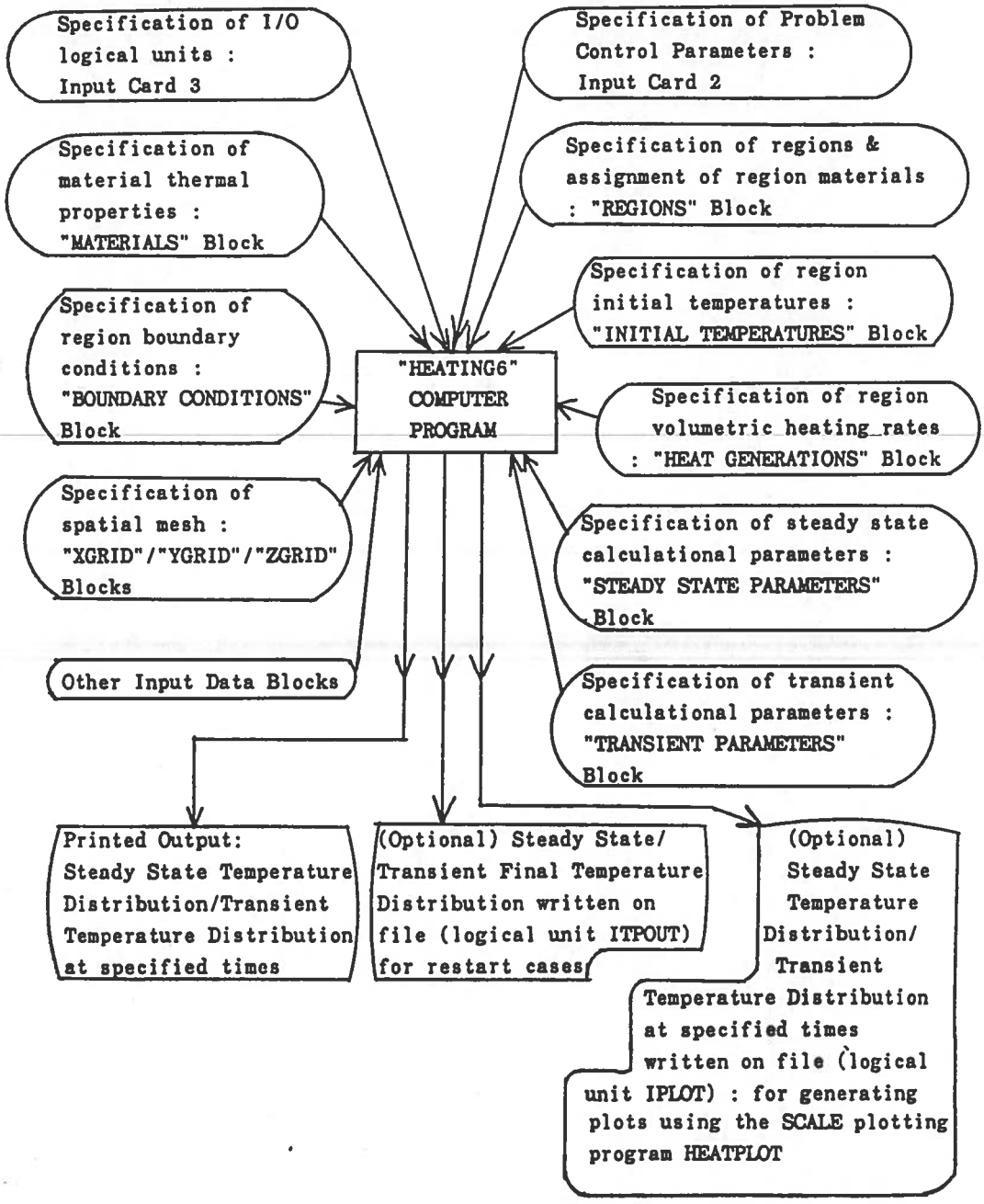

Fig. 5.3 Block diagram of HEATING6 input and output

6. MODIFICATIONS TO "HEATING6" FOR COMPUTING THE NUCLEAR HEAT SOURCE

6.1 Kerma Factors

Nuclear heating rates can be calculated from particle transport results for any system if "kerma factors" for the materials of the system are known [6.1]. Kerma is an acronym for kinetic energy released in materials. Kerma factors are sometimes also referred to as "fluence-to-kerma factors", a term introduced by the International Commission on Radiological Units and Measurements. The volumetric heat generation rate due to nuclear heating at some spatial point $\hat{r}$ in the system is given by

$$q_N(\hat{r}) = \int_E \Sigma^k(\hat{r},E)\Phi(\hat{r},E)dE \qquad (6.1)$$

where $\Sigma^k(\hat{r},E)$ is the macroscopic kerma factor of the material at $\hat{r}$ for particles of energy E ; $\Phi(\hat{r},E)$ is the scalar flux at $\hat{r}$ and energy E. The macroscopic kerma factor of a mixture of nuclides is given by

$$\Sigma^k(E) = \sum_j N_j \sigma_j^k(E) \qquad (6.2)$$

where $\sigma_j^k(E) = \sum_i \sigma_{ij}^k(E)$ (6.3) and $\sigma_{ij}^k(E) \equiv \sigma_{ij}(E)E_{ij}(E)$ (6.4)

where N_j is the atom density of the nuclide 'j' ; $\sigma_j^k(E)$ is the microscopic kerma factor of nuclide 'j' for particles of energy E ; $\sigma_{ij}^k(E)$ is the microscopic kerma factor of the nuclide 'j' for reaction type 'i' for particles of energy E ; σ_{ij} is the microscopic cross section of nuclide 'j' for reaction type 'i' for particles of energy E ; and E_{ij} is the energy deposited by a particle with energy E per reaction for reaction type 'i' in nuclide 'j'. Multigroup kerma factors are defined

in a manner similar to multigroup cross sections (Eqn. (4.6)). Like multigroup microscopic cross sections , multigroup microscopic kerma factors for various energy group structures are generated from basic nuclear data using an appropriate weighting function for the generic problem of interest and are stored on tape in the form of data libraries for multigroup codes to access.

The multigroup expression for the volumetric nuclear heating rate at some spatial point $\hat{r}$ is given by

$$q_N(\hat{r}) = \sum_{g=1}^{IGM} \Sigma_g^k(\hat{r})\Phi_g(\hat{r}) \qquad (6.5)$$

where $q_N(\hat{r})$ = volumetric nuclear heating rate ($J/cm^3/sec$) at spatial point $\hat{r}$.

$\Sigma_g^k(\hat{r})$ = group 'g' macroscopic kerma factor (J/cm) for the material at spatial point $\hat{r}$.

$\Phi_g(\hat{r})$ = group 'g' scalar flux ($particles/cm^2/sec$) at spatial point $\hat{r}$.

IGM = total number of energy groups.

6.2 Coupling "DOT-IV" and "HEATING6"

If the atom densities and microscopic cross section of the nuclides do not vary significantly with temperature, then the steady state Boltzmann transport equation can be solved independently of the heat conduction equation. Thus DOT-IV may be run in the usual manner to obtain the multigroup scalar flux $\Phi_g(\hat{r})$. The HEATING6 code may then be used to solve the heat conduction equation (Eqn. (5.1)) with the volumetric nuclear heating rate $q_N(\hat{r})$ being calculated using Eqn. (6.5).

In the present study, the nuclear heating source is allowed to be combined with any other heating source that can be treated by the original HEATING6 code. In other words the volumetric heat source term $q=q(\hat{r},t)$ in the heat conduction equation (Eqn. (5.1)) is separated into two components ; viz. $q_E=q_E(\hat{r},t)$ which is the external (non-nuclear) contribution as originally treated by the standard HEATING6 code (specified by the user in the HEAT GENERATIONS block in the code input or supplied as a subroutine), and $q_N(\hat{r})$ which is the contribution due to nuclear heating (assumed to be time-independent). Therefore the parameter P_i in Eqn. (5.3) can be expressed as

$$P_i = (P_i)_E + (P_i)_N \qquad (6.6)$$

and $P_i^{n+\theta}$ in Eqn. (5.9) can be written as

$$P_i^{n+\theta} = (P_i^{n+\theta})_E + (P_i)_N \qquad (6.7)$$

where

$$(P_i)_E = \sum_{l=1}^{L_i} (q_{i,l})_E \, V_{i,l} \qquad (6.8)$$

$$(P_i^{n+\theta})_E = \sum_{l=1}^{L_i} (q_{i,l}^{n+\theta})_E \, V_{i,l} \qquad (6.9)$$

$$(P_i)_N = \sum_{l=1}^{L_i} (q_{i,l})_N \, V_{i,l} \qquad (6.10)$$

The volumetric nuclear heating rate for the 'l'th subregion of node 'i' may be written (from Eqn. (6.5)) as

$$(q_{i,l})_N = \sum_{g=1}^{IGM} \Sigma_{g,i,l}^k \; \bar{\Phi}_{g,i,l} \qquad (6.11)$$

where $\Sigma_{g,i,l}^k$ is the group 'g' macroscopic kerma factor for the material

in the 'l'th subregion of node 'i' and $\bar{\Phi}_{g,i,l}$ is the average group 'g' scalar flux for the 'l'th subregion of node 'i' which is taken to be the value of Φ_g at the center of the node subregion. The scalar fluxes from the DOT-IV transport run which are saved in the VARFLM file will not correspond to points which are centers of the subregions associated with HEATING6 nodes because of differences in the way the DOT-IV and HEATING6 meshes are defined :

(a) HEATING6 does not treat variable meshes as DOT-IV does. HEATING6 can treat only fixed meshes.

(b) even if the same fixed mesh were to be used for both DOT-IV and HEATING6, the DOT-IV nodes where the scalar fluxes are computed will not coincide with the HEATING6 nodal subregion centers (the DOT-IV nodes will lie on the corners of the HEATING6 nodal control volume boundaries). Fig. 6.1 illustrates this inconsistency for the simple HEATING6 fixed meshes pertaining to Fig. 5.1 in chapter 5.

Therefore invariably, the scalar flux at the center of a subregion associated with a HEATING6 node always has to be obtained from the computed DOT-IV fluxes in the VARFLM file by interpolation. Substituting the expression for $(q_{i,l})_N$ from Eqn. (6.11) into Eqn (6.10) results in the following expression for the time independent nuclear heat source :

$$(P_i)_N = \sum_{l=1}^{L_i} \sum_{g=1}^{IGM} \Sigma^k_{g,i,l} \, \bar{\Phi}_{g,i,l} \, V_{i,l} \qquad (6.12)$$

Changing the order of summation, Eqn. (6.12) may be rewritten as

$$(P_i)_N = \sum_{g=1}^{IGM} \sum_{l=1}^{L_i} \Sigma^k_{g,i,l} \, \bar{\Phi}_{g,i,l} \, V_{i,l} \qquad (6.13)$$

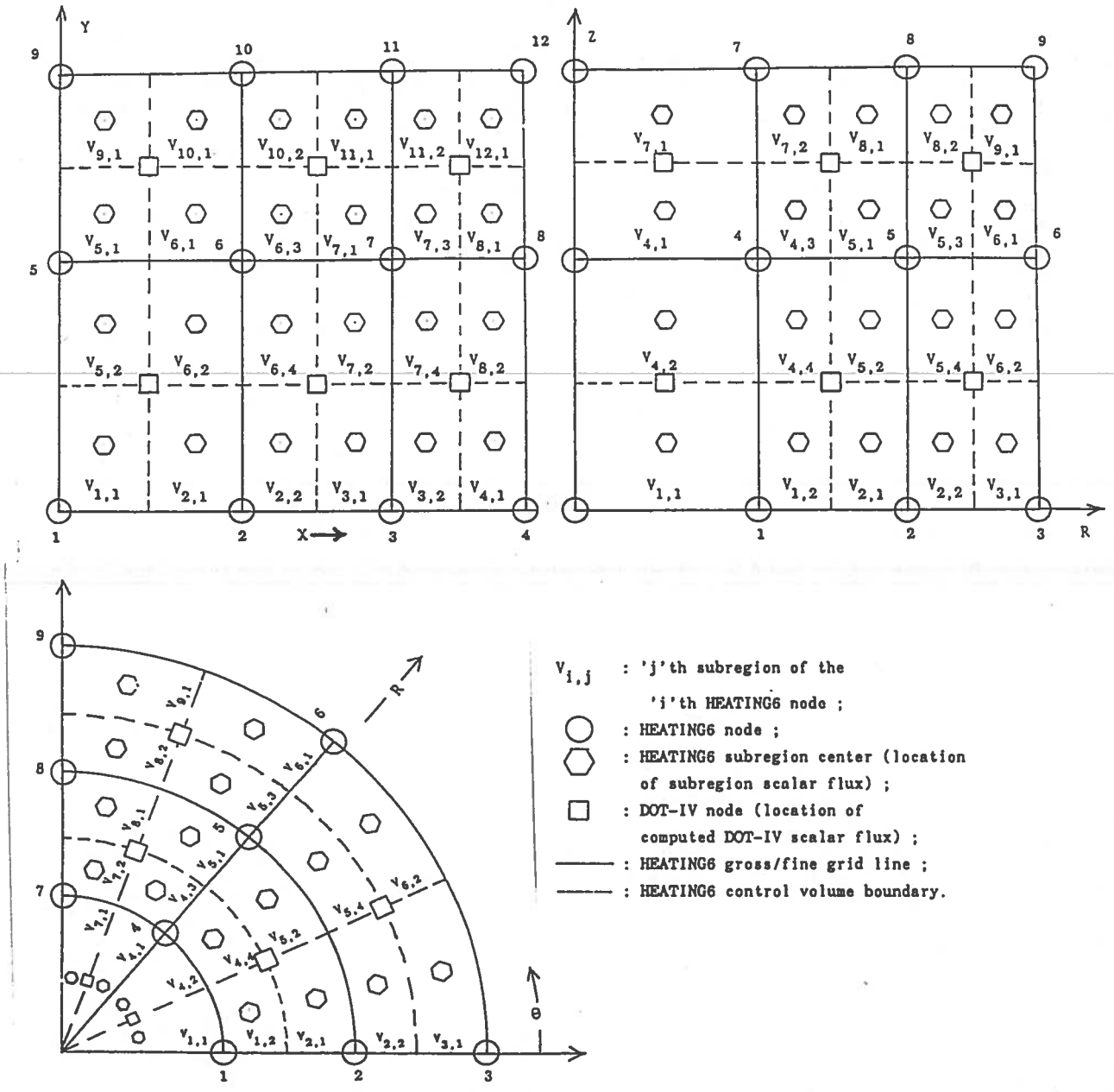

Fig. 6.1 Diagram showing the location of subregion scalar fluxes, i.e., points where the scalar flux must be determined (by interpolation from DOT-IV scalar fluxes) in order to calculate the nuclear heating source

In order to perform only a nuclear heating calculation, the external heat source is set to zero in the heat conduction equation. It is therefore clear that the following features will have to be incorporated into the existing HEATING6 code in order to couple DOT-IV and HEATING6 for nuclear heating calculations :

(1) Capability to read the multigroup scalar fluxes saved in the DOT-IV VARFLM file,

(2) Provision for multigroup macroscopic kerma factors of all materials involved to be input to HEATING6,

(3) Capability to interpolate scalar fluxes from the DOT-IV to the HEATING6 mesh,

(4) Capability to calculate the nuclear heat source $(P_i)_N$ for i=1..NT according to Eqn. (6.13),

(5) Provision for the nuclear heat source to be combined with the external heat source. In other words : (a) (P_i) in Eqn. (5.3) must be set to $(P_i)_E + (P_i)_N$,i=1..NT before steady state calculations commence ; and (b) $(P_i^{n+\theta})$ in Eqn. (5.9) must be set to $(P_i^{n+\theta})_E + (P_i)_N$,i=1..NT before transient calculations commence.

6.3 DOS-HEATING6

The HEATING6 code has been modified to incorporate the five features discussed in Section 6.2, allowing coupled radiation transport-thermal analysis studies to be conducted for any system that can be modeled with DOT-IV and HEATING6.

The modified code is called "DOS-HEATING6" [6.2], and has been incorporated as a module in the DOS system [4.2]. DOS-HEATING6 may be

used to perform nuclear heating calculations by appropriately setting the value of the newly introduced DOS-HEATING6 integer option control parameter "IDOT". A positive value of IDOT causes the five steps necessary for a nuclear heating calculation (mentioned in section 6.2) to be carried out. Setting IDOT to zero causes these five steps to be skipped : this corresponds to a normal HEATING6 run.

DOS-HEATING6 New Input Features

The format of the DOS-HEATING6 input data cards describing the problem to be solved is the same as that for HEATING6 except for the following two changes : (1) the value of the parameter IDOT must be supplied on the first input data card along with other variables belonging to the NAMELIST /OPTION/ group. For nuclear heating calculations, the logical unit number assigned to the VARFLM file containing the DOT-IV fluxes must be equal to IDOT ; (2) for nuclear heating calculations, the card/cards describing a particular material in the MATERIALS block should be followed by an additional "card K" containing the IGM macroscopic group-wise kerma factors of the corresponding material starting with group one. Card K must be placed after card M (if the material corresponding to card M does not undergo change of phase) or after card PC (if the material correponding to card M can undergo change of phase).

DOS-HEATING6 Program Structure

HEATING6, which is coded mostly in standard FORTRAN-IV, consists of about 19000 source statements containing about 123 subroutines. The main routine (MAIN-HEATING6) and eight subroutines of the HEATING6 source code

(HEATN6, INPUT, READER, MATERL, CALQLT, TRANO, DIRECT, DIFFER) have been modified for DOS-HEATING6. DOS-HEATING6 also contains three new subroutines (DOTR, DOTQ, DWOT) and one new function subprogram (TERP). A listing of the new routines DOTR, DOTQ, TERP, and DWOT is given in Appendix A. Calculation of the nuclear heat source is accomplished by calling the new subroutine DOTR. Except for the conditional call to DOTR whenever nuclear heating calculations need to be performed, the interconnection and calling sequence of all the other HEATING6 routines remains unaltered.

A new labled common block /DOT/ containing the parameter IDOT and some DOT-IV calculational parameters (IGM, NEUT, JM, LM, IMA, MMA, ISM, IMSISM, ISBT) has been defined and inserted into all subroutines that either need to use or pass on the values of these parameters. Provision has also been made to reserve storage (in the main container arrays ICORE and CORE) for the variably dimensioned arrays (ISET, IMBIS, RD, ZD, DFLX, XKERM, VMAT, QNEUT, QGAM, Q, VGEN, VOL) defined in subroutine DOTR.

The MAIN-HEATING6 routine has been modified to include IDOT in the list of variables in NAMELIST /OPTION/. The main routine MAIN-HEATING6 reads the NAMELIST /OPTION/ data from the first user supplied input data card, checks logical I/O units for consistency and allocates buffer space in core for each logical I/O unit. MAIN-HEATING6 then calls the assembly subroutine ALOCAT to determine the amount of computer core available for the variably dimensioned arrays (this is calculated as the amount of core requested by the user less the size of DOS-HEATING6 less the buffer space for the I/O units). ALOCAT then calls subroutine H6. H6 releases the buffer space required for the I/O units and calls subroutine ECHO. ECHO

reads and tabulates user supplied input data cards and also writes them to a scratch file (logical unit number IN) which serves as the standard input file for any future references to input during the run. H6 then calls subroutine HEATN6.

HEATN6 initializes a number of parameters for the computations, and has been modified to read the DOT-IV calculational parameters into the labled common block /DOT/, from the third record of the VARFLM file, if IDOT > 0. It calculates the pointers in the container arrays CORE, ICORE, and LCORE indicating the starting indices of all the variably dimensioned arrays ; HEATN6 has been modified to calculate pointers to the newly defined variably dimensioned arrays in DOTR if IDOT > 0. It determines whether or not enough core is available for the variably dimensioned arrays, and calls entry points to a number of subroutines to either initialize variables or pass the starting addresses of the variably dimensioned arrays to those subroutines. It then calls three subroutines INPUT, POINTS, and CALQLT in succession. HEATN6 has been modified to call the new subroutine DOTR after the call to POINTS but before calling CALQLT if IDOT > 0.

Subroutine DOTR reads information pertaining to the DOT-IV mesh from the fourth and fifth records of the VARFLM file and then calls subroutine DOTQ. DOTQ reads the multigroup scalar fluxes from the remaining records of the VARFLM file and computes the nuclear heat source according to Eqn. (6.13). The function subprogram TERP is called from DOTQ to obtain the values of the fluxes at the DOS-HEATING6 nodal subregion centers by interpolation (linear) from the DOT-IV fluxes. Subroutine DWOT prints out any 1-D/2-D/3-D double precision array in a convenient tabular format

and is called by DOTQ and MATERL for printing out the map of nodal volumetric nuclear heat generation rates and the macroscopic multigroup kerma factors of a material respectively.

Subroutine INPUT reads most of the input data card images and prints them in tabular form, and also initializes many variables. Subroutine MATERL (called by INPUT indirectly through subroutine READER) which reads the card/cards for a particular material from the MATERIALS data block has been modified to additionally read the card K containing the macroscopic group-wise kerma factors of the corresponding material (by calling subroutines NEXTCD and DREAD) and print them out (by calling subroutine DWOT) if IDOT > 0. A correction has also been made in subroutine DIFFER, which is called by INPUT indirectly through subroutine WRITER, correcting the expression that calculates the nodal volumes. The correction does not affect the computed temperatures.

Subroutine POINTS generates nodal connections and calls subroutine THRMPR which determines the initial temperatures and thermal parameters (thermal conductance, thermal capacitance etc.) for all nodes. CALQLT then calculates the temperature distribution according to the method specified by the user and prints the results. CALQLT contains the steady state (SOR) and the transient explicit algorithms. CALQLT calls subroutine DIRECT (indirectly through subroutine INFACE) if steady state calculations need to be performed using the direct solution method. If the implicit transient method is to be used, CALQLT first calls subroutine TRANO to read data for implicit transient calculations and then calls entry TRANIM (contained in TRANO). Entry TRANIM computes the transient temperature distribution using a linear combination of the CIP

and CNP techniques. CALQLT, DIRECT, and TRANO may call entry THRM1 (in subroutine THRMPR) to update temperature dependent thermal parameters for all the nodes. Subroutines CALQLT, DIRECT, and TRANO have been modified so that if IDOT > 0, then the nuclear heat source is added to the external heat source for all nodes before solution of the finite difference heat balance equations commences. Fig. 6.2 shows the flowchart indicating the calling sequence of the major routines involved in DOS-HEATING6.

DOS-HEATING6 Output Features

Whenever a nuclear heating calculation is performed, DOS-HEATING6 outputs the following extra information in addition to the information that would normally be printed out by HEATING6 : (1) a listing of the macroscopic multigroup kerma factors of each material; (2) A listing of the DOT-IV calculational parameters and the DOT-IV mesh; (3) a listing of the HEATING6 mesh; (4) a map of the average nuclear volumetric heat generation rate associated with each node; and (4) a listing of the volume, mass, neutron heat generation rate, gamma heat generation rate, and total heat generation rate for each material as well as for the entire system.

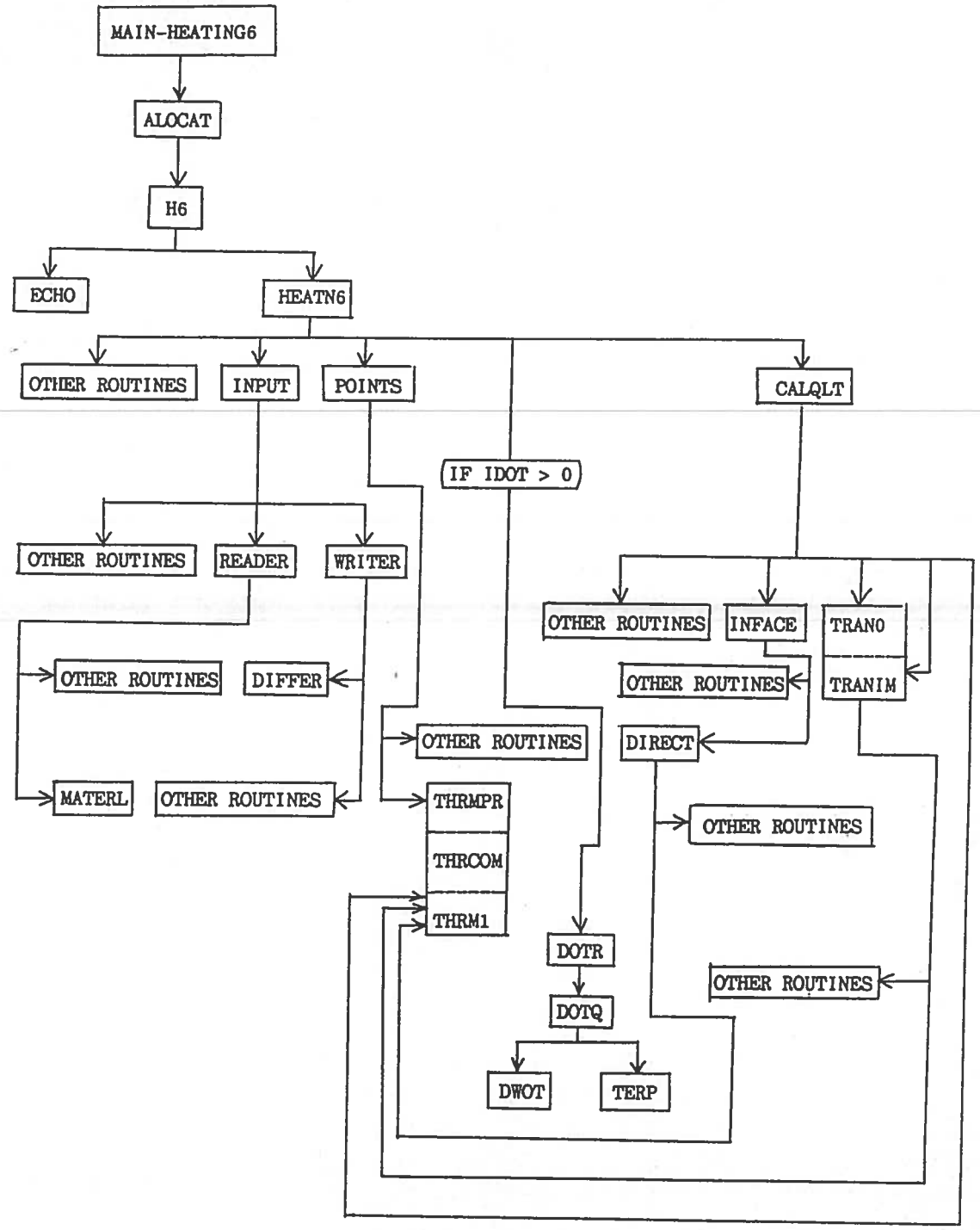

Fig. 6.2 Flowchart indicating the calling sequence of major DOS-HEATING6 routines

7. COUPLED RADIATION TRANSPORT - HEAT CONDUCTION CALCULATIONS FOR THE SHIELD OF AN SP-100 TYPE SPACE NUCLEAR REACTOR

Coupled radiation transport-heat conduction calculations have been performed for the radiation shield of an early version of a 100 kWe (2MWth) SP-100 space nuclear reactor developed by General Electric (GE) in 1984. DOT-IV has been used for transport calculations and subsequent heat conduction calculations have been performed using the new DOS-HEATING6 code.

7.1 Description of the Reactor-Shield System

Although a simple schematic diagram of the space reactor analyzed in the present study is not available, it is quite similar to the one shown in Fig. 7.1 which is a 300 kWe (6.8 MWth) version recently developed by General Electric [7.1].

Fig. 7.2 shows the 2-D axisymmetric RZ model of the 100 kWe (2 MWth) GE space nuclear reactor system considered in the present study (Henceforth, this model will be referred to as the "baseline model"). Traversing along the r = 0 centerline in the direction of increasing z values, the reactor subsystem starts at z = 0 cm and ends at z = 62.8 cm, the maximum radial dimension being 33.5 cm. The axial length of the core is 25.8 cm (z = 18.9 cm to z = 44.7 cm), the inner and outer radii being 5.6 cm and 17.7 cm respectively. The reactor is a liqiuid lithium cooled fast reactor using UO_2 (highly enriched in U^{235}) as fuel and Nb-1Zr as structural material (cladding, piping etc.). The reactor is surrounded by radial and axial reflectors composed of BeO to reduce neutron leakage. Reactor reactivity is controlled by varying the amount of neutron

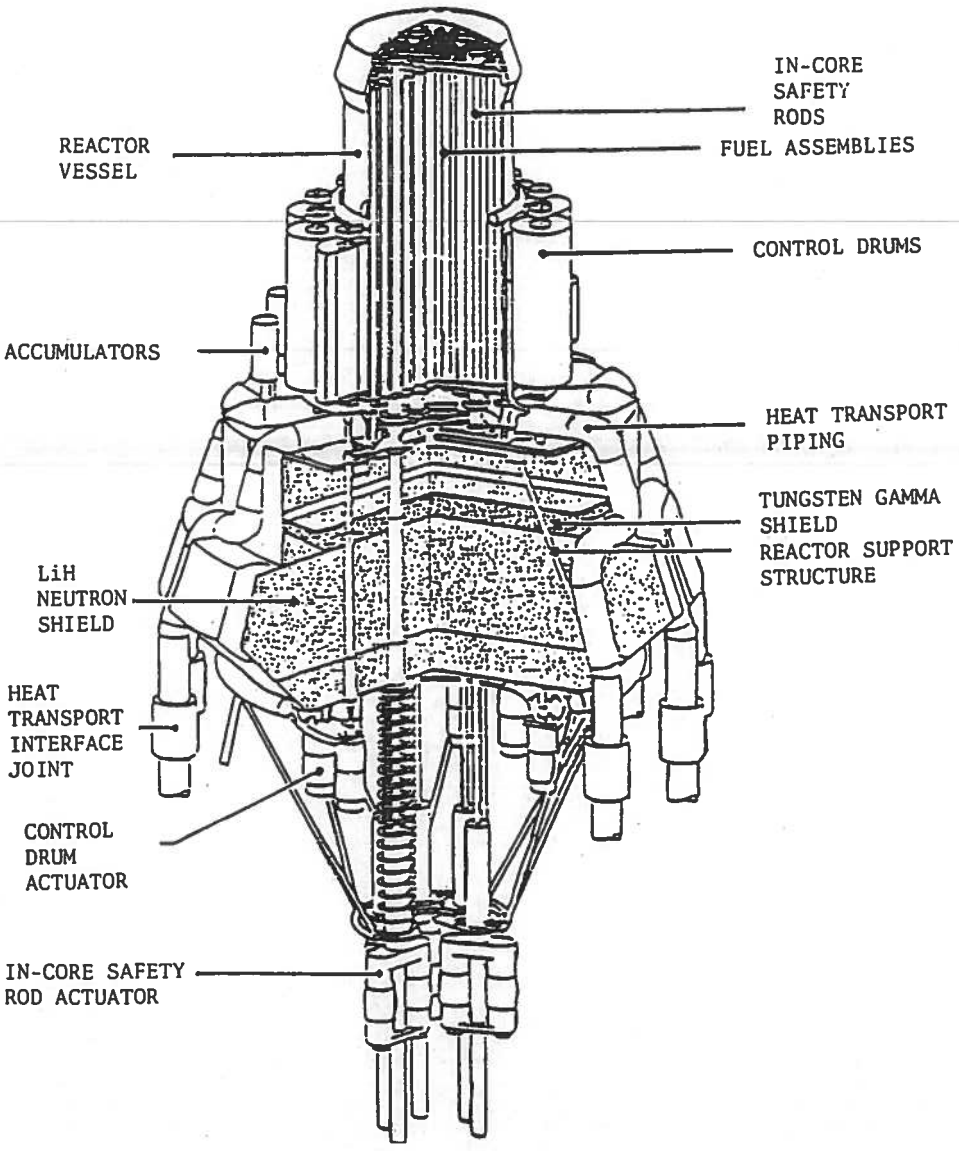

Fig. 7.1 A 300 kWe (6.8 MWth) SP-100 space nuclear reactor recently proposed by General Electric (Ref. [7.1])

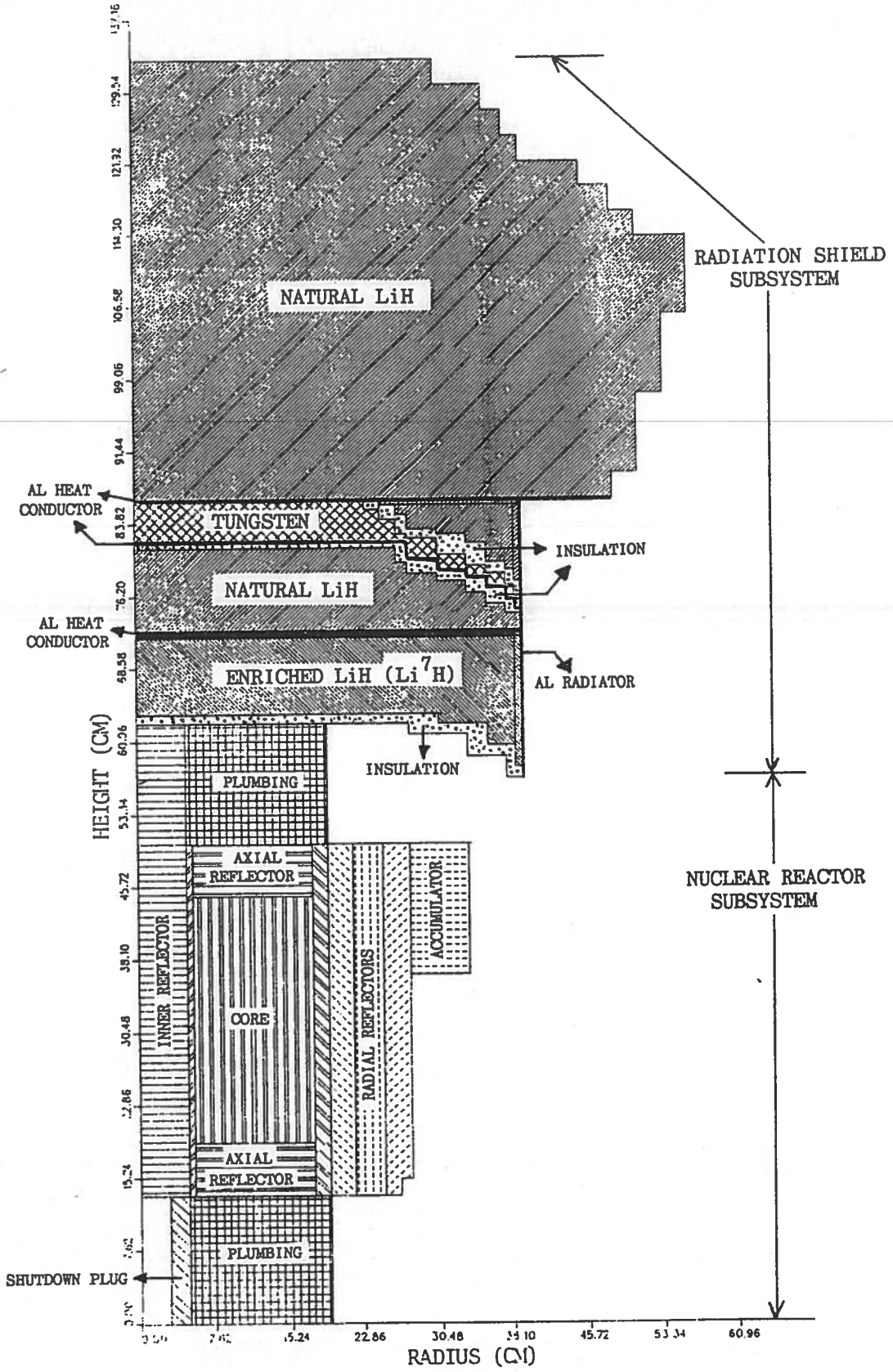

Fig. 7.2 2-D axisymmetric RZ model of the 100 kWe (2 MWth) General Electric SP-100 space nuclear reactor (baseline model) considered in the present study

absorption occuring in the radial reflectors achieved through rotation of the cylindrical control drums in the radial reflector system on the periphery of the reactor core. Each control drum is made up of two sectors one of which contains $^{10}B_4C$ neutron poison and the other sector containing BeO reflector material. The central safety plug composed of $^{10}B_4C$ neutron poison is for reactor shutdown in the event of accident conditions. Core heat pipes extend from the reactor core, bend around the radiation shield and finally carry the coolant to the "thermal to electric" power conversion module housed behind the radiation shield. The purpose of the accumulators is to take care of changes in the volume of the liquid metal coolant due to temperature variation as well as change of phase of the coolant from solid to liquid.

Located behind the reactor subsystem is a shadow shield (half cone angle ~17 degrees) made of LiH (the LiH portions of the shield are cast into a stainless steel (SS-347) matrix for structural integrity) for neutron attenuation and tungsten for gamma attenuation. Traversing along the r = 0 centerline in the direction of increasing z values, the shield subsystem begins at z = 63.8 cm (the outer radial region of the bottom end of the shield hangs down towards the reactor end going as low as z = 58.27 cm) and ends at z = 133 cm, the maximum radial dimension being 56.36 cm. A ZrO_2 multifoil insulation layer (~ 1 cm thick : z = 62.8 cm to z = 63.8 cm) separates the top of the reactor from the bottom of the shield. The bottom region of the shield (z = 63.8 cm to z = 71.8 cm) is composed of enriched LiH (almost 100% Li^7 enrichment in order to reduce charged particle heating due to the $[n,\alpha]$ reaction in Li^6). Behind the enriched LiH zone (z = 72.6 cm to z = 81.2 cm) is a natural LiH zone. A

radial aluminum heat conductor strip (0.8 cm thick : z = 71.8 cm to z = 72.6 cm) separates the enriched and natural LiH zones and is present to conduct heat from the inner region of the shield to the outer radial surface of the shield. Behind the natural LiH zone is a tungsten zone (~ 4.5 cm thick : z = 81.7 cm to z = 86.2 cm) which becomes very narrow as it runs diagonally through the shield down to z = 74.81 cm near the outer radius of the shield. The tungsten region is surrounded on its bottom and on its side by ZrO_2 multifoil insulation layers. The bottom insulation layer is approximately 0.2 cm thick (z = 81.2 cm to z = 81.4 cm). A thin radial aluminum heat conductor strip (~ 0.3 cm thick : z = 81.4 cm to z = 81.7 cm) lies sandwiched between the bottom insulation layer and the bottom of the tungsten zone. The insulation layer on the side is about 0.3 cm thick. The purpose of these two insulating layers is to isolate the gamma heating in the tungsten from the neutron heating in the surrounding natural LiH regions. A radial aluminum heat conductor strip (0.2 cm thick : z = 86.2 cm to z = 86.4 cm) lies behind the tungsten layer. The rest of the shield behind tungsten is composed of natural LiH. An axial aluminum strip (0.2 cm thick) forms the radiating outer surface of the shield between z = 58.27 cm and z = 89 cm.

- For the transport calculations, the r = 0 centerline is treated as a reflected boundary and the outer boundary of the entire reactor - shield system is treated as a void boundary.
- For heat conduction calculations, the r=0 centerline is treated as an insulated boundary (zero heat flux); the outer surface of the bottom portion of the shield at z = 63.8, and the outer surface of the top portion of the shield between z = 133 cm and z = 89 cm are

treated as insulated boundaries. Heat transfer across each of the two insulation layers that surround the tungsten zone is simulated using "surface-to- surface" radiative heat transfer (emissivity = 0.02) across a void region. The shield loses heat through its outer surface between z = 58.27 cm and z = 89 cm by radiation with an emissivity = 0.8, and an ambient temperature of 0°K. Results were found to be insensitive to the value assumed for the ambient temperatures up to a value of 300°K.

7.2 Steady State Thermal Analysis of the Radiation Shield

7.2.1 Calculational Procedure

The basic calculational procedure involved in the determination of the steady state temperature distribution in the shield (explained in Fig. 7.3 in the form of a flowchart) is as follows :

(1) Radiation transport calculations are first performed using DOT-IV for the entire reactor-shield configuration. This involves two DOT-IV runs. The first DOT-IV run is a "neutron only" k-eigenvalue calculation (10 inner (flux) iterations, 8 outer (source) iterations) to obtain the core fission source and the neutron flux. The neutron flux from the first DOT-IV run is then input as flux guess for the second DOT-IV calculation (a "coupled neutron-gamma" k-eigenvalue calculation : 10 inner iterations and 2 outer iterations) to obtain the final neutron and gamma scalar fluxes (saved in the VARFLM file). The fission source has been normalized to 1.55E17 neutrons/sec which corresponds to a 2 MWth reactor power level. DOT-IV input macroscopic cross sections for all materials involved have been

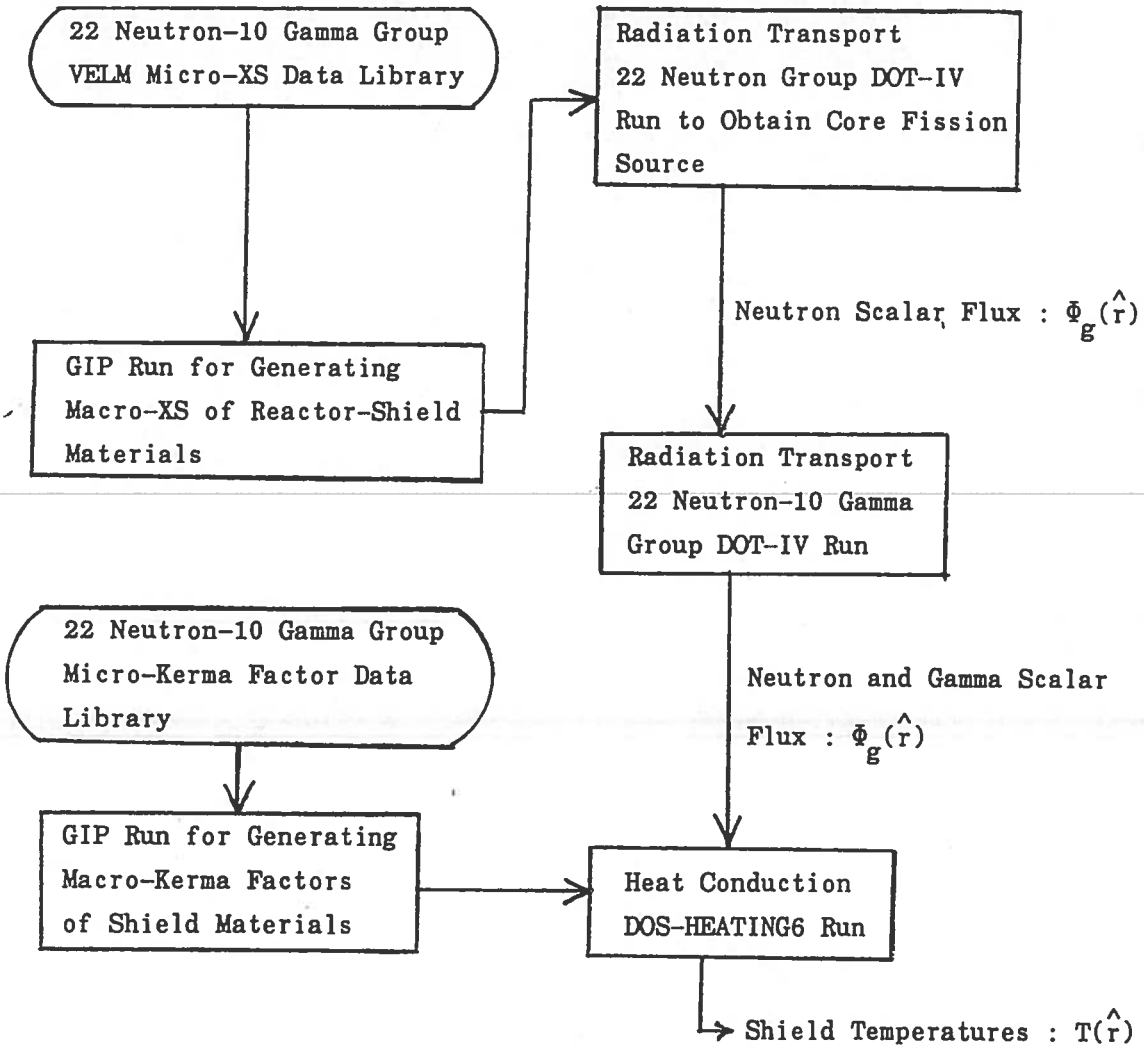

Fig. 7.3 Flowchart indicating the calculational procedure followed for steady state thermal analysis of the shield

generated by running the GIP program in conjunction with the 32 group (22 neutron groups and 10 gamma groups) VELM microscopic cross section data library [7.2] supplied by Oak Ridge National Laboratory (see Appendix B for the energy group structure associated with the library). The DOT-IV calculations use a P_3 Legendre expansion for the angle dependent scatter cross section (ISCT=3) and an S_6 quadrature containing 30 directions (MM=30) for the directional mesh.

(2) Subsequent heat conduction calculations are then performed for only the shield region using the DOS-HEATING6 program. The DOS-HEATING6 input macroscopic kerma factors for all materials involved have been generated by running the GIP program in conjunction with a 32 group microscopic kerma factor data library (based on the same energy group structure as the microscopic cross section data library) supplied by Oak Ridge National Laboratory (Appendix C contains a listing of the microscopic kerma factors of component nuclides of the shield materials). A steady state convergence criterion of 1.0D-12 has been used.

Two important points concerning the coupled calculations need to be mentioned :

(a) Calculation of nuclear heating rates in DOS-HEATING6 is based on linear interpolation of the DOT-IV fluxes to the DOS-HEATING6 mesh. Therefore the DOT-IV spatial mesh should be fine enough (especially in the vicinity of material interfaces where the flux may abruptly change due to abrupt cross section changes) for linear interpolation to give sufficiently good results. For a given problem, it is wise to repeat the

coupled calculations with different DOT-IV spatial meshes and make sure that the total heat generation rate comes out to be the same for each mesh.

(b) The default value of the steady state convergence criterion in DOS-HEATING6 is 1.0D-5. However, for nonlinear problems e.g. those that involve temperature dependent conductivities, radiative boundary conditions etc. it is possible that the SOR iterative process might be converging so slowly that a fairly lax convergence criterion like 1.0D-5 will be satisfied even though the temperature distribution has not yet converged. For this reason, a value of 1.0D-12 (maximum precision achievable on an IBM 370 computer) has been used as the steady state convergence criterion in DOS-HEATING6 calculations. As in (a), for a given problem, it is wise to repeat the coupled calculations using different values for the steady state convergence criterion and make sure that the temperature distribution comes out to be the same for each value.

Appendix D shows a zone-map of the baseline reactor-shield model (including the composition of each zone) used in transport calculations. Appendix E shows thermal property data of shield materials, needed for heat conduction calculations (thermal property data have been taken from the Materials Properties Library [7.3] that comes along with the HEATING6 code). Notice that the LiH zones in the shield actually occur mixed with stainless steel (the LiH is cast in a stainless steel (SS-347) honeycomb matrix). The thermal conductivities of these LiH zones for heat conduction calculations have been taken to be equal to that of pure LiH since there is no simple way to ascertain the thermal conductivity of the

heterogeneous mixture. However while calculating the mass densities of the LiH zones, the prescence of stainless steel has been accounted for.

All contour plots for fluxes/activities from DOT-IV calculations have been obtained by running the "ISOPLOT4" plotting program [7.4] in conjunction with the DOT-IV scalar fluxes in the VARFLM file. Because of the unavailability of the "HEATPLOT" plotting program [7.5], surface profiles/contours of the shield steady state temperatures obtained from the DOS-HEATING6 run (stored in logical unit ITPOUT) have been plotted using ISOPLOT4. However, ISOPLOT4 requires that the plot file containing the data to be plotted be in a VARFLM format. To this end, the DOS-HEATING6 temperatures have been interpolated from the DOS-HEATING6 mesh to the DOT-IV mesh and written into a file in VARFLM format so that subsequent plotting using ISOPLOT4 is possible.

7.2.2 Description of Calculations

First of all, coupled radiation transport-heat conduction calculations have been performed for the baseline reactor-shield model described in section 7.1 in order to determine the reference steady state temperature distribution in the shield. The coupled calculations require a total cpu time (on the IBM 370 mainframe computer) of about 48 minutes (25 minutes for the first DOT-IV run, 5 minutes for the second DOT-IV run, and 18 minutes for the DOS-HEATING6 run). The DOS-HEATING6 calculation requires 6721 iterations for convergence (steady state convergence criterion = 1.0D-12) for a spatial mesh consisting of 2691 nodes. Fig. 7.4 shows the energy-integrated neutron flux contours for E > 1.0 MeV for which the peak values of the neutron flux (0.0 cm $\leq$ r $\leq$ 39.43 cm) are found to be 3.94E12 neutrons/cm^2/sec and 5.12 E6

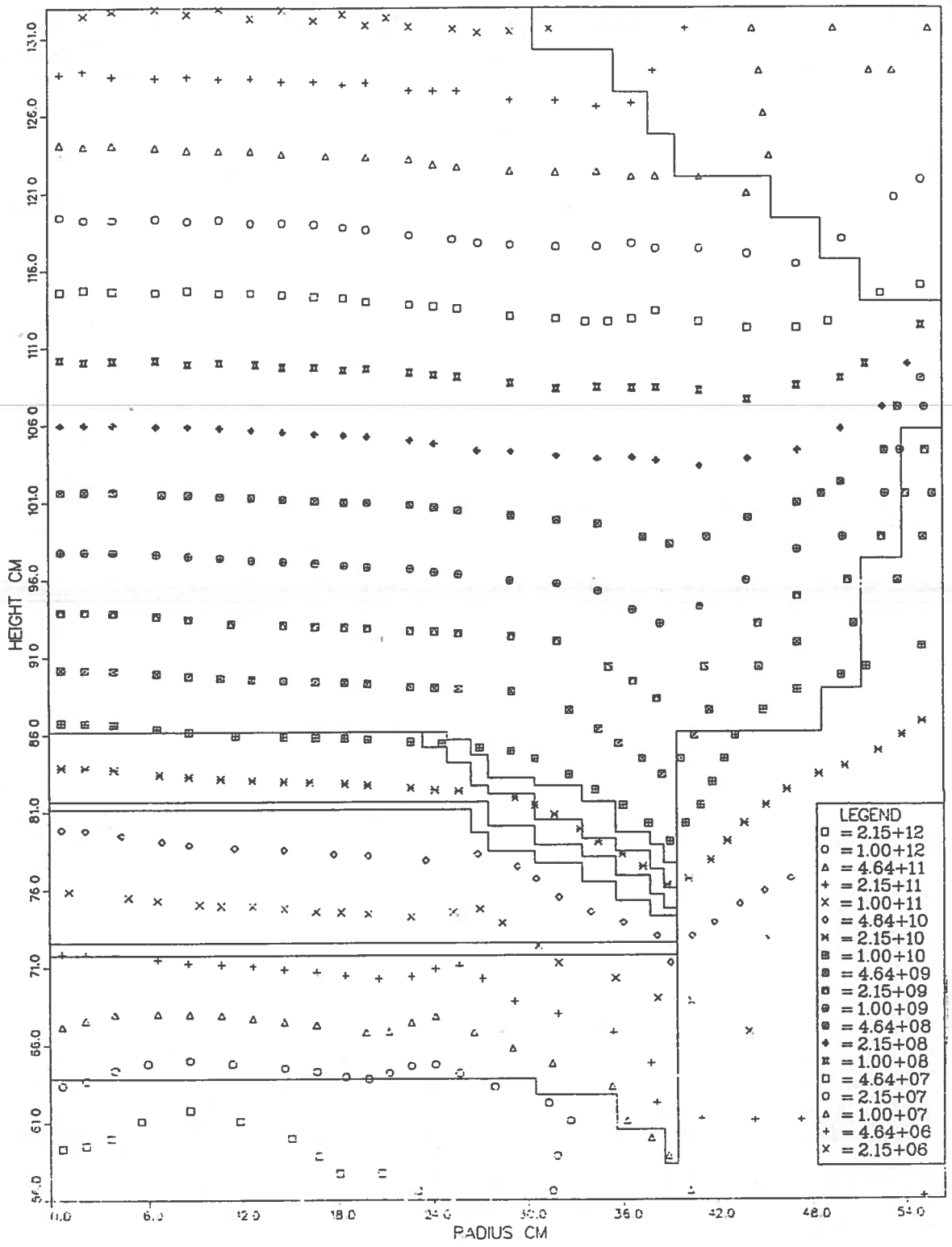

Fig. 7.4 Energy-integrated neutron flux [neutrons/cm^2/sec] contours (E > 1.0 MeV) for the baseline shield model

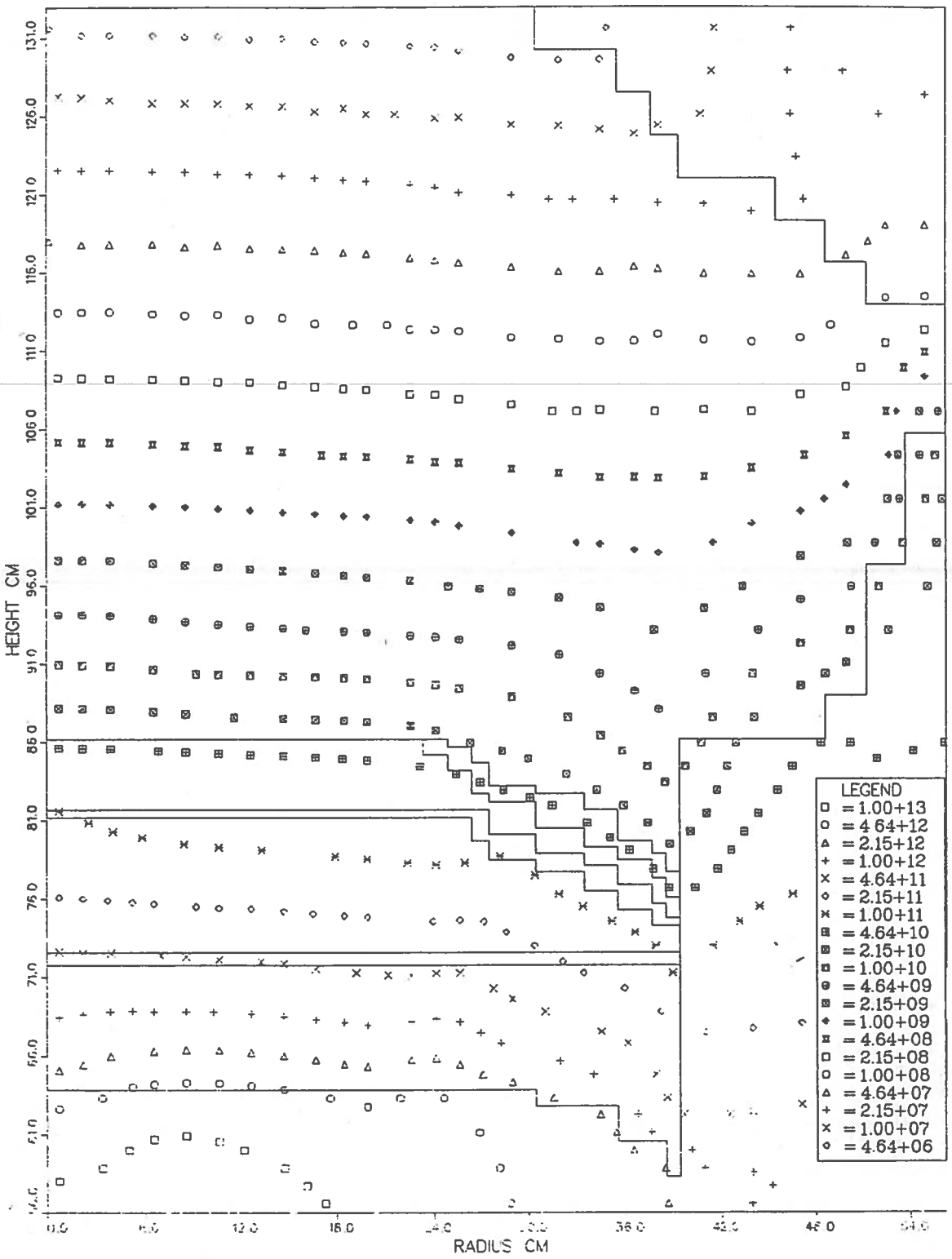

Fig. 7.5 Energy-integrated neutron flux [neutrons/cm^2/sec] contours (E > 0.1 MeV) for the baseline shield model

neutrons/cm^2/sec at the bottom and top of the shield, respectively. This corresponds to an attenuation factor of about 1.3E-6. Fig. 7.5 shows the energy-integrated neutron flux contours for E > 0.1 MeV for which the peak values of the neutron flux (0.0 cm $\leq$ r $\leq$ 39.43 cm) are found to be 1.57E13 neutrons/cm^2/sec and 7.91E6 neutrons/cm^2/sec at the bottom and top of the shield, respectively. This corresponds to an attenuation factor of about 5E-7. Fig. 7.6, Fig. 7.7, and Fig. 7.8 show the shield neutron, gamma, and total volumetric heat generation rate profiles, respectively. It may be observed that the neutron heating rate peaks at the interface of the enriched and natural LiH regions. This is because fast neutrons that thermalize in the enriched LiH region at the bottom of the shield give rise to charged particle heating in the adjoining natural LiH region due to the (n,α) reaction with Li^6 in natural LiH. On the other hand, the gamma heating rate peaks in the tungsten region since most of the gamma attenuation occurs in the tungsten region. The total nuclear heating rate in the shield is found to be 6.33 kW (neutron heating rate : 3.49 kW ; gamma heating rate : 2.84 kW). Fig. 7.9 and Fig. 7.10 show the shield temperature profile and shield temperature contours, respectively. The maximum temperature occurs in the bottom portion of the shield at a z level of 63.8 cm on the r=0 centerline in the enriched LiH region, whereas the minimum temperature occurs in the top portion of the shield at a z level of 86.2 cm near the outer boundary of the shield in the natural LiH region. The maximum temperature is found to be 880°K (200°K or 29% above the 680°K upper limit recommended for LiH) and the minimum temperature is found to be 532°K (68°K or 11% below the 600°K lower limit recommended for LiH). Although the melting

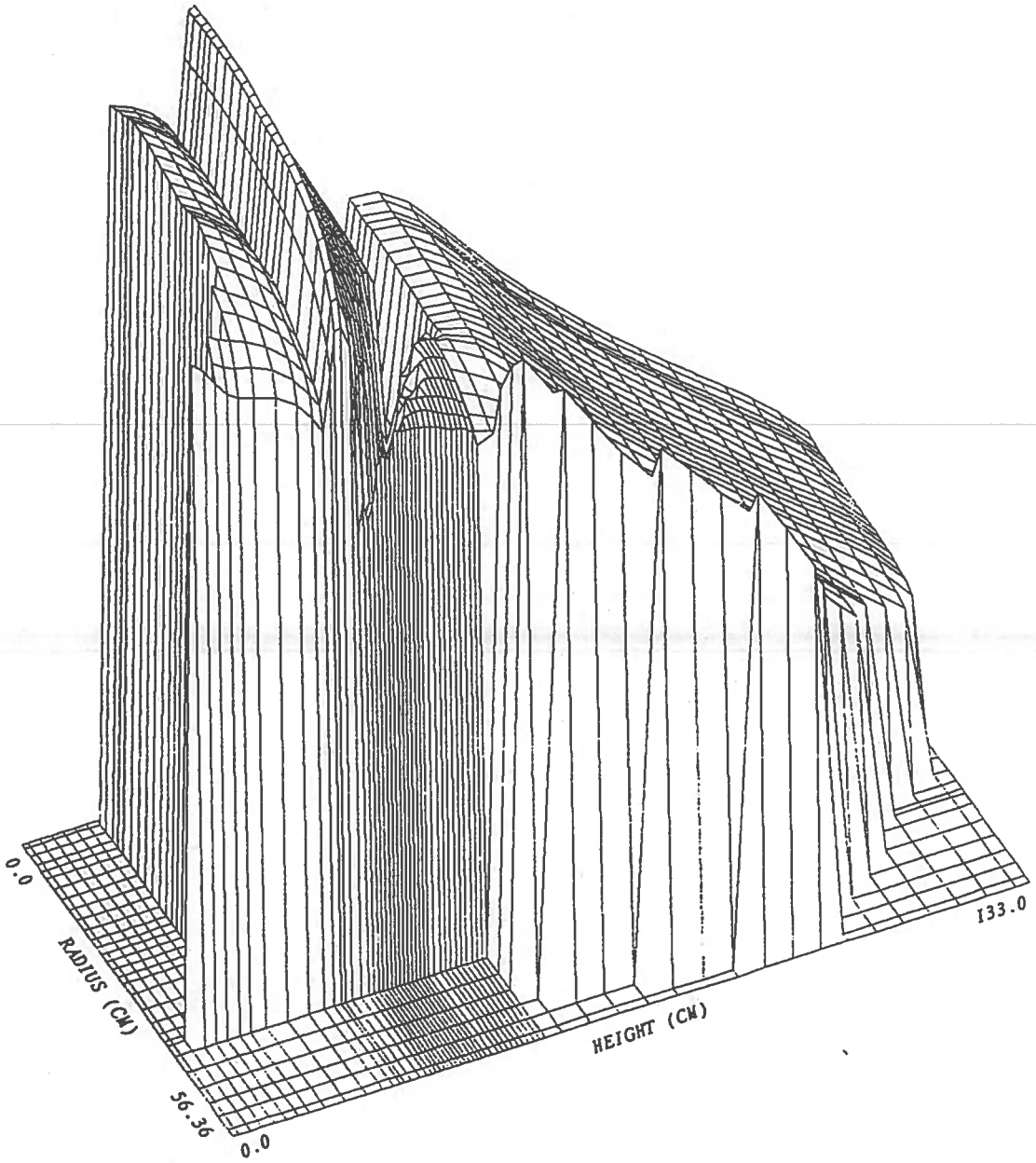

Fig. 7.6 Neutron volumetric heat generation rate (logarithmic) profile for the baseline shield model

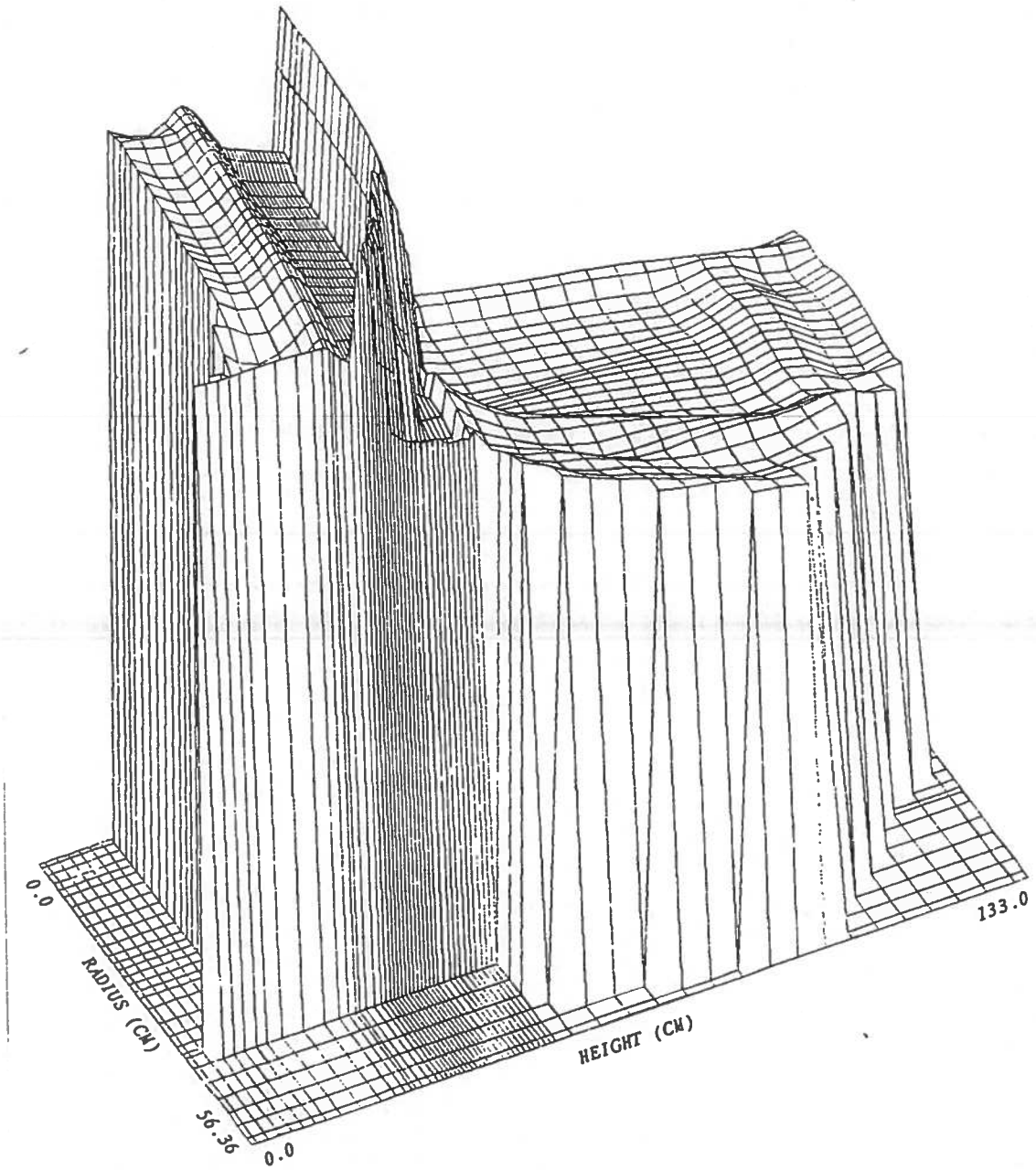

Fig. 7.7 Gamma volumetric heat generation rate (logarithmic) profile for the baseline shield model

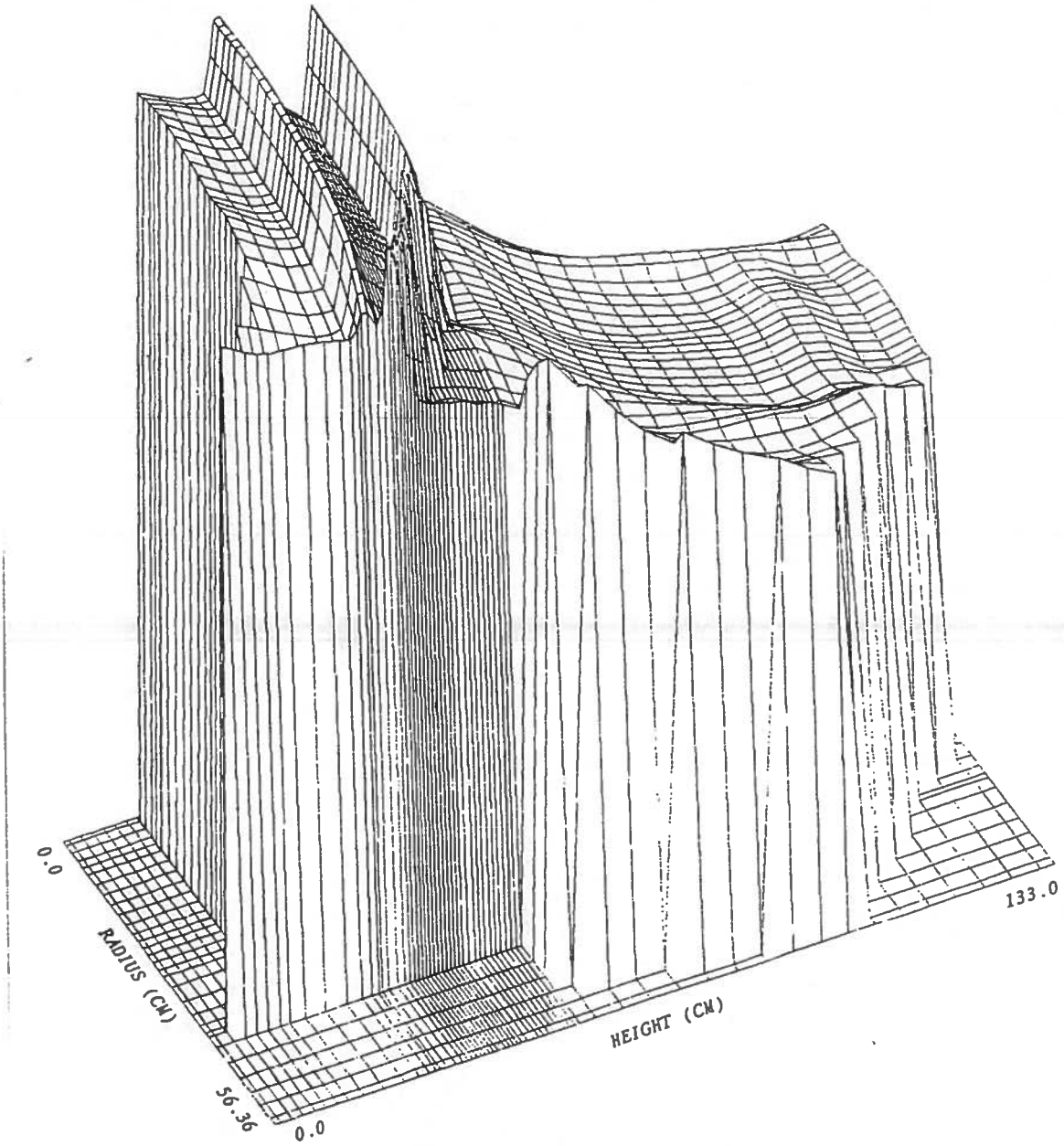

Fig. 7.8 Total (neutron plus gamma) volumetric heat generation rate (logarithmic) profile for the baseline shield model

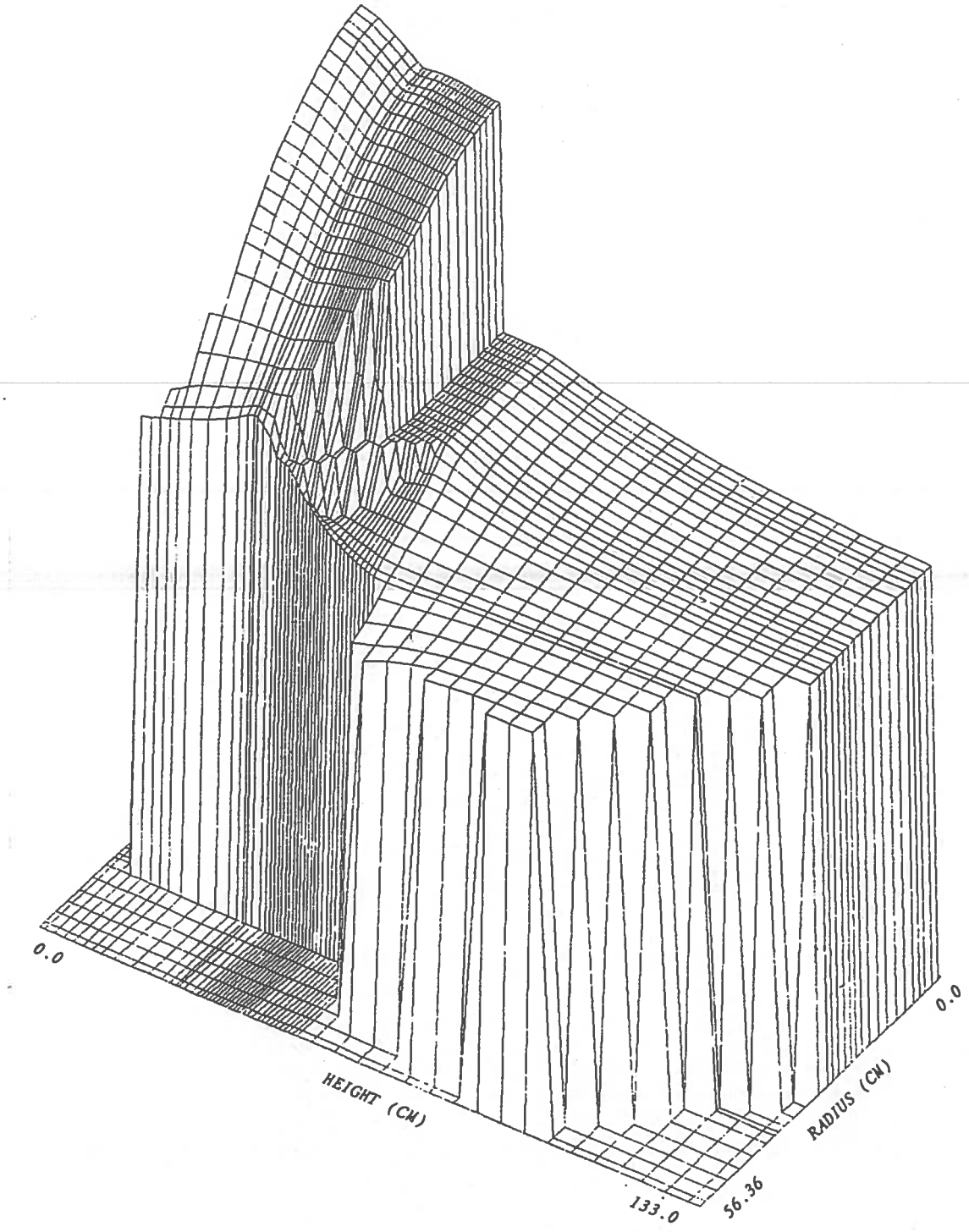

Fig. 7.9 Temperature [°K] profile for the baseline shield model

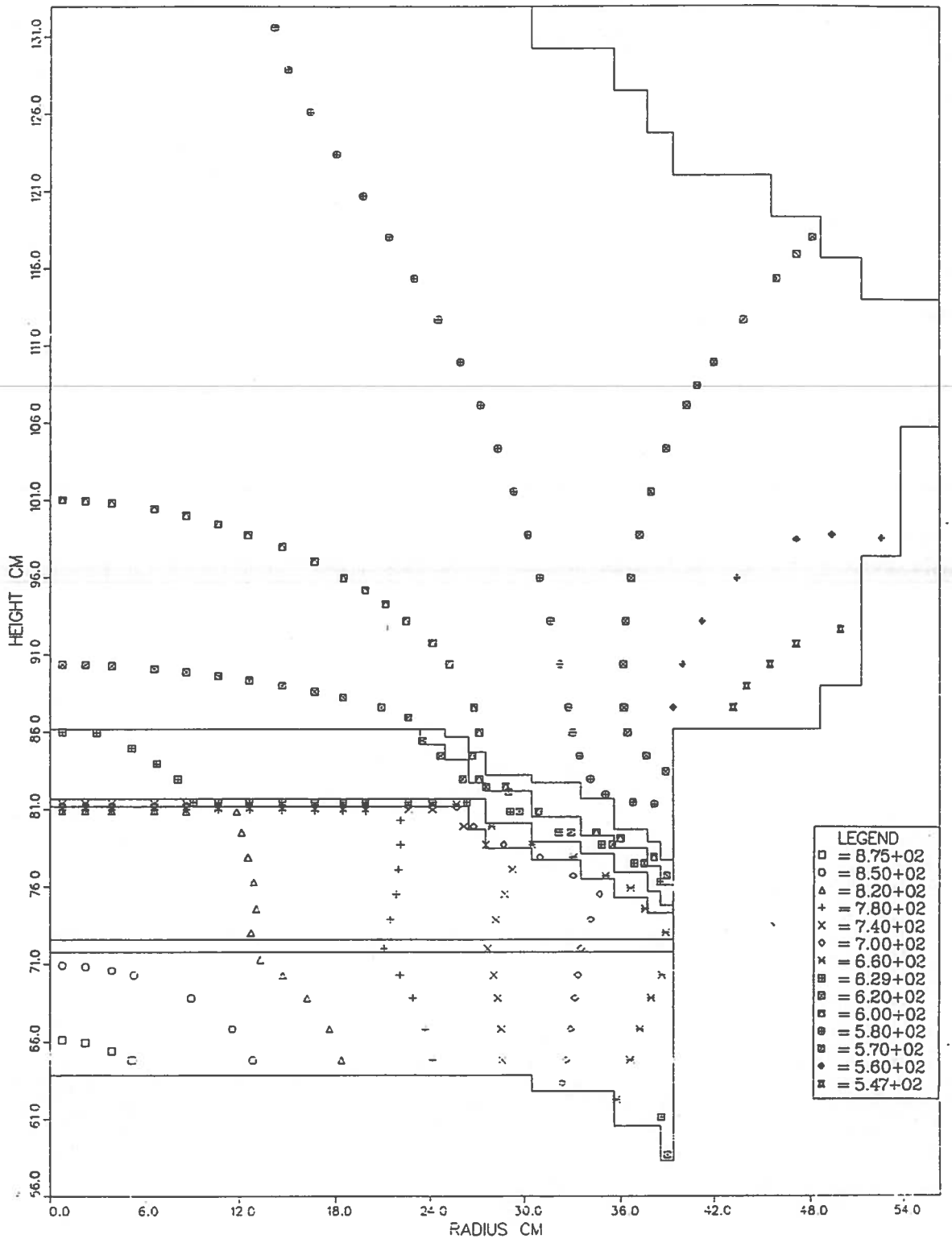

Fig. 7.10 Temperature [°K] contours for the baseline shield model

points of the shield materials are not exceeded, temperatures in the LiH zones are not in the desired 600°K-680°K range. In order to satisfy the temperature constraints for LiH, the baseline shield model needs modifications in a way so as to lower the maximum temperature and raise the minimum temperature. The shield weight is found to be 716 kg which is quite satisfactory (the SP-100 limit on the shield weight is about 790 kg).

From the description of the baseline reactor-shield system in section 7.1, it may be seen that there is a 0.8 cm aluminum heat conductor strip at the interface of the enriched and natural LiH regions in the bottom portion of the shield where considerable nuclear heating takes place. The heat generated in this region cannot be conducted away to the top of the shield because of the prescence of the insulation layer below the tungsten. The only way this heat may be rejected is by conduction in the radial direction to the radiative outer surface of the shield. The radial aluminum heat conductor strip was proposed by General Electric to serve this purpose. There are also two insulation layers surrounding the tungsten region. The purpose of these insulation layers in the G.E. design is not clear. Supposedly they are there to insulate the natural LiH regions from the tungsten region which is a source of considerable gamma heat [7.6]. Intuitively it would seem that the two insulation layers would worsen the temperature distribution by acting barriers, preventing heat flow in the axial direction. In order to study the effect of the aluminum heat conductor and the insulating gaps on the temperature distribution, coupled calculations have been repeated for the baseline reactor-shield model with the following design perturbations

made to the shield :

Case 1 : The radial aluminum heat conductor strip between z = 71.8 cm and z = 72.6 cm has been removed and replaced by the neighbouring enriched LiH material.

Case 2 : The thickness of the radial aluminum heat conductor strip between z = 71.8 cm and z = 72.6 cm has been doubled; i.e, the strip now lies between z = 71.4 cm and z = 73.0 cm.

Case 3 : The two insulation layers surrounding the tungsten region have been removed and replaced by the neighbouring natural LiH material.

For cases 1 thru 3, it was found that the maximum and minimum temperatures occur at the same locations in the shield as those for the baseline shield model. For Case 1, the maximum temperature is found to be 1148°K (468°K or 69% above the 680°K recommended upper limit for LiH) and the minimum temperature is found to be 528°K (72°K or 12% below the 600°K recommended lower limit for LiH). This indicates that the radial aluminum heat conductor strip at the enriched and natural LiH interface significantly helps to reduce the maximum temperature and the temperatures in the bottom portion of the shield. The minimum temperature and temperatures in the top portion of the shield are almost unaffected. For Case 2, the maximum temperature is found to be 832°K (152°K or 22% above the 680°K recommended upper limit for LiH) and the minimum temperature is found to be 537°K (63°K or 10% below the 600°K recommended lower limit for LiH). This indicates that the temperature distribution is not very sensitive to increases in the original thickness of the radial aluminum heat conductor strip located at the interface if the enriched and natural LiH regions. For Case 3, the maximum

temperature is found to be 799°K (119°K or 18% above the 680°K recommended lower limit for LiH) and the minimum temperature is found to be 561°K (39°K or 6% below the 600°K recommended lower limit for LiH). Results of Case 3 indicate that removal of the insulation layers around the tungsten region not only reduces the maximum temperature and other temperatures in the bottom portion of the shield but also raises the minimum temperature and other temperatures in the top portion of the shield. Although the temperatures are still outside the desired 600°K-680°K range, removal of the insulation layers does improve the shield design in that the temperature distribution is at least driven towards the 600°K-680°K band.

Recently, replacement of the LiH and aluminum regions in the shield by beryllium has been suggested [7.6] as a means to reduce nuclear heating in the shield, and also to improve heat conduction to the shield surface in view of the high thermal conductivity of beryllium (about 25 times more than that of LiH). The replacement of aluminum by beryllium is justifiable since beryllium is lighter (mass density of beryllium is about 0.7 times that of aluminum) and has a comparable thermal conductivity (thermal conductivity of beryllium is about 0.8 times that of aluminum). Beryllium also has a high melting point (1556°K as compared to 960°K for LiH). However, beryllium has the following disadvantages in comparison with LiH :

(1) its neutron moderating capability is not as good as that of LiH (the value of ξ, the average logarithmic decrement in energy of a neutron per collision is 0.97 for LiH as compared to 0.21 for beryllium).

(2) it is much more heavier than LiH (its mass density is about 2.2

times that of LiH).

(3) it is extremely toxic.

In view of the superior thermal properties of beryllium it is desirable to replace all the LiH regions in the shield by beryllium. However, doing this will greatly increase the weight of the shield because of the higher mass density of beryllium in comparison to LiH. Therefore the substitution of LiH by beryllium has been suggested only for the enriched LiH region in the bottom part of the shield where nuclear heating is very high. The effect of using beryllium has therefore been studied by repeating the coupled calculations for the baseline reactor-shield model with the following modification made to the shield :

Case 4 : The enriched LiH region at the bottom of the shield reactor end and all aluminum regions have been removed and replaced by beryllium.

For Case 4, the total nuclear heating rate is found to be 5.55 kW. The maximum temperature occurs at a z level of 77.81 cm on the r=0 centerline in the natural LiH zone. The location of the maximum temperature is 14.01 cm further up into the shield as compared to that for the baseline shield model. However, the location of the minimum temperature in the shield is the same as that for the baseline shield model. The maximum temperature is found to be 714°K (34°K or 5% above the 680°K recommended upper limit for LiH) and the minimum temperature is found to be 495°K (105°K or 18% below the 600°K recommended lower limit for LiH).

The use of beryllium results in :

(1) less nuclear heating (0.78 kW or 12% less than that for the baseline shield model) in the shield.

(2) the maximum temperature and other temperatures in the bottom portion of the shield reduces.

(3) reduction in the radial temperature gradient across the bottom portion of the shield.

(4) the minimum temperature and other temperatures in the top portion of the shield reduce further.

(5) an increased shield weight (743 kg). Although the shield weight is satisfactory, it is heavier than the baseline shield model by 27 kg or 4% due to the higher mass density of beryllium as compared to LiH.

Effects (1) and (2) are desirable but effect (3) worsens the shield design. The maximum and minimum temperature are still outside the 600°K-680°K range. The maximum temperature needs to be reduced and the minimum temperature needs to be raised. The temperature distribution for the Case 4 shield model, however, is better than the temperature distribution for the baseline shield model or for the shield models corresponding to cases 1 thru 3.

From the Case 3 results, it may be observed that removal of the insulation layers around the tungsten region not only reduces the maximum temperature and other temperatures in the bottom portion of the shield but also raises the minimum temperature and other temperatures in the top portion of the shield. Therefore, it would seem that if the insulation layers around the tungsten region are removed in the Case 4 shield model, the temperature distribution should move into the 600°K-680°K range. Finally, therefore, coupled calculations have been repeated for the baseline reactor-shield model with the following change made to the shield with the hope that satisfactory temperatures will result :

Case 5 : The two insulation layers around the tungsten gamma shield have been removed and replaced by neighbouring LiH, and the enriched LiH region at the bottom of the shield near the reactor end plus the aluminum regions have been replaced with beryllium.

Fig. 7.11 shows the energy-integrated neutron flux contours for E > 1.0 MeV, for which the peak values of the neutron flux are found to be 4.04E12 neutrons/cm^2/sec and 4.91E6 neutrons/cm^2/sec for the bottom and top of the shield, respectively. This corresponds to an attenuation factor of about 1.2E-6. Fig. 7.12 shows the energy-integrated neutron flux contours for E > 0.1 MeV, for which the peak values of the neutron flux are found to be 1.68E13 neutrons/cm^2/sec and 7.59E6 neutrons/cm^2/sec at the bottom and top of the shield, respectively. This corresponds to an attenuation factor of about 4.5E-7. The total nuclear heating rate is found to be 5.77 kW (neutron heating rate = 3.51 kW ; gamma heating rate = 2.26 kW). Fig. 7.13 and Fig. 7.14 show the shield temperature profile and shield temperature contours, respectively. The maximum temperature occurs at a z level of 77.81 cm at the r=0 centerline in the bottom portion of the shield in the natural LiH zone. The location of the maximum temperature in the shield is 10.51 cm further up into the shield as compared to that for the baseline shield model. However, the location of the minimum temperature is the same as that for the baseline shield model. The maximum and minimum temperatures are found to be 658°K and 526°K (74°K or 12% below the 600°K recommended lower limit for LiH), respectively. The Case 5 shield design appears to be the best among all the shield models evaluated so far. The maximum temperature and other temperatures in the bottom part of the shield in the LiH regions are

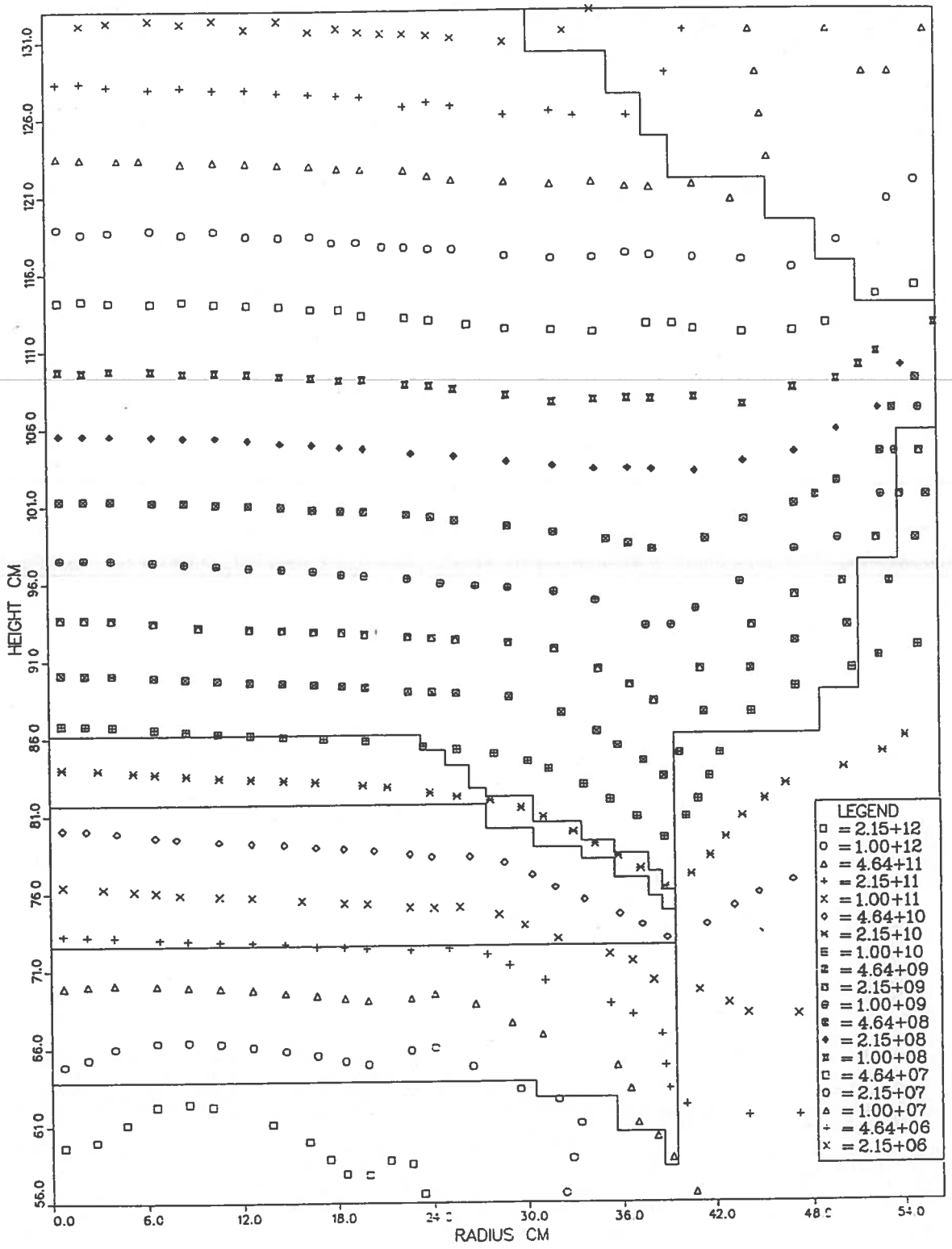

Fig. 7.11 Energy-integrated neutron flux [neutrons/cm^2/sec] contours (E > 1.0 MeV) for the Case 5 shield model

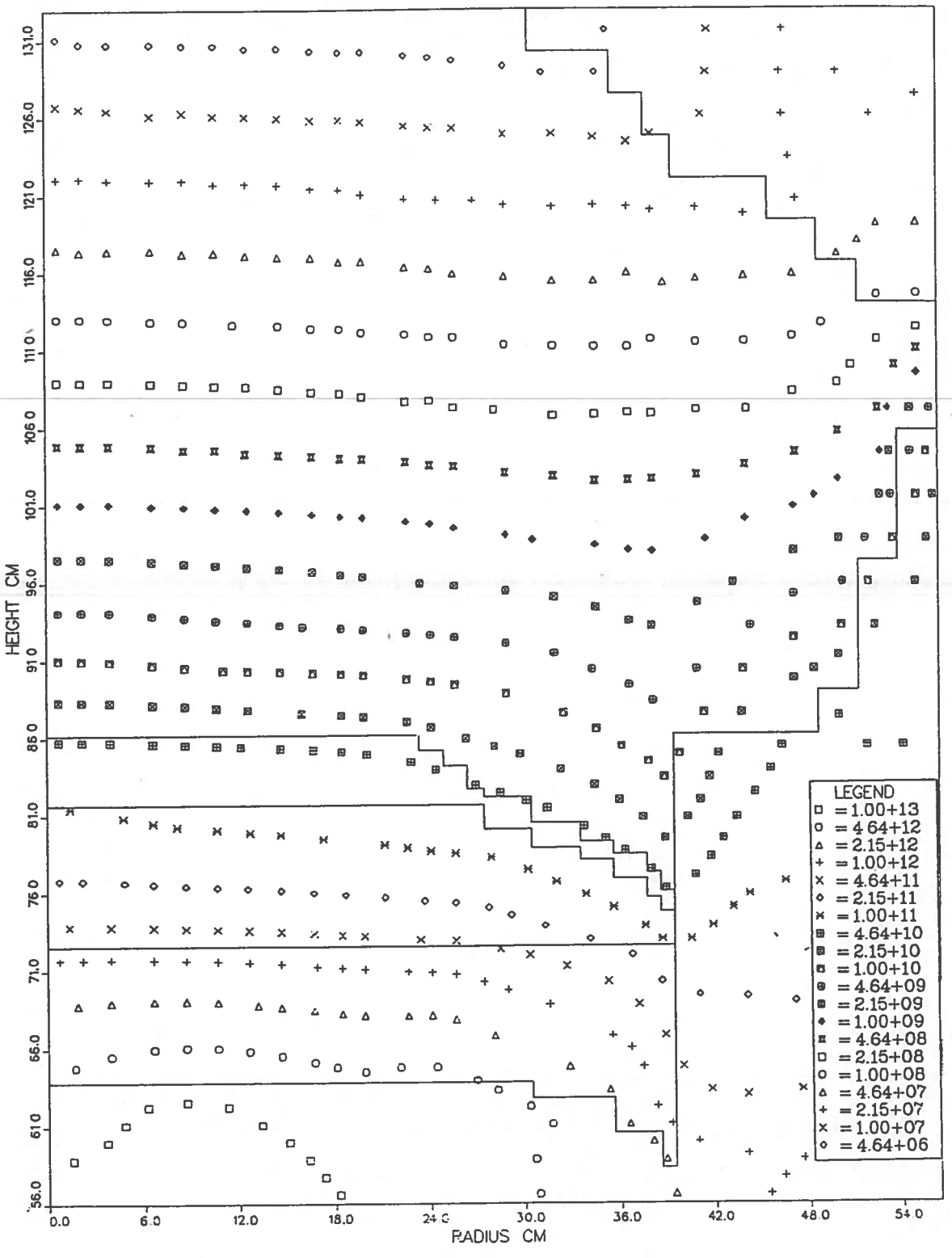

Fig. 7.12 Energy-integrated neutron flux [neutrons/cm^2/sec] contours (E > 0.1 MeV) for the Case 5 shield model

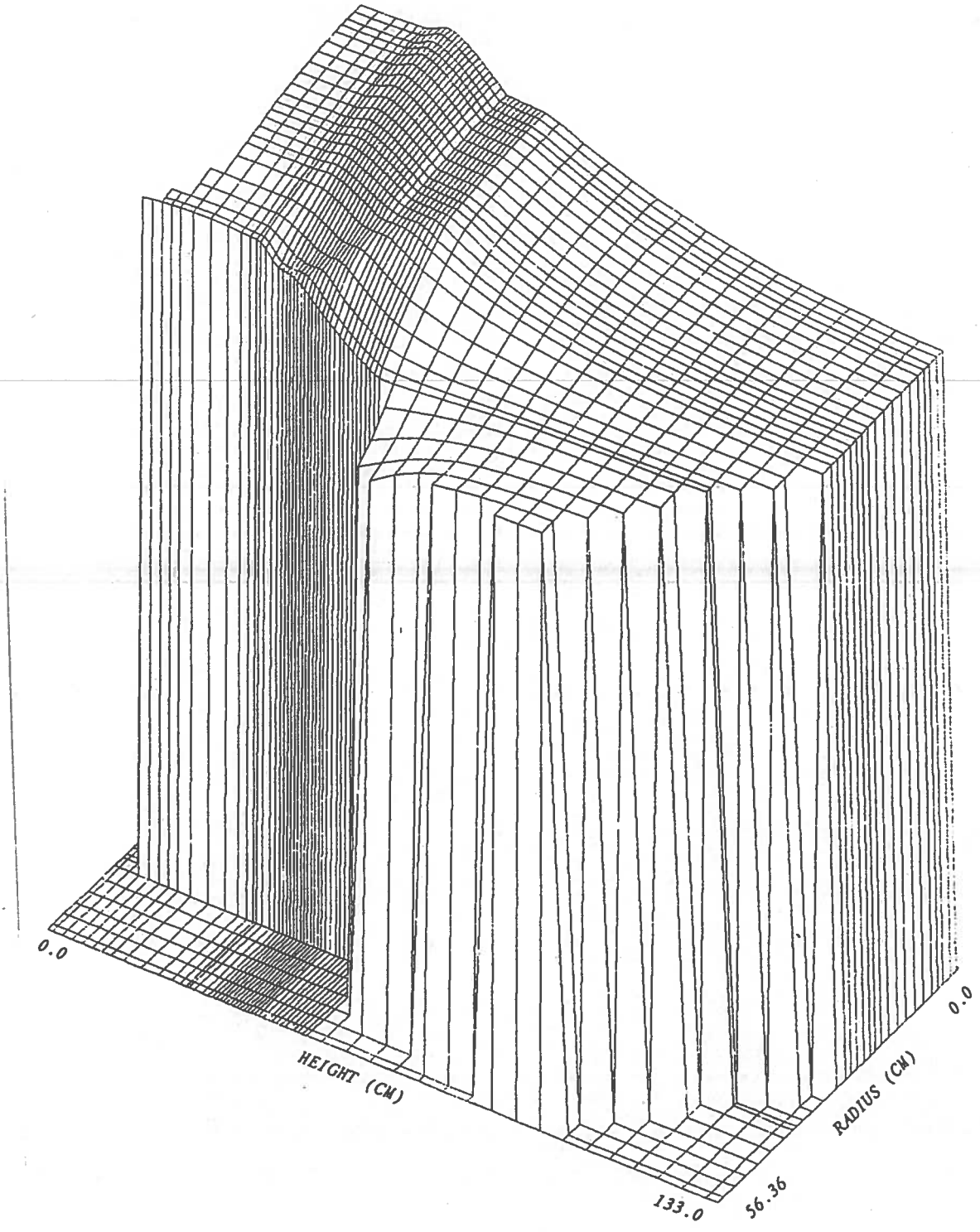

Fig. 7.13 Temperature [°K] profile for the Case 5 shield model

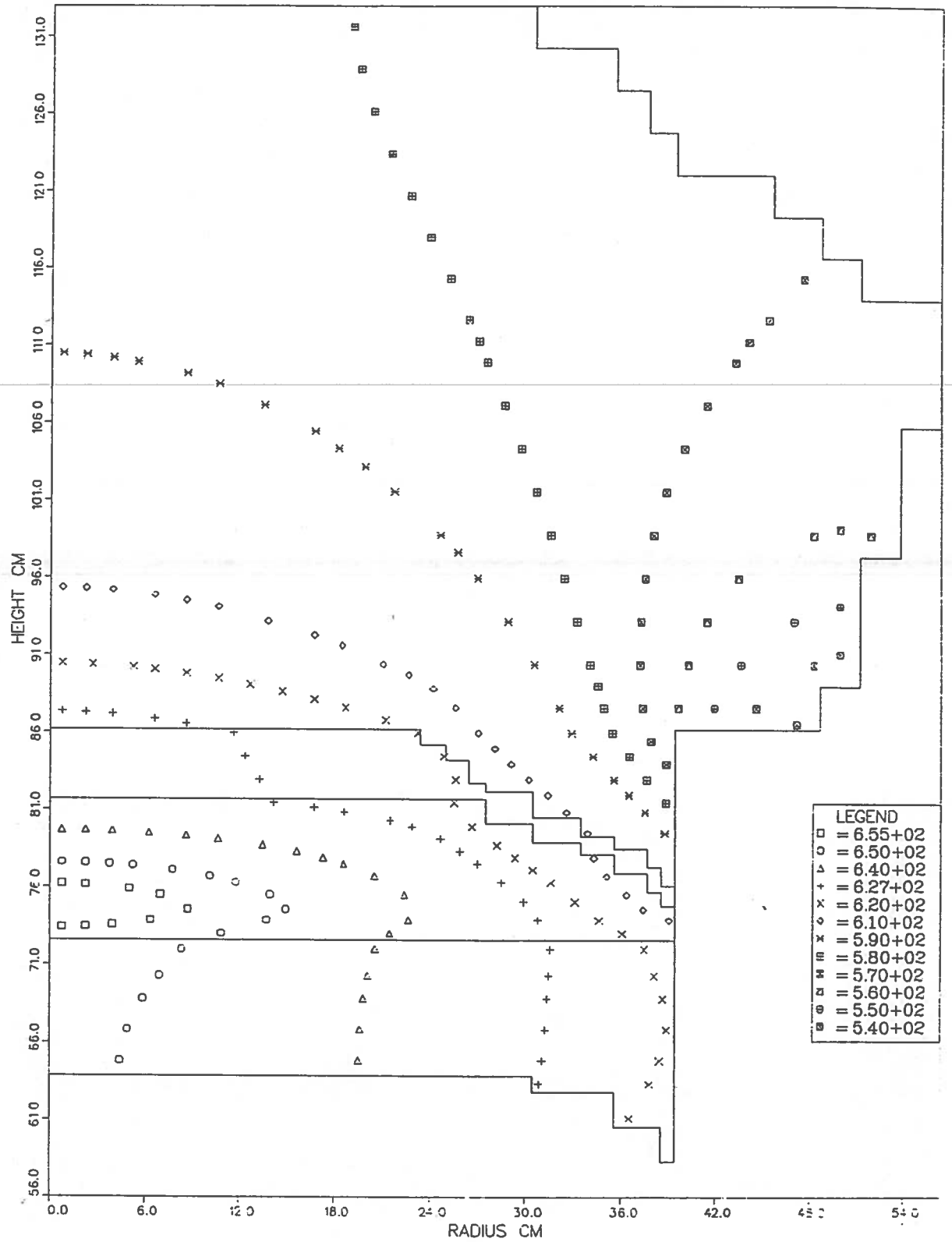

Fig. 7.14 Temperature [°K] contours for the Case 5 shield model

within the 680°K recommended upper limit for LiH. However, the minimum temperature and some of the temperatures in the top portion of the shield need to be raised. The total shield weight is found to be 752 kg which is satisfactory although it is 36 kg (5%) heavier than that for the baseline shield model owing to the higher mass density of beryllium as compared to LiH.

One way of raising the minimum temperature and temperatures in the top portion of the Case 5 shield model is to push the tungsten layer (and therfore the gamma heating source) a little further up into the shield (in the increasing z direction). This should cause heating in the top portion of the shield to increase, thereby driving the minimum temperature from 526°K to a higher value, hopefully, above 600°K resulting in a satisfactory shield design. Another alternative is to add axial heat conductor strips to transport some of the heat in the bottom of the shield towards the top. However, these modifications to the baseline shield model have not been investigated in the present study.

It should be noted that each of the cases (Case 1 thru Case 5) involves modifications only to the shield portion of the baseline reactor-shield system. The reactor subsystem and boundary conditions for the shield subsystem remain unaltered. The DOT-IV and DOS-HEATING6 spatial grid structures for each case run remain the same as those used in the baseline shield model computations. Coupled calculations for each case have been performed by appropriately modifying the DOT-IV and DOS-HEATING6 card input corresponding to the baseline reactor-shield design so as to reflect the changes made to the baseline shield model for that particular case.

Table 7.1 Summary of some important results of coupled radiation transport-steady state heat conduction calculations for the for the baseline shield model and for the shield models corresponding to Cases 1 thru 5.

Shield Model	Nuclear Heating [kW]	Maximum Shield Temperature [°K]	Minimum Shield Temperature [°K]	Shield Mass [kg]
Baseline	6.33	880.5	531.9	716
Case 1	6.20	1147.5	527.6	710
Case 2	6.63	831.8	536.6	722
Case 3	6.68	799.0	561.0	725
Case 4	5.56	713.9	495.4	742
Case 5	5.77	657.8	526.2	752

Table 7.1 summarizes some of the important results for steady state nuclear heating calculations for the baseline shield model and for the shield models corresponding to cases 1 thru 5 described in the present section.

7.3 Radiation Dosage Calculations

7.3.1 Radiation Dose at the Top of the Shield

The neutron fluence and gamma dose in the shield region has been calculated for the baseline shield model and for the Case 5 shield model. Multigroup dose factors for gammas are given in Appendix F. Fig. 7.15 and Fig. 7.16 show the seven year neutron fluence and gamma dose contours, respectively, for the baseline shield model. Fig. 7.17 and Fig. 7.18 show the seven year neutron fluence and gamma dose contours, respectively, for the Case 5 shield model. Table 7.2 lists the seven year neutron fluence and gamma dose along the top surface of the shield at z = 133.0 cm for the baseline and Case 5 shield models. Along the top surface of the shield (for 0.0 cm $\leq$ r $\leq$ 30.5 cm), the peak values of the seven year neutron fluence are found to be 1.19E15 neutrons/cm^2 and 1.09E15 neutrons/cm^2 for the baseline shield model and the Case 5 shield model, respectively, while the peak values of the seven year gamma dose are found to be 1.22E3 Mrad and 1.03 Mrad for the baseline shield model and the Case 5 shield model, respectively.

7.3.2 Radiation Dose at 25 m Dose Plane

To estimate the seven year neutron fluence and gamma dose at the 25 m doseplane (25 m behind the reactor midplane), a somewhat crude method has been used. The top of the shield at z = 133 cm (from r=0.0 cm

Table 7.2 Seven year neutron fluence (NVT) and gamma dose at the shield top (z = 133.0 cm) for the baseline and Case 5 shield models.

Radius [cm]	NVT[neutrons/cm^2] for Baseline Shield Model	NVT[neutrons/cm^2] for Case 5 Shield Model	Gamma Dose [Mrad] for Baseline Shield Model	Gamma Dose [Mrad] for Case 5 Shield Model
0.75	1.19E15[(a)]	1.09E15[(a)]	0.83E3	0.60E3
2.25	1.02E15	0.94E15	0.89E3	0.69E3
3.95	1.06E15	0.96E15	0.91E3	0.70E3
5.25	1.08E15	1.00E15	0.89E3	0.67E3
6.61	1.07E15	0.97E15	0.88E3	0.68E3
8.63	1.02E15	0.94E15	0.96E3	0.76E3
10.64	1.05E15	0.95E15	1.10E3	0.91E3
12.66	0.96E15	0.88E15	1.18E3	1.00E3
14.68	1.04E15	0.95E15	1.22E3[(a)]	1.03E3[(a)]
16.69	0.93E15	0.84E15	1.20E3	1.03E3
18.50	1.00E15	0.90E15	1.14E3	0.99E3
19.95	0.90E15	0.85E15	1.11E3	0.96E3
21.25	0.98E15	0.86E15	1.05E3	0.92E3
22.65	0.89E15	0.82E15	0.99E3	0.86E3
24.15	0.93E15	0.83E15	0.96E3	0.84E3
25.65	0.85E15	0.77E15	0.94E3	0.82E3
26.95	0.82E15	0.76E15	0.93E3	0.81E3
29.00	0.76E15	0.67E15	0.90E3	0.80E3
32.00	0.80E15	0.77E15	0.92E3	0.82E3
34.55	1.38E15	1.27E15	1.02E3	0.91E3
36.66	2.51E15	2.53E15	1.17E3	1.07E3
38.14	2.50E15	2.45E15	1.29E3	1.21E3
39.00	1.92E15	1.90E15	1.47E3	1.40E3
40.97	2.32E15	2.24E15	2.16E3	2.15E3
44.06	5.16E15	5.20E15	2.94E3	3.07E3
47.15	7.29E15	7.37E15	2.66E3	2.87E3
49.97	5.42E15	5.39E15	1.92E3	2.01E3
52.52	4.14E15	4.15E15	2.09E3	2.01E3
55.08	5.19E15	5.15E15	2.84E3	2.57E3

[(a)] Peak values for 0.0 cm $\leq$ radius $\leq$ 30.5 cm

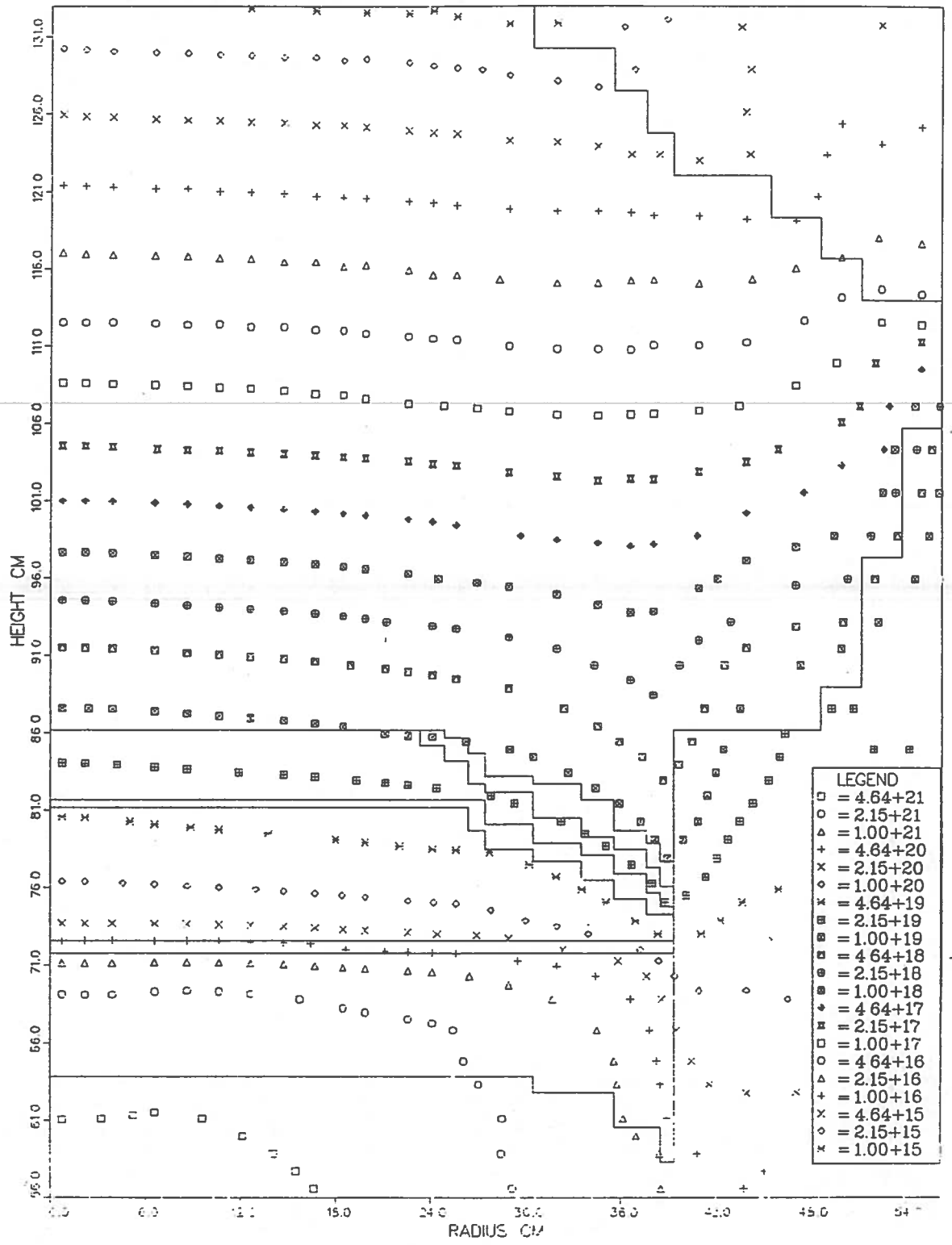

Fig. 7.15 Seven year neutron fluence [neutrons/cm^2] contours for the baseline shield model

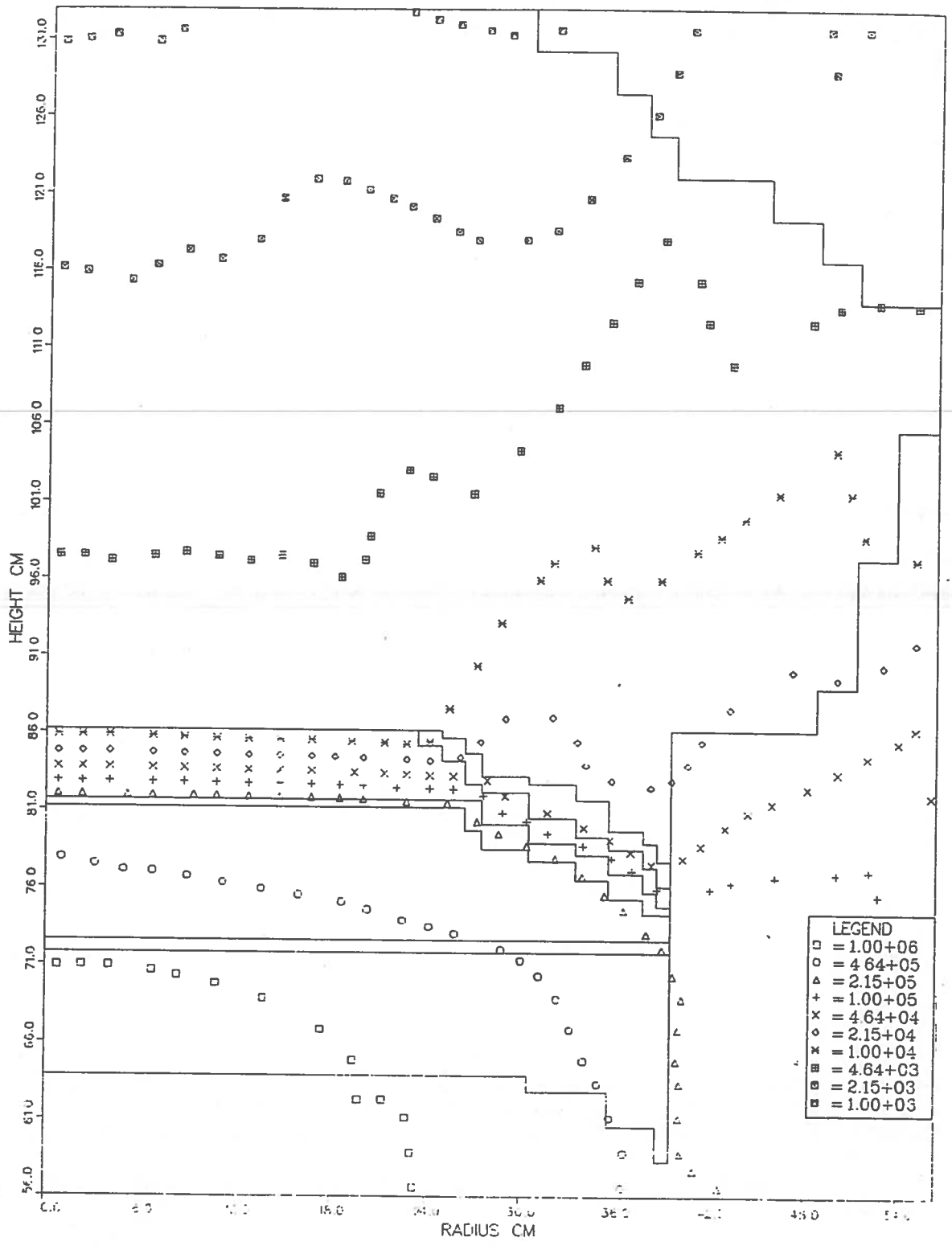

Fig. 7.16 Seven year gamma dose [Mrad] contours for the baseline shield model

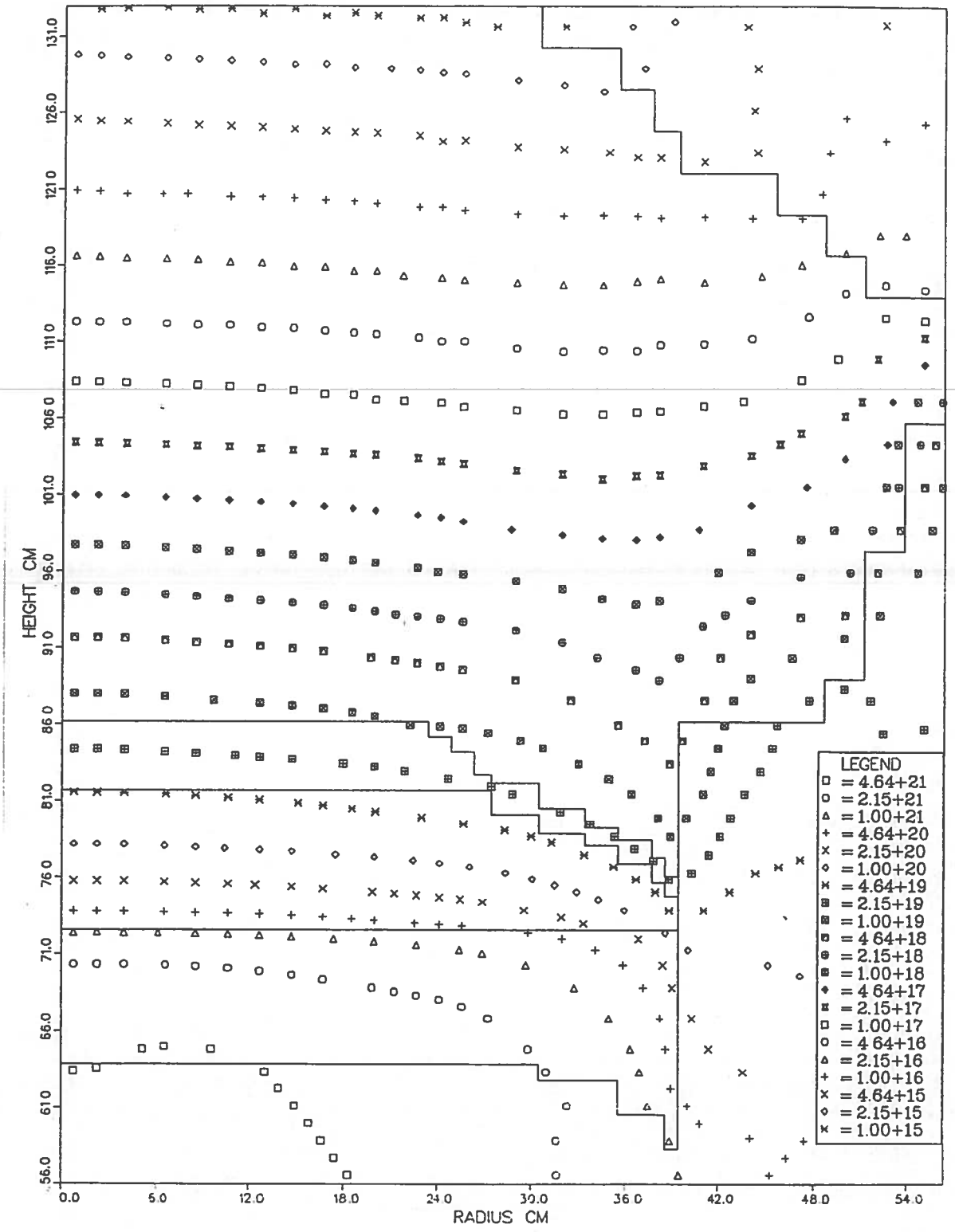

Fig. 7.17 Seven year neutron fluence [neutrons/cm^2] contours for the Case 5 shield model

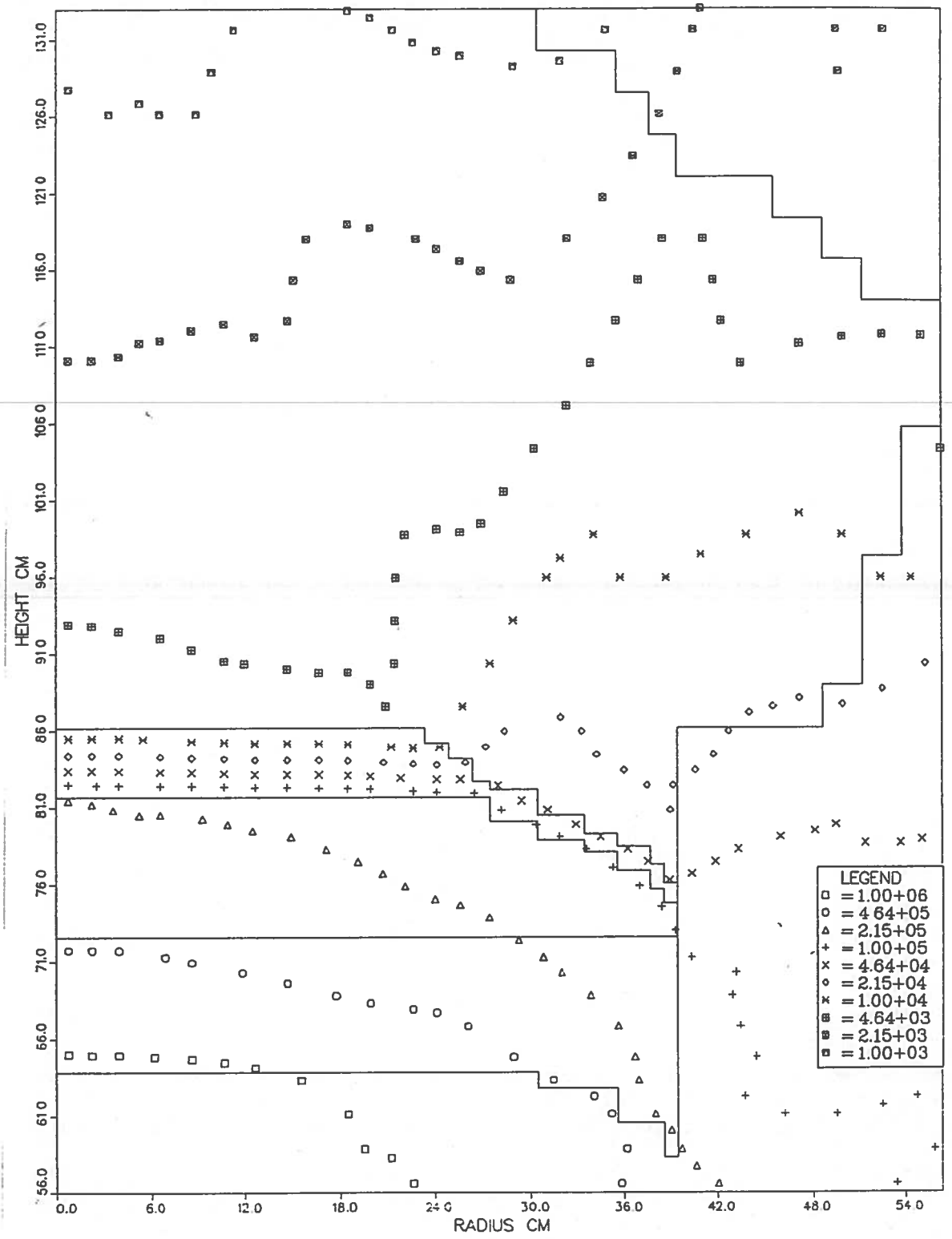

Fig. 7.18 Seven year gamma dose [Mrad] contours for the Case 5 shield model

to r=56.36 cm) has been considered to be an isotropic disk source. The equivalent source strengths of the disk source for neutrons and gammas have been calculated from their respective total leakages out of the top of the shield (this information may be obtained from the printout of the DOT-IV run). The detector response at a point 'P' located on the central axis of an isotropic disc source of radius 'a' at a distance 'h' from the center of the disc is given by [7.7]

$$R(P) = \pi \hat{R} S_a \ln(1+a^2/h^2) \qquad (7.1)$$

where S_a ≡ source strength.

$R(P)$ ≡ detector response at point P.

$\hat{R}$ ≡ detector response due to a point source at one unit distance from the source in the abscence of any attenuating medium, if the point source has a strengh of unity.

$\hat{R}$ in Eqn. (7.1) may be written as $\Re / 4\pi$ where $\Re$ is the detector response function. Therefore Eqn. (7.1) may be written as

$$R(P) = \Re S_a \ln(1+a^2/h^2) / 4 \qquad (7.2)$$

Maximum radial dimension of the shield = 56.36 cm. Therefore the value of 'a' in Eqn. (7.2) = 56.36 cm.

Neutron fluence and gamma dose calculations have been made at a point 'P' located on the r=0 centerline at a distance of 25 m from the reactor midplane (see Fig. 7.19). The axial position of the reactor midplane is at z = 31.8 cm ; Therefore the value of 'h' in Eqn. (7.2) = 2500 cm - (133 cm - 31.8 cm) = 2398.8 cm. Cross sectional area of the equivalent disc source = $\pi(56.36)^2$ = 9979.11 cm^2.

Seven Year Neutron Fluence Calculations

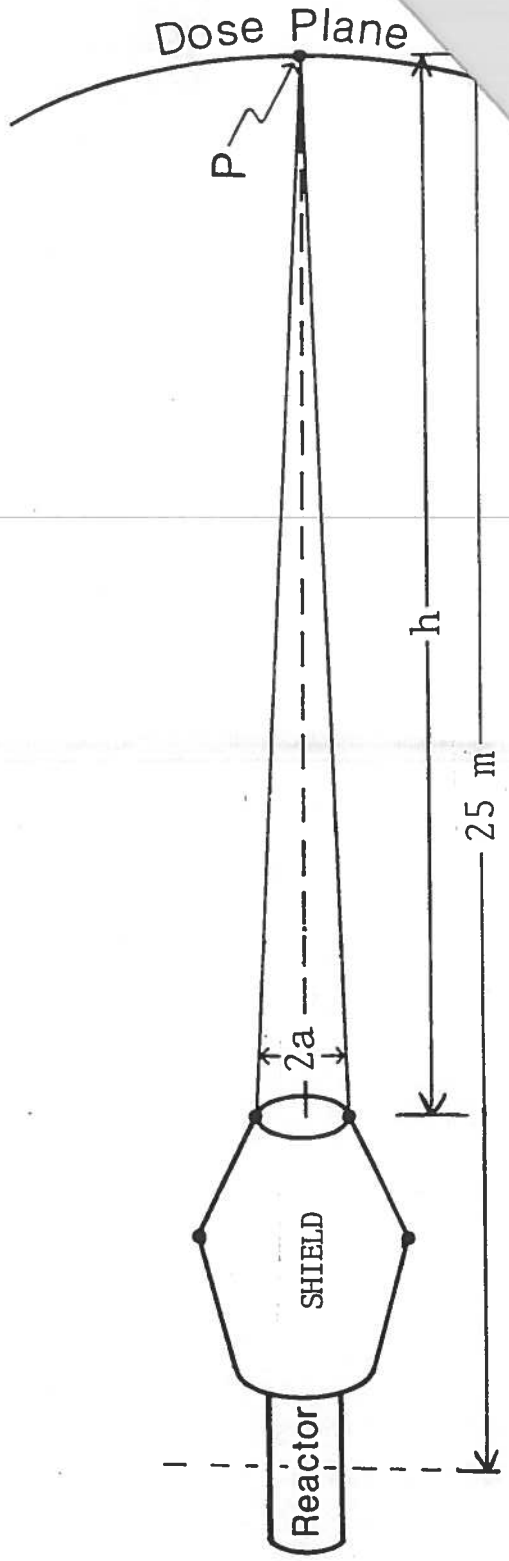

Fig. 7.19 Treatment of the top surface of the shield as a disk source for radiation dose calculations at point 'P' on the 25 m dose plane

(a) Baseline Shield Model

Total neutron outflow from top of shield at z = 133.0 cm = $\sum_{g=1}^{g=22} n_g$

where 'n_g' is the group 'g' neutron outflow [neutrons/sec] from the top of the shield,

= 1.119874E11 neutrons/sec.

Strength of equivalent isotropic disc source, S_a =

(2)(1.119847E11)/9979.11 = 2.244436628E7 neutrons/cm^2/sec.

From Eqn. (6.2), with $\Re$=1, R(P) = (2.244436628E7)ln(1+56.36^2/2398.8^2)/4 = 3096.573543 neutrons/cm^2/sec.

Seven year neutron fluence at point P =

(3096.573543)(7)(365.25)(24)(3600) = 6.84043E11 neutrons/cm^2.

(b) Case 5 Shield Model

Total neutron outflow from top of shield at z = 133.0 cm = $\sum_{g=1}^{g=22} n_g$

= 1.113520E11 neutrons/sec.

Calculations similar to those for the baseline shield model in (a), yield a seven year neutron fluence of 6.8016185E11 neutrons/cm^2.

Seven Year Gamma Dose Calculations

(a) Baseline Shield Model

($\Re$)(S_a) in Eqn. (7.2) may be written as

$$(\Re)(S_a) = \sum_{g=23}^{g=32} 2\, g_g\, D_g / A = (2/A) \sum_{g=23}^{g=32} g_g\, D_g \quad ..(7.3)$$

where g_g = group 'g' gamma outfow from top of shield [gammas/sec].

D_g = Dose factor for group 'g' [Mrad/hr per gammas/cm^2/sec].

A = Area of shield [cm^2].

Using the multigroup dose factors for the gammas listed in Appendix F and the values of g_g yields

$$\sum_{g=23}^{g=32} g_g D_g = 2.494247E2 \text{ Mrad-cm}^2/\text{hr}.$$

Therefore from Eqn. (6.3), $(\Re)(S_a) = (2/9979.11)(2.494247E2) =$ 4.9989368E-2 Mrad/hr.

From Eqn. (7.2), $R(P) = (4.9989368E-2)\ln(1+56.36^2/2398.8^2)/4 = 6.897E-6$ Mrad/hr.

Seven year gamma dose = (6.897E-6)(7)(365.25)(24) = 0.423205401 Mrad.

(b) Case 5 Shield Model

Using the multigroup dose factors for gammas listed in Appendix F and the values of g_g yields

$$\sum_{g=23}^{g=32} g_g D_g = 2.42587E2 \text{ Mrad-cm}^2/\text{hr}.$$

Calculations similar to those for the baseline shield model in (a), yield a seven year gamma dose of 0.411603697 Mrad.

Table 7.3 summarizes the results of radiation dosage calculations for the baseline and Case 5 shield models. For the baseline shield model as well as for the Case 5 shield model, the seven year neutron fluence and gamma dose at the 25 m doseplane are well within the SP-100 nominal specifications (maximum neutron fluence = 1.0E13 neutrons/cm^2; maximum gamma dose = 0.5 Mrad). The radiation attenuation performance of the Case 5 shield is slightly better than that of the baseline shield.

7.4 Transient Heat Conduction Analysis of the Radiation Shield

Table 7.3 Summary of radiation dosage calculations for the baseline shield model and for the Case 5 shield model.

Shield Model	7 Year NVT [neutrons/cm^2] at Shield Top (z=133.0 cm)	7 Year Gamma Dose[Mrad] at Shield Top (z=133.0 cm)	7 Year NVT [neutrons/cm^2] at 25 m Dose Plane	7 Year Gamma Dose[Mrad] at 25 m Dose Plane
Base-line	1.19E15	1.22E3	6.84E11	0.42
Case 5	1.09E15	1.03E3	6.80E11	0.41

Transient heat conduction calculations have been performed for the shield corresponding to the Case 5 design in order to get an estimate of the thermal response time of the shield. Initially, the reactor power is considered to be zero and the shield temperatures to be equal to the ambient temperature ($0^{\circ}K$). At t=0 hours, the reactor power jumps to 100% full power in a step fashion.

Two methods have been used for transient analysis. The first method is a crude analytical method wherein the shield has been modelled as a singly lumped system. The other method uses DOS-HEATING6 to perform the transient calculations utilizing the two dimensional RZ model of the Case 5 shield. The latter method should give a fairly accurate picture of the transient, though it was found to require a large amount of computing time.

Transient Calculations Using the Singly Lumped Analytical Model

This model assumes that the temperature does not vary spatially in the shield. Although this assumption is not justifiable, it should serve the purpose of obtaining a rough estimate of the average transient temperature response of the shield.

Application of heat balance to the shield yields the following differential equation :

$$\sum_{i=1}^{i=M} (\rho)_i (v_i)(c_p)_i \frac{dT}{dt} = Q_N - \sigma\epsilon A(T^4 - T_A^4) \qquad (7.4)$$

where $(\rho)_i$ ≡ mass density of the 'i'th material in the shield [kg/m^3].

(v_i) ≡ volume of the 'i'th material in the shield [m^3].

$(c_p)_i$ ≡ specific heat of the 'i'th material in the shield [$J/kg/^{\circ}K$].

M ≡ total number of materials in the shield.

T ≡ shield temperature [°K].

Q_N ≡ total time-independent nuclear heat generation rate in the shield [J/hr].

σ ≡ stefan-boltzmann contant = 2.0412E-4 J/hr/m^2/°K^4.

ϵ ≡ emissivity of the radiating outer surface of the shield.

A ≡ surface area of the radiating outer surface of the shield [m^2].

T_A ≡ ambient temperature [°K].

Letting $\sum_{i=1}^{i=M} (\rho_i)(v_i)(c_p)_i \equiv X$, Eqn. (7.4) becomes

$$X \frac{dT}{dt} = Q_N - \sigma\epsilon A(T^4 - T_A^4) \qquad (7.5)$$

or

$$\frac{dT}{Q_N - \sigma\epsilon A(T^4 - T_A^4)} = \frac{dt}{X} \qquad (7.6)$$

Integration of Eqn. (7.6) and further simplification results in the following expression for the time response of the shield :

$$t = \frac{X}{2\sigma\epsilon A T_{ss}^3}\left[\frac{1}{2}\ln\left[\frac{(1+\tilde{T}(t))(1-\tilde{T}(0))}{(1+\tilde{T}(0))(1-\tilde{T}(t))}\right] + \tan^{-1}(\tilde{T}(t)) - \tan^{-1}(\tilde{T}(0))\right] \qquad (7.7)$$

where T_{ss} ≡ steady state temperature of shield = $\left[\frac{Q_N}{\sigma\epsilon A} + T_A^4\right]^{\frac{1}{4}}$ (7.8)

where $\tilde{T}(t) \equiv \frac{T(t)}{T_{ss}}$ = normalized shield temperature at time = t hours.

$\tilde{T}(0) \equiv \frac{T(0)}{T_{ss}}$ = normalized shield temperature at time t = 0 hours.

The value of A in eqn. (7.4) = $2\pi(39.43)(86.2-58.27)+\pi(48.69^2-39.43^2)+$
$2\pi(49.69)(88.989-86.2)+\pi(51.246^2-48.69^2)$

$\approx$ 11139 cm^2 = 1.1139 m^2.

The value of σ in Eqn. (7.4) = 2.0412E-4 $J/hr/m^2/°K^4$.

The value of ϵ in Eqn. (7.4) = 0.80.

The value of T_A in Eqn. (7.4) = 0.0°K.

The value of Q_N in Eqn. (7.4) = 20772.648 J/hr (this value has been obtained from the printout of the steady state DOS-HEATING6 run for the Case 5 shield model).

On substituting the values of A, σ, ϵ, Q_N, and T_A into Eqn. (7.8), the steady state temperature, T_{ss} corresponding to a nuclear heating rate of Q_N is found to be 581.32°K. Recall that in the previous DOS-HEATING6 steady state analysis, the temperature varied spatially between values of 526°K and 658°K.

There are three materials in the shield viz. beryllium, LiH, and tungsten. Therefore the value of M in Eqn. (7.4) is 3.

Table 7.4 lists the thermal data of these three materials used in the transient calculations. Using data from Table 7.4, the value of X in Eqn. (7.4) is found to be 1549502.926 J/°K.

Using the above data, the transient thermal response of the shield as indicated by Eqn. (7.7) has been graphically depicted in Fig. (7.20). It takes approximately 172 hours for the shield to attain steady state

Transient Calculations using DOS-HEATING6

Transient calculations have been performed on the same two dimensional RZ model of the Case 5 shield as that employed in steady state heat conduction calculations. The Crank-Nicholson implicit scheme has been chosen as the method of solution of the transient equation. The initial

Table 7.4 Thermal property data used in transient heat conduction calculations for the Case 5 shield model.

Note : Specific heat and thermal conductivity data listed below are the values at 290°K except for the thermal conductivity of LiH whose value at 600°K has been listed due to the insufficiency of data to be able to extrapolate confidently to 290°K.

Material	Volume [cm^3]	Mass Density [kg/cm^3]	Specific Heat [J/kg/°K]	Thermal Conductivity [W/cm/°K]
Beryllium	51508.6	1.848E-3	1789.0	1.836
LiH	401508.6	0.82E-3	4084.4	0.0711
Tungsten	13296.3	19.3E-3	134.2	1.7948

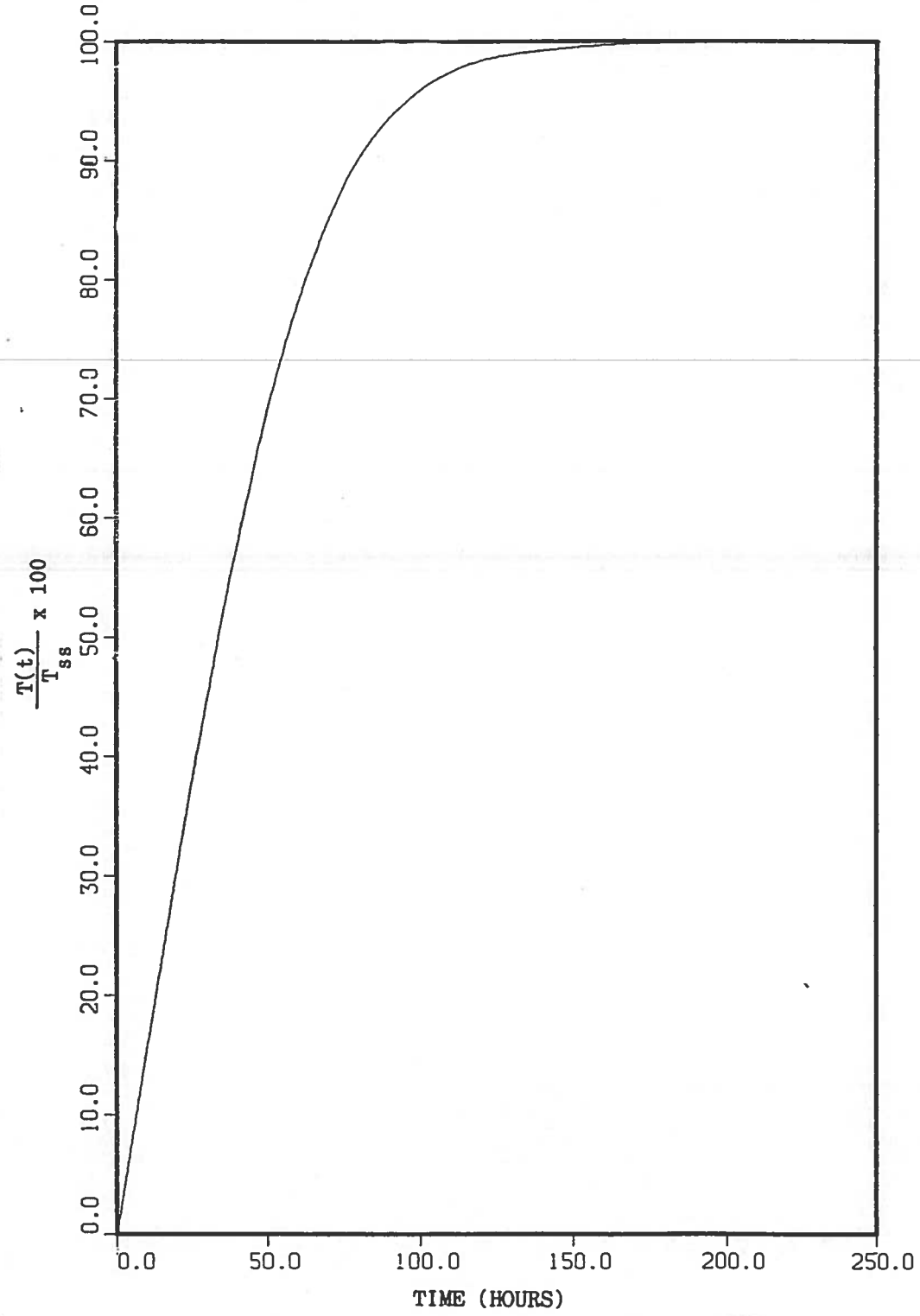

Fig. 7.20 Transient temperature variation (analytical solution) for the Case 5 shield model-the shield being modelled as a singly lumped system, for a step increase in reactor power level from 0% full power to 100% full power.

time step input to the code is 0.015 seconds. DOS-HEATING6 then varies the time step size implicitly by keeping the maximum relative temperature change at a node to 2.5% over a time step. After performing numerous trial runs it was found that an inordinate amount of cpu time is required for the transient calculations if temperature-dependent thermal properties are used in the model. To this end, constant values have been used for the thermal conductivity and specific heat data of the shield materials (see Table 7.4) and a coarse spatial mesh has been employed (1342 nodes as opposed to 2720 nodes used in the steady state calculations). A total cpu time (on the IBM 370 mainframe computer) of about 1.5 hours is required for simulating 130 hours of the transient. Fig. 7.21 shows the transient temperature variation in the shield centerline (r=0.0) temperature. It takes about 130 hours for the peak shield temperature to reach 99.82% of its full power steady state value. According to the singly lumped analytical model it would take about 93 hours for the shield temperature to reach 99.82% of the full power steady state value.

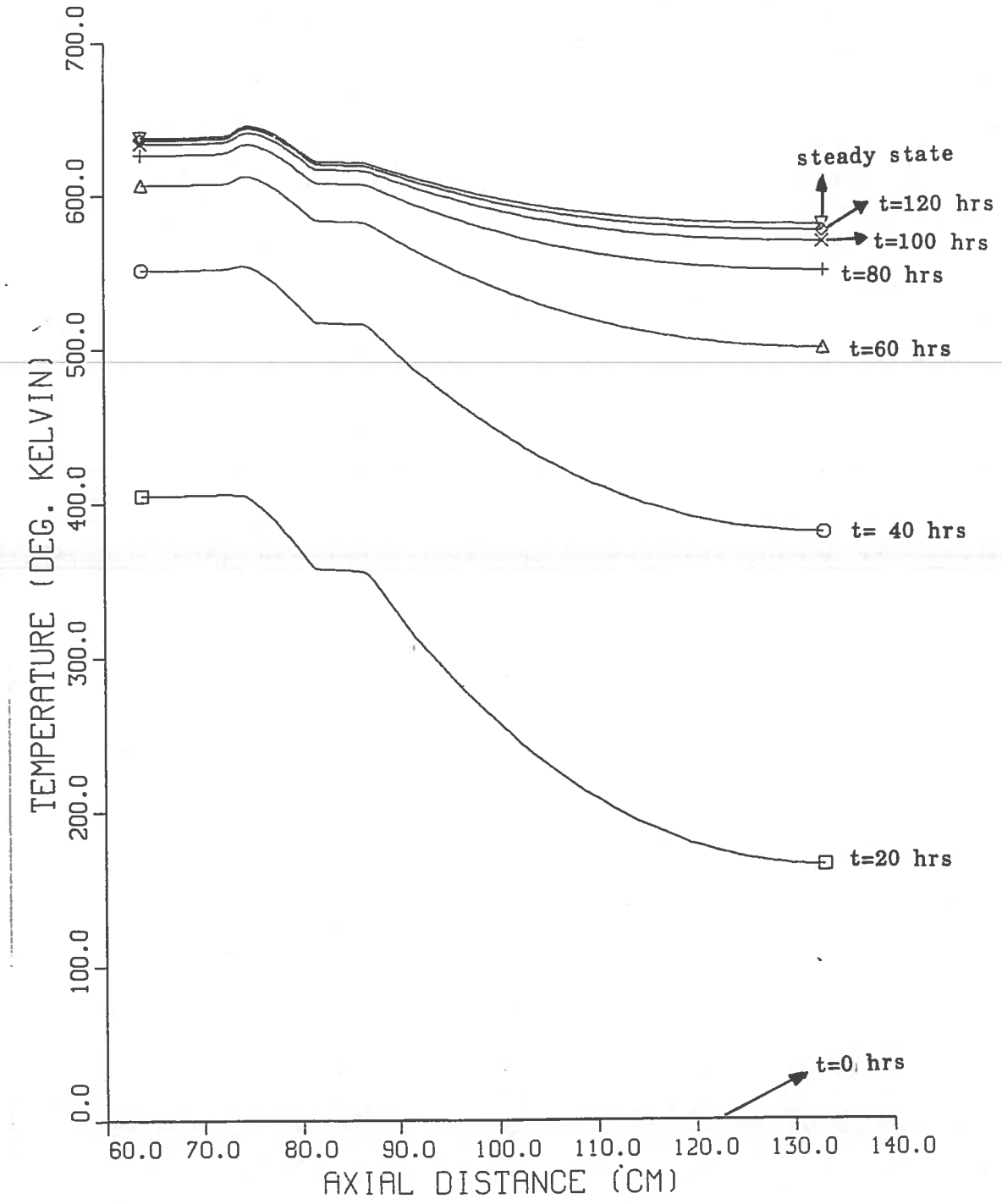

Fig. 7.21 Transient temperature (centerline temperatures at r=0) variation for the Case 5 shield model obtained using the DOS-HEATING6 computer code, for a step increase in reactor power level from 0% full power to 100% full power.

8. SUMMARY AND CONCLUSIONS

In this study, two dimensional (RZ) radiation transport-heat conduction calculations have been carried out for the radiation shield of a 100 kWe (2 MWth) SP-100 space nuclear reactor designed by General Electric in 1984 (in this study, this model is referred to as the "baseline model"), in order to determine the steady state and transient temperature distribution in the shield resulting from nuclear (neutron and gamma) heating occuring in the shield, as well as neutron and gamma dose behind the shield. The DOT-IV computer code has been used for radiation transport calculations, and subsequent heat conduction calculations have been performed using the DOS-HEATING6 computer code, which contains programming modifications made during this study to allow nuclear heating analysis.

The total nuclear heating rate in the baseline shield is found to be 6.33 kW. The maximum and minimum temperatures in the shield are found to be 880°K and 532°K, respectively. These temperatures are outside the stipulated 600°K-680°K band and therefore the shield design requires modifications. The radiation shielding performance of the baseline shield is acceptable. The seven year neutron fluence and gamma dose at the 25 m dose plane are found to be 6.84E11 nvt and 0.42 Mrad, respectively, which are well within the SP-100 dose limits of 1.0E13 nvt for neutrons and 0.5 Mrad for gammas. The total baseline shield weight is 716 kg (which is within the SP-100 upper limit of about 790 kg).

Two unique features of the G.E. shield design that clearly stand out are the prescence of a 0.8 cm thick radial aluminum heat conductor strip

at the bottom of the shield (near the reactor end) and the prescence of two insulation layers surrounding the tunsgten gamma shield. Calculations reveal that removal of the aluminum heat conductor strip raises the maximum temperature from 880°K to 1147°K whereas doubling the thickness of this aluminum strip reduces the maximum temperature from 880°K to 832°K. Thus the aluminum heat conductor strip proves to be very effective in reducing the peak temperature, however increasing the thickness of the strip does not affect the peak temperature much. The radial conductor is therefore an indispensible feature in the baseline shield design. It was found that removal of the insulation layers surrounding the tungsten region not only causes the maximum temperature to be reduced from 880°K to 799°K but also causes the minimum temperature to be raised from 532°K to 561°K, both of which are desirable. Removal of the insulation layers also reduces temperatures in the bottom portion of the shield and raises temperatures in the top portion of the shield. Therefore the insulation layers should be removed from the baseline shield design.

Using beryllium in place of Li^7H in the bottom portion of the shield reduces the total nuclear heating rate in the shield from 6.33 kW to 5.56 kW. The maximum temperature is reduced significantly (from 880°K to 714°K), while the minimum temperature is affected very little. Beryllium also reduces the radial gradient in the temperature across the bottom portion of the shield. The main negative feature of the beryllium is the increased weight of the shield (shield weight increases from 716 kg to 742 kg) caused by the higher mass density of beryllium as compared to Li^7H.

A combination of the previous two changes in the shield designs,

i.e., replacing the Li^7H region by beryllium and removal of the insulation layers around the tungsten reduces the maximum temperature drastically from 880°K to 658°K, but the minimum temperature is affected very little. The total nuclear heating rate in the shield is reduced from 6.33 kW to 5.77 kW, at the expense of an increase in shield weight from 716 kg to 752 kg (the weight is within the SP-100 upper limit of about 790 kg). The seven year neutron fluence and gamma dose at the 25 m dose plane are found to be 6.80E11 nvt and 0.41 Mrad, respectively for this design, which are almost the same as for the baseline shield model, and within the SP-100 dose limits. This design change made to the baseline shield design gives a better temperature distribution than any of the other designs examined. The maximum temperature and temperatures in the bottom portion of the shield are now satisfactory. However, the minimum temperature (526°K) and some of the temperatures in the top portion of the shield still need to be raised above 600°K in order to obtain an acceptable temperature distribution. One way this could be done is to push the gamma heating source (tungsten layer) further up into the top portion of the shield. However, this change has not been examined in this thesis.

DOS-HEATING6 has also been used to carry out transient heat conduction calculations for the shield design containing beryllium and having the insulation layers removed. Starting with an initial temperature distribution equal to the ambient temperature (0°K), the time taken for shield temperatures to achieve steady state following a step increase in the reactor power level from 0% full power to 100% full power is found to be of the order of 130 hours. Thus, if the reactor were to

operate as a pulsed power source, the steady state temperature corresponding to pulsed mode operation of the reactor should remain well below the steady state temperature distribution corresponding to 100% full power operation. Moreover since the shield temperatures vary so slowly with time, the shield should not develop very high thermal stresses due power-up and power-down operations.

REFERENCES

1.1 M. S. El-Genk, D. M. Woodall, V. F. Dean, and D. L. Y. Louie, "Review of the Design Status of the SP-100 Space Nuclear Power System," in Space Nuclear Power Systems 1984, M. S. El-Genk and M. D. Hoover eds., Orbit Book Co., Malabar, FL, 1985.

1.2 J. A. Angelo Jr. and D. Buden, Space Nuclear Power, Orbit Book Co., Malabar, FL, 1985.

1.3 V. C. Truscello and H. S. Davis, "Nuclear Electric Power in Space," I.E.E.E. Spectrum, 1984.

1.4 D. Buden and J. Angelo Jr., "Opening Up the Future in Space with Nuclear Power," Transactions of the Second Symposium on Space Nuclear Power Systems, CONF-850103-SUMMS, Albuquerque, NM, Jan. 14-16, 1985.

1.5 V.C. Truscello, "Status of the SP-100 GES Project," Transactions of the Fourth Symposium on Space Nuclear Power Systems, CONF-870118-SUMMS, Albuquerque, NM, Jan. 15, 1987.

1.6 S. Bailey, S. Vaidyanathan, and J. VanHoomissen, "Liquid Metal Cooled Reactors for Space Power Applications," in Space Nuclear Power Systems 1984, M.S. El-Genk and M.D. Hoover eds., Orbit Book Co., Malabar, FL, 1985.

1.7 A. T. Josloff, A. Kirpich, and J. D. Stephen, "Tradeoffs and Studies of the SP-100 concept," Transactions of the Fourth Symposium on Space Nuclear Power Systems, CONF-870118-SUMMS, Albuquerque, NM, Jan. 15, 1987.

1.8 D. E. Carlson, "Minimum Mass Configurations of Tungsten and Lithium

Hydride in the Shadow Shield of the SP-100 Reactor," Transactions of the Second Symposium on Space Nuclear Power Systems, CONF-850103-SUMMS, Albuquerque, NM, Jan. 14-16, 1985.

1.9 W. J. Barattino, M. S. El-Genk, and S.S. Voss, "Review of Previous Shield Analysis for Space Reactors," in Space Nuclear Power Systems 1984, M. S. El-Genk and M. D. Hoover eds., Orbit Book Co., Malabar, FL, 1985.

1.10 F. Beiriger Jr., Thermal Analysis - Advanced ZrH_2 Reactor, TI-696-20-001, Atomics International, May, 1968.

1.11 Thompson and Schwab, Nuclear Heating in Reference ZrH_2 Shield, TI-696-23-040, Atomics International, December, 1969.

1.12 F. Keshishian et al., Radiation Shielding for Zirconium Hydride Systems, AI-AEC-13081, Atomics International, Canoga Park, CA, 1973.

1.13 W. J. Barattino and M. S. El-Genk, "Thermal Analysis of Radiation Shields for Space Reactors using Analytical and Finite Element Methods," in Space Nuclear Power Systems 1984, M. S. El-Genk and M. D. Hoover eds., Orbit Book Co., Malabar, FL, 1985.

1.14 W. J. Barattino, M. S. El-Genk, and P. J. McDaniel, "A Coupled Radiation Transport-Thermal Analysis of the Radiation Shield for an SP-100 Type Reactor," in Space Nuclear Power Systems 1985, M. S. El-Genk and M. D. Hoover eds., Orbit Book Co., Malabar, FL, 1985.

1.15 W. J. Barattino, Coupled Radiation Transport/Thermal Analysis of the Radiation Shield for a Space Nuclear Reactor, PhD. dissertation, Department of Chemical and Nuclear Engineering, The

University of New Mexico, Albuquerque, NM, 1985.

2.1 Chapter 13 titled "Heat Generation in Shields," pp. 172-184, in Reactor Handbook, Vol. III, Part B (Shielding), 2nd Edition, E. P. Blizard and L. S. Abbott eds., Interscience Publishers (a division of John Wiley & Sons, Inc.), 1962.

4.1 W. J. Rhoades and R. L. Childs, An Updated Version of the DOT4 One-and Two-Dimensional Neutron/Photon Transport Code, ORNL-5851, Oak Ridge National Laboratory, 1982.

4.2 W. A. Rhoades and M. B. Emmett, DOS : The Discrete Ordinates System, ORNL/TM-8362, Oak Ridge National Laboratory, 1982.

4.3 R. D. O'Dell and R. E. Alcouffe, Transport Calculations for Nuclear Analyses: Theory and Guidelines for Effective Use of Transport Codes, LA-10983-MS, UC-32, Los Alamos National Laboratory, September, 1987 (This report is a revision of the chapter titled "Transport Calculations for Nuclear Reactors," written by the authors for Vol. 1 of the three-volume CRC Handbook of Nuclear Reactor Calculations, Y. Ronen editor, published by the CRC Press, Boca Raton, FL, 1986).

4.4 E. E. Lewis and W. F. Miller Jr., Computational Methods of Neutron Transport, John Wiley & Sons Inc., New York, 1974.

5.1 D. C. Elrod, G. E. Giles, and W. D. Turner, "HEATING6 : A Multi-dimensional Heat Conduction Analysis with the Finite-Difference Formulation," Section F.10 in SCALE : A Modular Code System for Performing Standardized Computer Analyses for Licensing Evaluation, Vol. II, NUREG/CR-0200, Nuclear Regulatory Commission, Washington D. C., 1984.

5.2 SCALE: A Modular Code System for Performing Standardized Computer Analyses for Licensing Evaluation, Rev. 3, Vol. I-III, NUREG/CR-0200, Nuclear Regulatory Commission, Washington D. C., 1984.

6.1 M. A. Abdou and C. W. Maynard, "Calculational Methods for Nuclear Heating-Part I: Theoretical and Computational Algorithms," Nuclear Science and Engineering, Vol. 56, pp. 360-380, 1975.

6.2 M. L. Williams, A. Yucel, and S. Nadkarny, DOS-HEATING6 : A General Conduction Code with Nuclear Heat Generation derived from DOT-IV Transport Calculations, ORNL/TM-10645, Oak Ridge National Laboratory, May, 1988.

7.1 S. Vaidyanathan, S. Kaplan, R. Protsik, and A. W. Dalcher, "Design Concepts for the GES SP-100 Reactor and shield," Transactions of the Fourth Symposium on Space Nuclear Power Systems, CONF-870118-SUMMS, Albuquerque, NM, Jan. 15, 1987.

7.2 C. Y. Fu and D. T. Ingersoll, VELM61 and VELM22: Multigroup Cross Section Libraries for Sodium-Cooled Reactor Shield Analysis, ORNL/TM-10302, Oak Ridge National Laboratory, April, 1987.

7.3 A. L. Edwards, A Compilation of Thermal Property Data for Computer Heat Conduction Calculations, Lawrence Radiation Laboratory, University of California, Livermore, CA, February 24, 1969 (UCRL-50589).

7.4 D. T. Ingersoll and C. O. Slater, "ISOPLOT4- A Code for Plotting DOT-IV Geometries and Isoflux Contours," in DOGS: A Collection of Graphics Support of Discrete Ordinates Codes, ORNL/TM-7188, Oak Ridge National Laboratory, March, 1980.

7.5 C. K. Cobb, "HEATPLOT-S: A Temperature Distribution Plotting Program for HEATING5/HEATING6," Section F.13 in SCALE: A Modular Code System for Performing Standardized Computer Analyses for Licensing Evaluation, Vol II, NUREG/CR-0200, Nuclear Regulatory Commission, Washington D. C., 1984.

7.6 W. H. Harless, Personal Communication, 1987.

7.7 A. B. Chilton, J. K. Shultis, and R. E. Faw, Principles of Radiation Shielding, Prentice-Hall, Inc., Englewood Cliffs, NJ, 1984.

APPENDIX A

Listing of New DOS-HEATING6 Routines

APPENDIX A

```
      SUBROUTINE DOTR(IMBIS,ISET,ZD,RD,DFLX,RH,TH,ZH,MATL,XKERM,NILFR,
     *   NILBR,NIRFR,NIRBR,NOLFR,NOLBR,NORFR,NORBR,NTPI,NTPJ,NTPK,
     *   G1M,G1P,G2M,G2P,G4M,G4P,G5M,G5P,G7M,G7P,Q,MAT,MATNAM,VMAT,
     *   QNEUT,QGAM,VGEN,VOL,DENSTY)
C     SUBROUTINE DOTR IS CALLED FROM HEATING6 SUBROUTINE HEATN6 (IF
      IDOT  > 0) I.E. IF NUCLEAR HEATING CALCULATIONS NEED TO BE
      PERFORMED. SUBROUTINE DOTR CALLS SUBROUTINE DOTQ.
      IMPLICIT REAL*8 (A-H,O-Z)
      REAL*8 MATNAM
      REAL*4 ZD,RD,DFLX
      INTEGER*2 NILFR(1),NILBR(1),NIRFR(1),NIRBR(1),NOLFR(1),
     *   NOLBR(1),NORFR(1),NORBR(1),NTPI(1),NTPJ(1),NTPK(1),MATL,MAT
      DIMENSION IMBIS(1),ISET(1),ZD(1),RD(1),DFLX(IMA,1),
     *   RH(1),TH(1),ZH(1),MATL(1),XKERM(IGM,1),G1M(1),G1P(1),G2M(1),
     *   G2P(1),G4M(1),G4P(1),G5M(1),G5P(1),G7M(1) G7P(1),Q(1),MAT(1),
     *   MATNAM(1),VMAT(1),QNEUT(1),QGAM(1),VGEN(IT,1),VOL(1),DENSTY(1)
      COMMON /GRDLIN/ IT,JT,KT,NGX,NGY,NGZ,IGT,JGT,KGT,NGXP1,NGYP1,
     *               NGZP1,NGGR,NGG
      COMMON /DOT/ IDOT,IGM,NEUT,JM,LM,IMA,MMA,ISM,IMSISM,ISBT
C
C     ** DEBUG PRINT HEATING6 VARIABLES **
      WRITE(6,41) (RH(I),I=1,IT)
   41 FORMAT(//2X,'HEATING6 R MESH',/2X,(8E12.5))
      WRITE(6,42) (TH(J),J=1,JT)
   42 FORMAT(//2X,'HEATING6 Y MESH',/2X,(8E12.5))
      WRITE(6,43) (ZH(K),K=1,KT)
   43 FORMAT(//2X,'HEATING6 Z MESH',/2X,(8E12.5))
C     ************************************
C     ** READ DOT4 71$$ AND 73$$ ARRAYS **
      READ(IDOT) (LMBIG,IG=1,IGM),(IMBIS(IS),IS=1,ISM),(ISET(J),J=1,JM)
C     ************************************
      JM1=JM+1
      ITOT=IMSISM+ISM
C     ** READ DOT4 Z AND R MESHES (MAY BE VARIABLY DIMENSIONED) **
      READ(IDOT) (ZD(J),J=1,JM1),(RD(I),I=1,ITOT)
C     ********************************************************************
C     ** DEBUG PRINT **
      WRITE(6,60) IGM,NEUT,JM,LM,IMA,ISM,IMSISM,ISBT
   60 FORMAT(/2X,'IGM,NEUT,JM,LM,IMA,ISM,IMSISM,ISBT=',8I4)
      WRITE(6,61) (IMBIS(IS),IS=1,ISM)
   61 FORMAT(//2X,'IMBIS:',(1X,30I4))
      WRITE(6,62) (ISET(J),J=1,JM)
   62 FORMAT(//2X,'ISET:',(1X,30I4))
      WRITE(6,63) (ZD(J),J=1,JM1)
   63 FORMAT(//2X,'ZD:',(1X,10E12.5))
      WRITE(6,64) (RD(I),I=1,ITOT)
   64 FORMAT(//2X,'RD:',(1X,10E12.5))
C     ******************
      CALL DOTQ(IDOT,NEUT,IGM,JM,IMA,IMBIS,ISET,ZD,RD,DFLX,RH,TH,ZH,
     *   MATL,XKERM,NILFR,NILBR,NIRFR,NIRBR,NOLFR,NOLBR,NORFR,NORBR,
     *   NTPI,NTPJ,NTPK,G1M,G1P,G2M,G2P,G4M,G4P,G5M,G5P,G7M,G7P,Q,
     *   MAT,MATNAM,VMAT,QNEUT,QGAM,VGEN,VOL,DENSTY)
      RETURN
      END
C
      SUBROUTINE DOTQ(IDOT,NEUT,IGM,JM,IMA,IMBIS,ISET,ZD,RD,DFLX,RH,TH,
     *   ZH,MATL,XKERM,NILFR,NILBR,NIRFR,NIRBR,NOLFR,NOLBR,NORFR,NORBR,
     *   NTPI,NTPJ,NTPK,G1M,G1P,G2M,G2P,G4M,G4P,G5M,G5P,G7M,G7P,Q,MAT,
     *   MATNAM,VMAT,QNEUT,QGAM,VGEN,VOL,DENSTY)
C     THIS SUBROUTINE CALCULATES THE NUCLEAR HEAT GENERATION RATE
```

```
C     ASSOCIATED WITH THE CONTROL VOLUME OF EACH HEATING6 NODE.
C     SUBROUTINE DOTQ IS CALLED FROM SUBROUTINE DOTR. SUBROUTINE DOTQ
      CALLS FUNCTION TERP AND SUBROUTINE DWOT.
      IMPLICIT REAL*8 (A-H,O-Z)
      REAL*4 RD,ZD,DFLX
      REAL*8 MATNAM
      INTEGER*2 NILFR,NILBR,NIRFR,NIRBR,NOLFR,NOLBR,NORFR,NORBR,
     *   NTPI,NTPJ,NTPK,MATL,MAT
      DIMENSION IMBIS(1),ISET(1),ZD(1),RD(1),DFLX(IMA,1),RH(1),ZH(1),
     *   TH(1),MATL(1),XKERM(IGM,1),NILFR(1),NILBR(1),NIRFR(1),NIRBR(1),
     *   NOLFR(1),NOLBR(1),NORFR(1),NORBR(1),NTPI(1),NTPJ(1),NTPK(1),
     *   G1M(1),G1P(1),G2M(1),G2P(1),G4M(1),G4P(1),G5M(1),G5P(1),G7M(1),
     *   G7P(1),Q(1),MAT(1),MATNAM(1),VMAT(1),QNEUT(1),QGAM(1),
     *   VGEN(IT,1),VOL(1),DENSTY(1)
      DIMENSION MREG(2,2,2),G1(2),G2(2),G4(2),G5(2),G7(2)
      COMMON /GRDLIN/ IT,JT,KT,NGX,NGY,NGZ,IGT,JGT,KGT,NGXP1,NGYP1,
     *                NGZP1,NGGR,NGG
      COMMON /PRBTYP/ NT,NPBT,NGEOM,NTYPE,NSET,KF,IDEGRE
      COMMON /ARYLNG/ MAXANA, MAXBDC, MAXCP , MAXFGL, MAXGGL, MAXHGN,
     .                MAXINT, MAXMAT, MAXNSN, MAXPAR, MAXPBT, MAXPRS,
     .                MAXPRT, MAXPTS, MAXREG, MAXRFG, MAXSPC, MAXSPL,
     .                MAXSUR, MAXTBL, MAXTFG, MAXZFG
C     ** LAST NEUTRON GRP 'LNG' = NEUT **
      LNG=NEUT
C     ************************************
C     ** INITIALIZE HEAT SOURCE FOR EACH NODE **
      DO 10 N=1,NT
   10 Q(N)=0.0
C     ******************************************
C     ** INITIALIZE QNEUT,QGAM,AND VMAT **
      DO 4 MM=1,MAXMAT
      QNEUT(MM)=0.0D0
      QGAM(MM)=0.0D0
      VMAT(MM)=0.0D0
 4    CONTINUE
C     ******************************************
      FACTR=1.0
      IF(NGEOM.EQ.2) FACTR=0.159155
C     ** BEGIN GROUP LOOP **
      DO 100 IG=1,IGM
C        ** BEGIN J LOOP **
         DO 50 J=1,JM
         M=ISET(J)
         ILIM=IMBIS(M)
         READ(IDOT) (DFLX(I,J),I=1,ILIM)
   50    CONTINUE
C        ** END J LOOP **
C     ** READ BOUNDARY FLUX **
      READ(IDOT)
C     ************************
C     ** LOOP OVER HEATING-6 NODES **
      DO 500 N=1,NT
      IX=NTPI(N)
      JY=NTPJ(N)
      KZ=NTPK(N)
      R=RH(IX)
      Z=ZH(KZ)
      IF(NGEOM.EQ.2.OR.NGEOM.EQ.7) Z=TH(JY)*FACTR
      G1(1)=G1M(IX)
      G1(2)=G1P(IX)
```

```
      G2(1)=G2M(IX)
      G2(2)=G2P(IX)
      G4(1)=G4M(JY)
      G4(2)=G4P(JY)
      G5(1)=G5M(KZ)
      G5(2)=G5P(KZ)
      G7(1)=G7M(IX)
      G7(2)=G7P(IX)
      MREG(1,1,2)=NILFR(N)
      MREG(1,1,1)=NILBR(N)
      MREG(1,2,2)=NIRFR(N)
      MREG(1,2,1)=NIRBR(N)
      MREG(2,1,2)=NOLFR(N)
      MREG(2,1,1)=NOLBR(N)
      MREG(2,2,2)=NORFR(N)
      MREG(2,2,1)=NORBR(N)
      IF(IG.EQ.1) VSUM=0.0D0
C     ** LOOP OVER NEIGHBORING INTERVALS **
      DO 980 I=1,NGXP1
      V1=G1(I)*G2(I)*G7(I)
      DO 980 J=1,NGYP1
      V2=V1*G4(J)
      DO 980 K=1,NGZP1
      NOREG=MREG(I,J,K)
      IF(NOREG.LT.1)GO TO 980
      MATRL=MATL(NOREG)
      IF(MATRL.LT.1)GO TO 980
      V=V2*G5(K)
      IF(IG.EQ.1) VSUM=VSUM+V
      IN=IX+2*I-3
      JN=JY+2*J-3
      KN=KZ+2*K-3
C     RN AND ZN ARE COORDS OF NEIGHBOURING NODE
      RN=RH(IN)
      ZN=ZH(KN)
      IF(NGEOM.EQ.2.OR.NGEOM.EQ.7) ZN=TH(JN)*FACTR
C     RPT AND ZPT ARE MIDPOINTS OF 'NODE SECTION'(IE, 1/4 NODE IN 2D)
      SIG=XKERM(IG,MATRL)
      RPT=(RN-R)*.25 + R
      ZPT=(ZN-Z)*.25 + Z
      PHI=TERP(DFLX,ZD,RD,IMBIS,ISET,IMA,JM,RPT,ZPT)
C     ** CALCULATE THE VOLUME AND HEAT GEN RATE FOR EACH MATERIAL **
      DO 985 MM=1,MAXMAT
      IF(MATRL.NE.MM) GO TO 985
      PSV=PHI*SIG*V
      IF(IG.GT.LNG) GO TO 61
      QNEUT(MM)= QNEUT(MM)+PSV
      GO TO 59
   61 QGAM(MM)= QGAM(MM)+PSV
   59 IF(IG.EQ.1) VMAT(MM)=VMAT(MM)+V
  985 CONTINUE
C     ***************************************************************
      Q(N)=Q(N)+PHI*SIG*V
  980 CONTINUE
      IF(IG.EQ.1) VOL(N)=VSUM
  500 CONTINUE
C     ** END OF LOOP OVER NODES **
  100 CONTINUE
C     ** END OF GROUP LOOP **
C     ** DETERMINE THE VOL. HEAT GEN RATE FOR EACH NODE **
```

```
C     ** AND PRINT IT OUT USING SUBROUTINE DWOT  *********
      IF(NGEOM.NE.2.AND.NGEOM.NE.7) GO TO 298
      NLIM=JT
      GO TO 299
  298 NLIM=KT
  299 CONTINUE
      DO 307 I=1,IT
      DO 307 J=1,NLIM
      VGEN(I,J)=0.0D0
  307 CONTINUE
      DO 301 N=1,NT
      IX=NTPI(N)
      JY=NTPJ(N)
      KZ=NTPK(N)
      IF(NGEOM.NE.2.AND.NGEOM.NE.7) GO TO 311
      VGEN(IX,JY)=Q(N)/VOL(N)
      GO TO 301
  311 VGEN(IX,KZ)=Q(N)/VOL(N)
  301 CONTINUE
      WRITE(6,302)
  302 FORMAT(//1X,'MAP OF VOLUMETRIC HEAT GEN RATES FOR ALL NODES : ',/
     $1X)
      IF(NGEOM.EQ.2) GO TO 312
      IF(NGEOM.EQ.7) GO TO 313
      IF(NGEOM.EQ.3) GO TO 314
      IF(NGEOM.EQ.8) GO TO 315
  312 CALL DWOT(VGEN,IT,NLIM,1,' R ',' T ',' 0 ',6)
      GO TO 304
  313 CALL DWOT(VGEN,IT,NLIM,1,' X ',' Y ',' 0 ',6)
      GO TO 304
  314 CALL DWOT(VGEN,IT,NLIM,1,' R ',' Z ',' 0 ',6)
      GO TO 304
  315 CALL DWOT(VGEN,IT,NLIM,1,' X ',' Z ',' 0 ',6)
  304 CONTINUE
C     *********************************************************
C     ** CALCULATE THE MASS OF EACH MATERIAL AND PRINT THE VOLUME, **
C     ** HEAT GEN RATES AND THE MASS OF EACH MATERIAL              **
      WRITE(6,18)
   18 FORMAT(////1X,'MAT. NO.',2X,'MAT. NAME',6X,'VOLUME',12X,'MASS',7X,
     $'NEUTRON HEAT GEN. RATE',4X,'GAMMA HEAT GEN. RATE',4X,'TOTAL HEAT
     $GEN. RATE',/1X)
      TMASS=0.0D0
      TVOL=0.0D0
      TNQ=0.0D0
      TGQ=0.0D0
      DO 800 MM=1,MAXMAT
      RMASS=DENSTY(MM)*VMAT(MM)
      QMM=QNEUT(MM)+QGAM(MM)
      WRITE(6,21) MAT(MM),MATNAM(MM),VMAT(MM),RMASS,QNEUT(MM),QGAM(MM),
     $            QMM
   21 FORMAT(1X,I5,5X,A8,4X,1PD12.5,3X,1PD12.5,4X,6X,D12.5,14X,D12.5,9X,
     $D12.5)
      TVOL=TVOL+VMAT(MM)
      TNQ=TNQ+QNEUT(MM)
      TGQ=TGQ+QGAM(MM)
      TMASS=TMASS+RMASS
  800 CONTINUE
      WRITE(6,806) TVOL ,TMASS
  806 FORMAT(//1X,'TOTAL VOLUME (EXCLUDING GAP REGIONS) = ',1PD12.5,//1X
     $,'TOTAL MASS OF ALL MATERIALS = ',1PD12.5,//1X)
```

```
      THEAT=TNQ+TGQ
      WRITE(6,802) TNQ,TGQ,THEAT
  802 FORMAT(/1X,'TOTAL NEUTRON HEAT GEN. RATE = ',1PD12.5,/1X,'TOTAL GA
     $MMA HEAT GEN. RATE = ',1PD12.5,/1X,'TOTAL NEUTRON AND GAMMA HEAT G
     $EN. RATE = ',1PD12.5,//1X)
C     ****************************************************************
      RETURN
      END
C
      FUNCTION TERP(DFLX,ZD,RD,IMBIS,ISET,IMA,JM,R,Z)
C     THIS SUBPROGRAM INTERPOLATES THE DOT FLUXES FROM THE
C     DOT MESH POINTS TO ANY HEATING6 MESH POINT. LINEAR
C     INTERPOLATION HAS BEEN USED.
C     INTERPOLATION IS FIRST DONE ALONG THE X OR R AXIS;
C     INTERPOLATION IS THEN DONE ALONG THE Y OR Z AXIS.
C     IF ANY INTERPOLATED FLUX VALUE TURNS OUT TO BE NEGATIVE,
C     IT IS SET TO THE VALUE OF THE FLUX AT THE NEAREST MESH POINT
C     AT WHICH THE FLUX IS POSITIVE. FUNCTION TERP IS CALLED FROM
C     SUBROUTINE DOTQ.
      IMPLICIT REAL*8(A-H,O-Z)
      REAL*4 RD,ZD,DFLX
      DIMENSION DFLX(IMA,1),ZD(1),RD(1),IMBIS(1),ISET(1)
      DO 10 J=1,JM
      IF(Z.GE.ZD(J).AND.Z.LE.ZD(J+1)) GO TO 5
      GO TO 10
    5 ZM=(ZD(J)+ZD(J+1))/2.0
      IF(J.EQ.1.OR.J.EQ.JM) GO TO 12
      IF(Z.GE.ZM) GO TO 15
   30 ZT=ZM
      JPHIT=J
      ZB=(ZD(J)+ZD(J-1))/2.0
      GO TO 20
   15 ZT=(ZD(J+1)+ZD(J+2))/2.0
      JPHIT=J+1
      ZB=ZM
      GO TO 20
   12 IF(J.EQ.1) GO TO 15
      GO TO 30
   10 CONTINUE
   20 CONTINUE
      JSRCH=JPHIT
   33 IISET=ISET(JSRCH)
      IISET1=IISET-1
      NSUM=0
      IF(IISET.EQ.1) GO TO 35
      DO 38 I=1,IISET1
      NSUM=NSUM+IMBIS(I)+1
   38 CONTINUE
   35 CONTINUE
      IL=NSUM+1
      IR=IL+IMBIS(IISET)
      IR1=IR-1
      DO 40 I=IL,IR1
      IF(R.GE.RD(I).AND.R.LE.RD(I+1)) GO TO 45
      GO TO 40
   45 IBRAC=I-NSUM
      RM=(RD(I)+RD(I+1))/2.0
      IF(I.EQ.IL.OR.I.EQ.IR1) GO TO 50
      IF(R.GE.RM) GO TO 55
   65 RR=RM
```

```
      IPHIR=IBRAC
      RL=(RD(I-1)+RD(I))/2.0
      GO TO 60
 55   RR=(RD(I+1)+RD(I+2))/2.0
      IPHIR=IBRAC+1
      RL=RM
      GO TO 60
 50   IF(I.EQ.IL) GO TO 55
      GO TO 65
 40   CONTINUE
 60   CONTINUE
      IF(JSRCH.NE.JPHIT) GO TO 80
      PHIT=DFLX(IPHIR-1,JSRCH)+(DFLX(IPHIR,JSRCH)-DFLX(IPHIR-1,JSRCH
     $))*(R-RL)/(RR-RL)
      IF(PHIT.LT.0.0D0) GO TO 100
 105  JSRCH=JSRCH-1
      GO TO 33
 100  IF(R.GT.RR) GO TO 101
      PHIT=DFLX(IPHIR-1,JSRCH)
      GO TO 102
 101  PHIT=DFLX(IPHIR,JSRCH)
 102  CONTINUE
      GO TO 105
 80   PHIB=DFLX(IPHIR-1,JSRCH)+(DFLX(IPHIR,JSRCH)-DFLX(IPHIR-1,
     $JSRCH))*(R-RL)/(RR-RL)
      IF(PHIB.LT.0.0D0) GO TO 110
      GO TO 115
 110  IF(R.GT.RR) GO TO 111
      PHIB=DFLX(IPHIR-1,JSRCH)
      GO TO 112
 111  PHIB=DFLX(IPHIR,JSRCH)
 112  CONTINUE
 115  TERP=PHIB+(PHIT-PHIB)*(Z-ZB)/(ZT-ZB)
      IF(TERP.GE.0.0D0) RETURN
      IF(Z.GT.ZT) GO TO 118
      TERP=PHIB
      GO TO 119
 118  TERP=PHIT
 119  CONTINUE
      RETURN
      END
C
      SUBROUTINE DWOT (X,II,JJ,KK,TOP1,TOP2,TOP3,NOU)
C     THIS SUBROUTINE PRINTS OUT A 1-D, 2-D, OR 3-D REAL ARRAY.
C     SUBROUTINE DWOT IS CALLED FROM SUBROUTINE DOTQ AND ALSO
      FROM HEATING6 SUBROUTINE MATERL (IF IDOT > 0).
      DIMENSION X(II,JJ,KK)
      REAL*8 TOP1,TOP2,TOP3,X
      DO 110 K=1,KK
      JO2 = 0
      JO3 = (JJ+8)/9
      IF  (KK.LE.1) GO TO 10
      WRITE (NOU,120)TOP3,K
   10 DO 100 JK=1,JO3
      JO1 = JO2 + 1
      JO2 = MIN0(JO1+8,JJ)
      WRITE (NOU,130)TOP1,(TOP2,J,J=JO1,JO2)
      NFLAG = 0
      DO 90 I=1,II
      SSUM = 0.0
```

```
      DO 20 J=JO1,JO2
   20 SSUM = SSUM + DABS(X(I,J,K))
      IF  (SSUM.NE.0.0) GO TO 30
      NFLAG=NFLAG+1
      IF  (I.LT.II) GO TO 90
   30 IF  (NFLAG-1) 80,60,40
   40 N=I-NFLAG
      IM1=I-1
      IF  ((I.LT.II).OR.(SSUM.NE.0.0)) GO TO 50
      N=N+1
      IM1=I
   50 WRITE (NOU,160)N,IM1,(X(IM1,J,K),J=JO1,JO2)
      GO TO 70
   60 IF  (SSUM.LE.0.0) GO TO 80
      IM1=I-1
      WRITE (NOU,140)IM1,(X(IM1,J,K),J=JO1,JO2)
   70 CONTINUE
      NFLAG=0
      IF  (SSUM.LE.0.0) GO TO 90
   80 WRITE (NOU,140)I,(X(I,J,K),J=JO1,JO2)
C     WRITE (NOU,150)
   90 CONTINUE
  100 CONTINUE
  110 CONTINUE
      WRITE (NOU,150)
      RETURN
C
C
  120 FORMAT  (/1H0,6X,A6,I5)
  130 FORMAT  (/1H0,6X,A6,   9(4X,A6,I3))
  140 FORMAT  (1H ,I10,4X,1P9E13.5)
  150 FORMAT  (1H )
  160 FORMAT  (1H ,I7,3H TO,I4,1P9E13.5)
      END
```

APPENDIX B

Energy Group Structure Associated with the "VELM" Microscopic Cross-Section Data Library/Microscopic Kerma Factor Data Library

APPENDIX B

Neutron Groups

Energy Group	Upper Limit (eV)	Lower Limit (eV)
1	1.4918E7	5.4881E6
2	5.4881E6	2.4660E6
3	2.4660E6	1.6530E6
4	1.6530E6	1.1080E6
5	1.1080E6	7.4273E5
6	7.4273E5	5.2340E5
7	5.2340E5	3.8774E5
8	3.8774E5	2.9849E5
9	2.9849E5	2.7324E5
10	2.7324E5	1.4996E5
11	1.4996E5	8.6517E4
12	8.6517E4	5.6562E4
13	5.6562E4	3.4307E4
14	3.4307E4	2.6058E4
15	2.6058E4	9.1188E3
16	9.1188E3	3.0354E3
17	3.0354E3	1.2341E3
18	1.2341E3	2.7536E2
19	2.7536E2	4.7851E1
20	4.7851E1	1.0677E1
21	1.0677E1	1.1253E0
22	1.1253E0	1.0000E-5

Gamma Groups

Energy Group	Upper Limit (eV)	Lower Limit (eV)
23	1.4000E7	8.0000E6
24	8.0000E6	6.0000E6
25	6.0000E6	4.0000E6
26	4.0000E6	2.0000E6
27	2.0000E6	1.0000E6
28	1.0000E6	6.0000E5
29	6.0000E5	3.0000E5
30	3.0000E5	1.0000E5
31	1.0000E5	4.5000E4
32	4.5000E4	1.0000E4

APPENDIX C

Listing of Microscopic Kerma Factors of Component Nuclides of Shield Materials

APPENDIX C

MATERIAL : LI-6
4.39655E6 3.20083E6 2.20285E6 1.82932E6 1.68433E6 1.88637E6 2.66068E6
5.41570E6 1.06450E7 1.14259E7 3.73593E6 3.37987E6 3.80300E6 4.39738E6
5.96830E6 1.00250E7 1.63875E7 3.02902E7 6.88739E7 1.53925E8 4.04906E8
4.00604E9 1.32237E6 1.00001E6 8.21863E5 6.02995E5 3.79044E5 2.29517E5
1.32448E5 5.28383E4 1.27820E4 5.13282E3
MATERIAL : LI-7
3.29982E6 1.60333E6 7.64470E5 5.22089E5 3.11800E5 1.70031E5 1.27172E5
1.41312E5 2.86020E5 1.51099E5 1.98731E4 1.35996E4 9.52538E3 6.93603E3
4.33914E3 2.41090E3 1.99289E3 2.61280E3 5.41391E3 1.16020E4 3.03040E4
2.96937E5 1.32237E6 1.00001E6 8.21863E5 6.02995E5 3.79044E5 2.29517E5
1.32448E5 5.28383E4 1.27820E4 5.13282E3
MATERIAL : H-1
4.47708E6 3.64131E6 2.93644E6 2.46092E6 2.04124E6 1.70933E6 1.46285E6
1.27642E6 1.16879E6 9.76587E5 6.96702E5 5.01150E5 3.54343E5 2.57223E5
1.48258E5 5.44164E4 2.01885E4 6.50152E3 1.32788E3 2.53803E2 4.34571E1
5.72491E-1 3.95107E5 3.14920E5 2.65100E5 1.98808E5 1.26266E5 7.65062E4
4.41492E4 1.76088E4 4.22346E3 9.64062E2
MATERIAL : AL
1.23147E6 3.66220E5 2.61189E5 2.02215E5 1.63522E5 1.28904E5 1.10839E5
8.44125E4 9.10511E4 6.35595E4 5.48517E4 2.38712E4 3.28234E4 1.96043E4
4.89469E3 8.56454E3 3.61325E3 2.75987E3 4.62510E3 9.89002E3 2.59843E4
2.56903E5 8.65090E6 5.52150E6 4.13530E6 2.75600E6 1.64857E6 9.96062E5
5.78332E5 2.55245E5 2.53387E5 2.44015E6
MATERIAL : BE
1.66882E6 1.43737E6 7.63673E5 5.14229E5 5.05923E5 4.64897E5 2.89185E5
2.40654E5 2.11609E5 1.68029E5 1.08662E5 7.12281E4 4.66560E4 3.19225E4
1.73815E4 6.00721E3 2.17769E3 6.98928E2 1.47919E2 4.08535E1 4.11762E1
3.61731E2 1.85420E6 1.37010E6 1.11353E6 8.08368E5 5.05556E5 3.06030E5
1.76602E5 7.04945E4 1.74138E4 1.31930E4
MATERIAL : SI
1.77064E6 3.82347E5 2.55764E5 1.84494E5 1.68745E5 1.20470E5 8.85568E4
8.06299E4 8.24983E4 9.05814E4 6.33903E3 8.93611E3 4.59771E3 3.00663E3
1.78838E3 7.91767E2 3.00276E2 1.14524E2 6.99782E1 1.18254E2 3.01320E2
2.96991E3 9.62647E6 6.07330E6 4.51650E6 2.98373E6 1.77627E6 1.07327E6
6.24103E5 2.81615E5 3.25009E5 3.32357E6
MATERIAL : CR
7.81103E5 2.76104E5 1.75132E5 1.32771E5 8.54279E4 5.75549E4 5.37345E4
2.98603E4 2.34141E4 3.49902E4 3.42801E4 6.80184E3 1.24383E4 4.92567E3
3.27782E3 6.85831E3 4.16174E3 7.33834E2 1.29168E3 2.79293E3 7.31153E3
6.98552E4 2.17636E7 1.25673E7 8.79670E6 5.39068E6 3.06807E6 1.86500E6
1.14182E6 8.76310E5 3.12763E6 2.87664E7
MATERIAL : MN
6.43334E5 2.54943E5 1.74283E5 1.36346E5 8.67769E4 6.38976E4 5.57677E4
4.27271E4 3.41436E4 4.56762E4 3.45480E4 4.46494E4 4.50441E4 5.02230E4
6.74815E4 3.73766E4 2.08428E5 4.31174E6 4.67935E5 3.95985E5 9.46769E5
8.91352E6 2.32146E7 1.33123E7 9.27151E6 5.64523E6 3.19982E6 1.94805E6
1.20297E6 9.77780E5 3.64426E6 3.31500E7
MATERIAL : FE
1.05249E6 2.97031E5 1.56552E5 1.05630E5 6.56356E4 4.46113E4 5.48612E4
3.29072E4 3.25209E4 2.43535E4 1.73999E4 1.41622E4 9.84021E3 2.83877E4
1.71099E3 1.29034E3 5.08242E2 2.43645E2 9.30121E1 1.05474E2 2.60755E2
2.38904E3 2.47076E7 1.40745E7 9.75461E6 5.90223E6 3.33178E6 2.03040E6
1.25985E6 1.07275E6 4.31581E6 3.97348E7
MATERIAL : NI
4.60419E6 1.06280E6 2.20055E5 1.22185E5 7.35884E4 5.50199E4 5.17532E4
4.98187E4 6.01743E4 4.02979E4 2.08007E4 2.31475E4 9.11429E3 1.33871E4
1.89563E4 3.38512E3 1.36736E3 6.15343E2 6.43716E2 1.27589E3 3.31736E3
3.16775E4 2.77986E7 1.56563E7 1.07542E7 6.42503E6 3.59872E6 2.20107E6
1.39105E6 1.32673E6 5.78898E6 5.22558E7

MATERIAL : NB
4.33477E5 1.72874E5 1.19629E5 8.95530E4 7.98242E4 7.07963E4 6.04077E4
5.16012E4 4.57207E4 3.48938E4 1.95209E4 9.27495E3 6.06792E3 4.21620E3
2.40161E3 1.22201E3 9.43916E2 7.45820E2 4.42500E2 7.19848E1 3.16857E1
2.97288E2 5.16750E7 2.76235E7 1.81480E7 1.01200E7 5.43616E6 3.48282E6
2.68772E6 5.20785E6 2.81032E7 1.08944E8
MATERIAL : TA
1.87777E5 1.09166E5 8.08428E4 6.17105E4 4.26205E4 3.16761E4 2.41655E4
1.93873E4 1.70578E4 1.33111E4 8.98689E3 6.47181E3 4.58018E3 3.24819E3
2.07273E3 1.11495E3 9.87453E2 1.78043E3 3.57494E3 8.26613E3 2.60589E4
2.00464E3 1.34392E8 6.89110E7 4.33997E7 2.24132E7 1.21349E7 1.02772E7
1.37193E7 4.66488E7 1.22989E8 2.95370E8
MATERIAL : W-182
1.72372E5 1.00207E5 7.32211E4 6.08605E4 4.70506E4 3.29386E4 2.47475E4
1.97594E4 1.73554E4 1.38264E4 9.54138E3 7.04185E3 5.08504E3 3.82043E3
2.41192E3 1.29018E3 7.05903E2 7.39935E2 1.44606E3 1.66146E4 1.74152E4
2.01567E3 1.37420E8 7.04243E7 4.43157E7 2.28368E7 1.23373E7 1.05217E7
1.43735E7 4.99090E7 1.23054E8 3.13324E8
MATERIAL : W-183
1.68915E5 9.65188E4 7.11878E4 5.68842E4 4.29142E4 3.12983E4 2.36828E4
1.90021E4 1.67984E4 1.37652E4 9.60251E3 7.10918E3 5.25250E3 4.01327E3
2.61192E3 1.44119E3 1.23258E3 2.14800E3 3.36325E3 2.15024E4 6.65370E3
1.39082E3 1.37420E8 7.04243E7 4.43157E7 2.28368E7 1.23373E7 1.05217E7
1.43735E7 4.99090E7 1.23054E8 3.13324E8
MATERIAL : W-184
1.71489E5 1.00486E5 7.65520E4 6.65426E4 5.50139E4 3.98467E4 3.18110E4
2.74638E4 2.55351E4 2.45333E4 2.82008E4 2.87862E4 2.86479E4 3.07692E4
3.97828E4 8.21039E4 2.30853E5 3.87075E5 6.36277E5 5.51650E3 1.69698E4
1.96967E5 1.37420E8 7.04243E7 4.43157E7 2.28368E7 1.23373E7 1.05217E7
1.43735E7 4.99090E7 1.23054E8 3.13324E8
MATERIAL : W-186
1.67610E5 1.03501E5 8.75502E4 7.42263E4 6.08511E4 5.03957E4 4.35960E4
3.87034E4 3.68905E4 3.74558E4 4.92457E4 5.26042E4 5.45765E4 5.95197E4
7.57166E4 1.53098E5 3.07887E5 1.29213E6 1.58879E6 1.10264E8 1.90898E6
1.10400E7 1.37420E8 7.04243E7 4.43157E7 2.28368E7 1.23373E7 1.05217E7
1.43735E7 4.99090E7 1.23054E8 3.13324E8

Note : microscopic kerma factor data presented in Appendix C have units of eV-cm^2/atom; multiply by a factor of 1.6021E-19 in order to convert to units of J-cm^2/atom.

APPENDIX D

Zone-Map of the Baseline Reactor-Shield Model

APPENDIX D

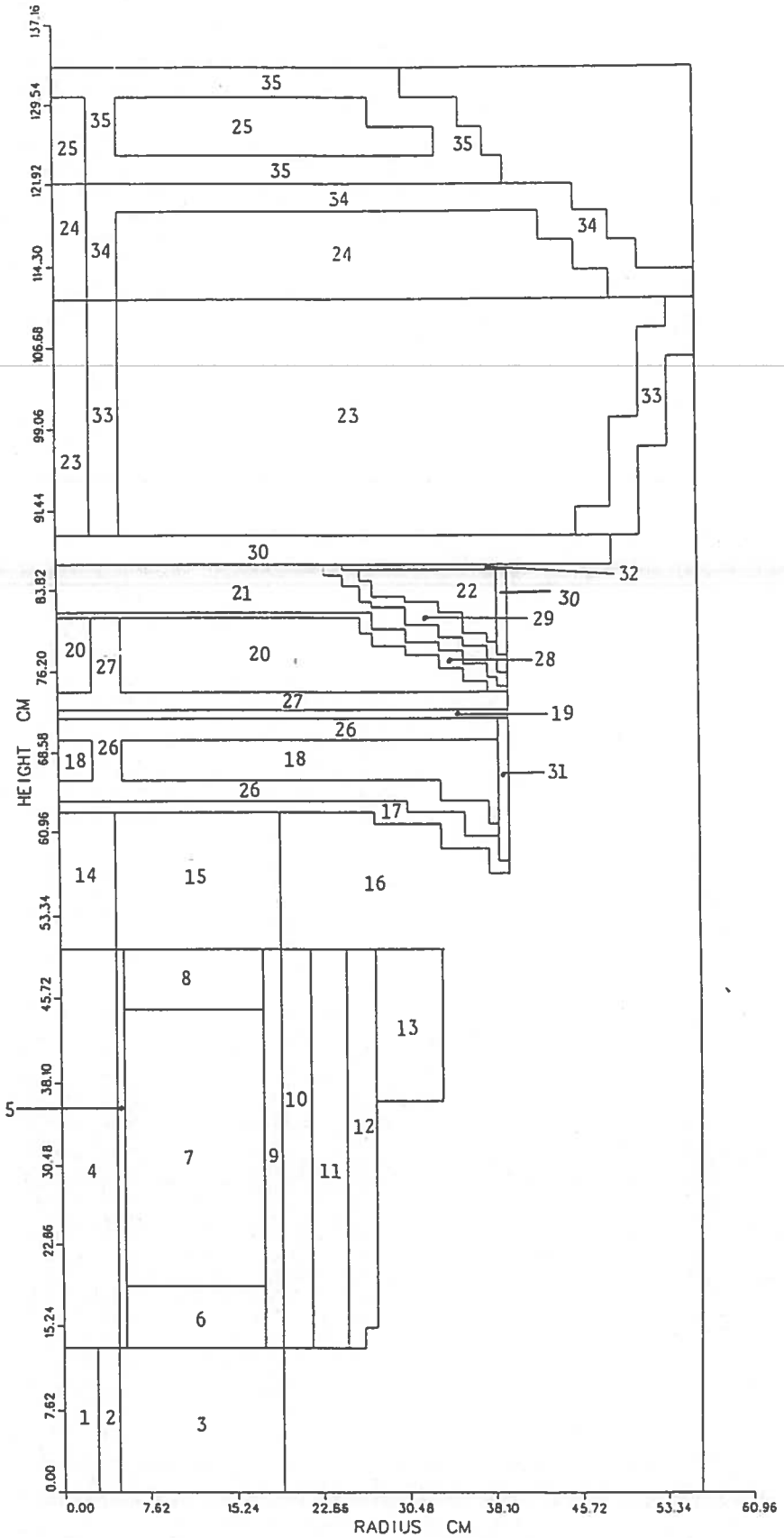
HEIGHT CM
RADIUS CM
0.00
7.62
15.24
22.86
30.48
38.10
45.72
53.34
60.96
68.58
76.20
83.82
91.44
99.06
106.68
114.30
121.92
129.54
137.16
1
2
3
4
5
6
7
8
9
10
11
12
13
14
15
16
17
18
19
20
21
22
23
24
25
26
27
28
29
30
31
32
33
34
35

APPENDIX D (continued)

Zone	Zone Description	Material	Volume Fraction	Component Nuclide	Atom Density [atoms/(barn-cm)]
1	Shutdown Plug Hole	Void	1.0000	-	-
2	Shutdown Plug	B_4C	0.8947	B^{10}	7.278E-2
				B^{11}	8.088E-3
				C	2.022E-2
		Nb-1Zr	0.1053	Nb	5.645E-3
				Zr	5.701E-5
3	Tip Plumbing	Nb-1Zr	0.3483	Nb	1.867E-2
				Zr	6.564E-4
		Insulation	0.0376	Mo	1.883E-3
				O	9.357E-4
		Li	0.2492	Li^7	9.961E-3
		Void	0.3649	-	-
4	Inner Reflector	Nb-1Zr	0.0404	Nb	2.163E-3
				Zr	2.185E-5
		BeO	0.9596	Be	6.103E-2
				O	6.103E-2
5	Inner Structure	Nb-1Zr	0.8291	Nb	4.444E-2
				Zr	4.489E-4
		Void	0.1709	-	-
6	Lower Axial Reflector	Nb-1Zr	0.1701	Nb	9.118E-3
				Zr	9.210E-5
		BeO	0.6259	Be	3.981E-2
				O	3.981E-2
		Li	0.2040	Li^7	8.154E-3
7	Core	UO_2	0.6259	U^{235}	1.241E-2
				U^{238}	3.838E-4
				O	2.559E-2
		Nb-1Zr	0.1701	Nb	9.118E-3
				Zr	9.210E-3
		Li	0.2040	Li^7	8.154E-3
8	Upper Axial Reflector	Nb-1Zr	0.1701	Nb	9.118E-3
				Zr	9.210E-5
		BeO	0.6259	Be	3.981E-2
				O	3.981E-2
		Li	0.2040	Li^7	8.154E-3
9	Outer Structure/ Coolant	Nb-1Zr	0.3173	Nb	1.701E-2
				Zr	1.718E-4
		Li	0.6827	Li^7	2.729E-2

APPENDIX D (continued)

10	Inner Radial Reflector	(a) Nb-1Zr	0.0755	Nb	4.061E-3
				Zr	4.102E-5
		BeO	0.9245	Be	5.907E-2
				O	5.907E-2
		(b) Nb-1Zr	0.1163	Nb	6.256E-3
				Zr	6.319E-5
		BeO		Be	3.484E-2
				O	3.484E-2
		B_4C		B^{10}	2.764E-2
				B^{11}	3.072E-3
				C	7.680E-3
11	Central Radial Reflector	(a) Nb-1Zr	0.0300	Nb	1.614E-3
				Zr	1.630E-5
		BeO	0.9700	Be	6.198E-2
				O	6.198E-2
12	Outer Radial Reflector	(a) Nb-1Zr	0.0712	Nb	3.830E-3
				Zr	3.868E-5
		BeO	0.9288	Be	5.935E-2
				O	5.935E-2
		(b) Nb-1Zr	0.1033	Nb	5.557E-3
				Zr	5.612E-5
		BeO		Be	4.029E-2
				O	4.029E-2
		B_4C		B^{10}	2.173E-2
				B^{11}	2.415E-3
				C	6.038E-3
13	Accumulator	Nb-1Zr	0.9700	Nb	5.200E-2
				Zr	5.252E-4
		Li	0.0300	Li^7	1.199E-3
14	Inner Reflector Extension	Nb-1Zr	0.0404	Nb	2.163E-3
				Zr	2.185E-5
		BeO	0.9596	Be	6.103E-2
				O	6.103E-2
15	Base Plumbing	Nb-1Zr	0.1078	Nb	5.779E-3
				Zr	5.561E-4
		Insulation	0.0400	Mo	2.004E-3
				O	9.954E-4
		Li	0.8488	Li^7	3.393E-2
		Void	0.0034	-	-
16	Void	Void	1.0000	-	-
17	Insulation	Insulation	1.0000	Mo	5.133E-2
				Zr	1.275E-2
				O	2.550E-2

18	Enriched Li^7H	Li^7H	0.9980	Li^7	5.504E-2
	LiH (Li^7H)			H_1	5.503E-2
	Neutron			H_2	8.255E-6
	Shield	SS-347	0.0020	Si	1.974E-6
	+			Mn	3.418E-6
	SS-347 Can			Cr	3.162E-5
				Ni	1.880E-5
				Fe	1.134E-4
				Nb	8.544E-7
				Ta	8.544E-7
19	Radial Aluminum Heat Conductor	Al	1.0000	Al	6.036E-2
20	Natural LiH	LiH	0.9980	Li^6	4.167E-3
	Neutron			Li^7	5.139E-2
	Shield			H_1	5.555E-2
	+			H_2	8.333E-6
	SS-347 Can	SS-347	0.0020	Si	1.974E-6
				Mn	3.418E-6
				Cr	3.162E-5
				Ni	1.880E-5
				Fe	1.134E-4
				Nb	8.544E-7
				Ta	8.544E-7
21	Tungsten	W	1.0000	W_{182}	1.673E-2
	Gamma			W_{183}	9.120E-3
	Shield			W_{184}	1.940E-2
				W_{186}	1.799E-2
22 23 24 25	..... SAME AS ZONE 20				

26	Enriched	Li^7H	0.9481	Li^7	5.229E-2
	LiH (Li^7H)			H_1	5.228E-2
	+			H_2	7.842E-6
	SS-347 Can	SS-347	0.0519	Si	5.121E-5
				Mn	8.870E-5
				Cr	8.205E-4
				Ni	4.878E-4
				Fe	2.942E-3
				Nb	2.217E-5
				Ta	2.217E-5
27	Natural	LiH	0.9396	Li^6	3.923E-3
	LiH			Li^7	4.838E-2
	+			H_1	5.230E-2
	SS-347 Can			H_2	7.846E-6
		SS-347	0.0604	Si	5.960E-5
				Mn	1.032E-4
				Cr	9.549E-4
				Ni	5.676E-4
				Fe	3.423E-3
				Nb	2.580E-5
				Ta	2.580E-5
28	Aluminum	SS-347	0.1429	Si	1.410E-4
	+			Mn	2.442E-4
	Insulation			Cr	2.259E-3
	+			Ni	1.343E-3
	SS-347 Can			Fe	8.100E-3
				Nb	6.105E-5
				Ta	6.105E-5
		Insulation	0.4286	Mo	2.200E-2
				Zr	5.465E-3
				O	1.093E-2
		Al	0.4286	Al	2.587E-2

APPENDIX D (continued)

29	Natural LiH + Insulation + SS-347 Can	SS-347	0.2000	Si	1.974E-4
				Mn	3.418E-4
				Cr	3.162E-3
				Ni	1.880E-3
				Fe	1.134E-2
				Nb	8.544E-5
				Ta	8.544E-5
		Insulation	0.6000	Mo	3.080E-2
				Zr	7.650E-3
				O	1.530E-2
		LiH	0.2000	Li^6	8.334E-4
				Li^7	1.028E-2
				H_1	1.111E-2
				H_2	1.667E-6
30	Natural LiH + Aluminum + SS-347 Can	SS-347	0.0376	Si	3.710E-5
				Mn	6.426E-5
				Cr	5.945E-4
				Ni	3.534E-4
				Fe	2.131E-3
				Nb	1.606E-5
				Ta	1.606E-5
		Al	0.0717	Al	4.328E-3
		LiH	0.8907	Li^6	3.712E-3
				Li^7	4.577E-2
				H_1	4.948E-2
				H_2	7.422E-6
31	Enriched LiH (Li^7H) + Aluminum + SS-347 Can	SS-347	0.1176	Si	1.160E-4
				Mn	2.010E-4
				Cr	1.859E-3
				Ni	1.105E-3
				Fe	6.666E-3
				Nb	5.024E-5
				Ta	5.024E-5
		Al	0.2326	Al	1.404E-2
		Li^7H	0.6499	Li^7	3.577E-2
				H_1	3.576E-2
				H_2	5.365E-6

32 33 34 35	..... SAME AS ZONE 27 .....

(a) composition without the "B_4C reactivity control wedge" in the radial reflector (this is the composition that has been used in the reactor model for radiation transport calculations, in the present study)

(b) composition with the "B_4C reactivity control wedge" in the radial reflector.

Note : When the reactor is in shutdown mode, the BeO inner reflector (zone 4) is replaced by the B_4C shutdown plug (zone 2) and the shutdown plug hole (zone 1).

APPENDIX E

Thermal Property Data of Shield Materials for Heat Conduction Calculations

APPENDIX E

(a) Thermal Conductivity Data

Note : Thermal conductivities have been presented as ordered pairs of the form [T, k(T)] where k(T) is the thermal conductivity [W/cm/°K] at temperature T [°K]; intermediate values obtained by linear interpolation.

Material	Thermal Conductivity
LiH	[600.0, 0.071128], [800.0, 0.06276]
Al	[273.0, 2.36], [300.0, 2.37], [350.0, 2.40], [400.0, 2.40], [500.0, 2.37], [600.0, 2.32], [700.0, 2.26], [800.0, 2.20], [900.0, 2.13]
W	[273.0, 1.82], [300.0, 1.78], [350.0, 1.70], [400.0, 1.62], [500.0, 1.49], [600.0, 1.39], [700.0, 1.33], [800.0, 1.28], [900.0, 1.24], [1000.0, 1.21], [1100.0, 1.18], [1200.0, 1.15]
Be	[298.0, 1.82], [473.0,1.464], [673.0, 1.17], [1073.0, 0.774], [1273.0, 0.6067], [1473.0, 0.523], [1556.0, 0.4937]
SS-347(1)	[8.0, 5.439E-3], [13.0, 9.205E-3], [23.0, 2.176E-2], [43.0, 5.021E-2], [73.0, 7.531E-2], [173.0, 1.3E-1], [373.0, 1.464E-1], [473.0,1.59E-1], [1173.0,2.636E-1], [1373.0, 2.72E-1], [1573.0, 2.9E-1]

(b) Specific Heat Data

Note : Specific heat data have been presented as ordered pairs of the form [T, C_p(T)] where C_p(T) is the specific heat [J/gm/°K] at temperature T [°K]; intermediate values obtained by linear interpolation.

Material	Specific Heat
LiH	[173.0, 2.301], [273.0, 3.933], [473.0, 5.648], [973.0, 7.95]
Al	[20.4, 1.004E-2], [33.0, 4.0E-2], [55.5, 1.803E-1], [77.2, 3.41E-1], [111.0, 5.439E-1], [173.0, 7.74E-1], [273.0, 8.996E-1], [773.0, 1.13E0]
W	[23.0, 2.1E-3], [33.0, 1.046E-2], [73.0, 6.485E-2], [98.0, 8.786E-2], [123.0, 1.025E-1], [148.0, 1.13E-1], [198.0, 1.3E-1], [273.0, 1.339E-1], [3683.0, 2.029E-1]
Be	[73.0, 6.276E-2], [98.0, 1.883E-1], [223.0, 1.423], [273.0, 1.715], [373.0, 2.134], [473.0, 2.364], [673.0,2.699]
SS-347(1)	[13.0, 4.0E-2], [123.0, 3.3E-1], [273.0, 4.477E-1], [473.0, 4.812E-1], [673.0, 5.565E-1], [1573.0, 7.113E-1]

(c) Miscellaneous Data

Material	Mass Density (gm/cc)	Melting Point [°K](1)	
LiH	0.82	960	687 °C
Al	2.703	933	660
W	19.3	3683	3410
Be	1.848	1556	1283
SS-347	7.92	1673	1400

(1) listed for the sake of information; these data have not been used in the calculations

APPENDIX F

Energy Group	Neutron Dose Factor (rem-hr^{-1}/neutrons-cm^{-2}-sec^{-1})[a]
1	1.5024E-04
2	1.3876E-04
3	1.2651E-04
4	1.2933E-04
5	1.2437E-04
6	1.0170E-04
7	8.4550E-05
8	6.6035E-05
9	5.5979E-05
10	4.3014E-05
11	2.5510E-05
12	1.6688E-05
13	1.1502E-05
14	8.4492E-06
15	5.1675E-06
16	3.5759E-06
17	3.6666E-06
18	3.8479E-06
19	4.1525E-06
20	4.4358E-06
21	4.5525E-06
22	3.7563E-06

Energy Group	Gamma Dose Factor (rem-hr^{-1}/photons-cm^{-2}-sec^{-1})
23	1.0270E-05
24	7.2945E-06
25	5.8030E-06
26	4.1681E-06
27	2.6213E-06
28	1.6777E-06
29	1.0730E-06
30	5.0699E-07
31	2.7018E-07
32	1.0251E-06

[a] listed for the sake of information; these data have not been used in the calculations